Optimising Localised Smart Grids with aFRR Services

The Synergy of PV, Heat Pumps, EVs and Battery Storage

S.A.M. Warmerdam

Delft University of Technology

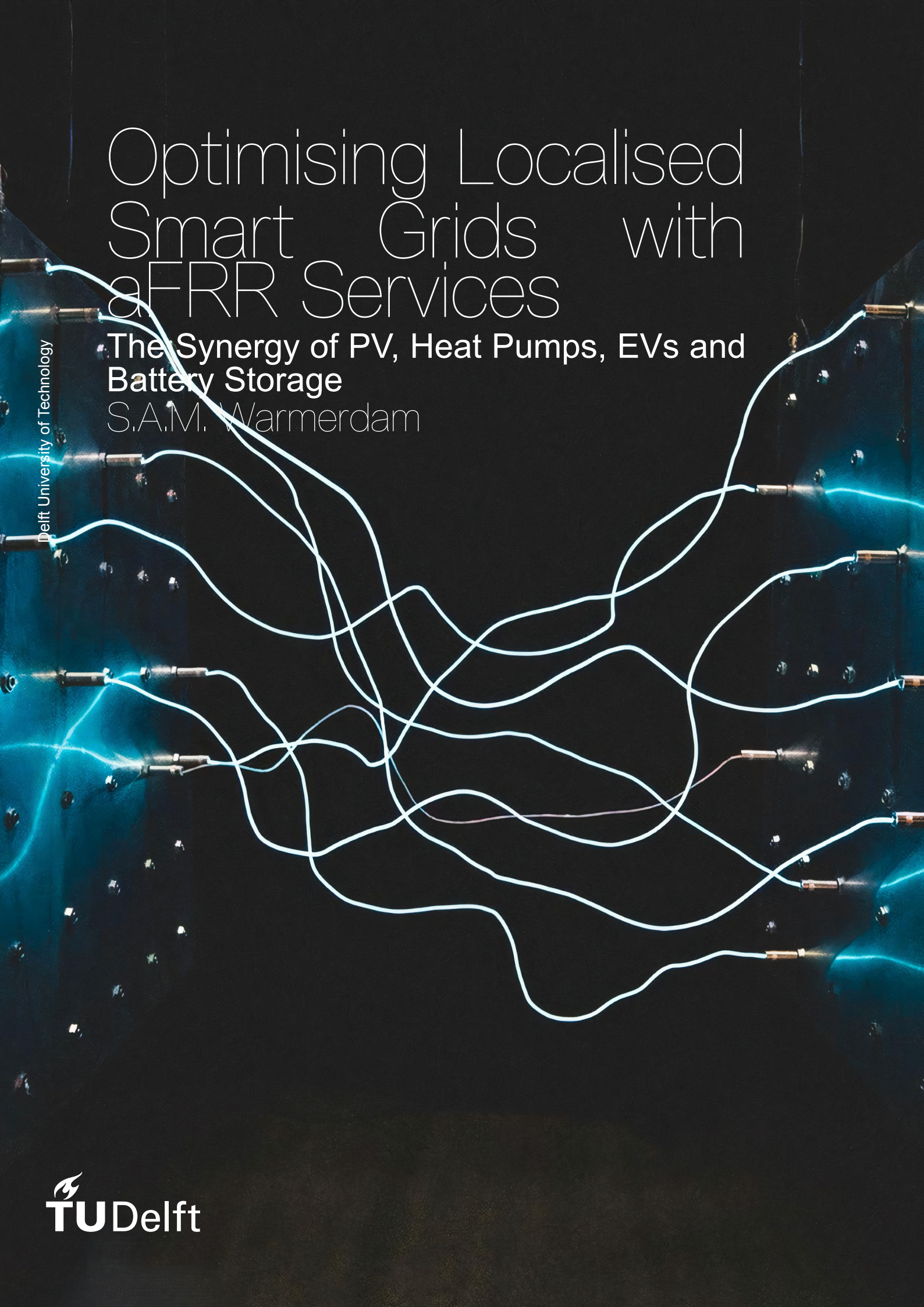

TU Delft

Optimising Localised Smart Grids with aFRR Services

The Synergy of PV, Heat Pumps, EVs and Battery Storage

by

S.A.M. Warmerdam

to obtain the degree of Master of Science
at the Delft University of Technology,
to be defended publicly on Friday May 24, 2024 at 14:00 PM.

Student number: 4609549
Project duration: June, 2023 – May, 2024
Thesis committee:

Prof. dr. ir. P. Bauer,	TU Delft, Coordinator
Dr. ir. G. R. Chandra Mouli,	Assistant Professor TU Delft
Dr. S. H. Tindemans,	Assistant Professor TU Delft

This thesis is confidential and cannot be made public until May 24, 2024.

TU Delft

Acknowledgements

I would like to extent my deepest gratitude to my thesis supervisor Nikolaos Damianakis, who worked long days (and sometimes nights) to solve the countless bugs that arose from the programming, when I could no more. His positive attitude and abundant knowledge of various topics resulted in long sparring sessions, taking up most of the progress meetings which gave me new energy to progress. Furthermore, I want to express my gratitude to Gautham Chandra Mouli for his support, guidance, and insightful contributions during our monthly meetings, which I was always looking forward for. Also, special thanks to Prof.dr.ir.Pavol Bauer for offering me the opportunity to conduct my thesis at the DCE&S department. In addition, a big thanks to Robert Bansco who enriched my knowledge on the energy market with his, without asking anything in return. This thesis would not have been possible without my family and the collective support and encouragement of each individual mentioned and many others who, although not named, have contributed immensely to my academic journey. Thank you.

S.A.M. Warmerdam
Delft, May 2024

Abstract

This study explores the integration of diverse flexible assets, including electric vehicles (EVs), stationary battery energy storage (BESS), heat-pumps and photovoltaics, into a localised smart grid to enhance aFRR ancillary service provision and lower overall grid costs. The performance of the grid was evaluated by simulating and analysing various loads, including residential and commercial building heating, EV charging profiles, as well as photovoltaic generation and battery energy storage. This analysis covered six cases across different seasons and years, with each case assessed over a one-day period. Within the grid, three different nodes are analysed; a Residential, Commercial and Mixed node, all with different power consumption and behaviour profiles differentiating between the seasons. The findings demonstrate the potential of EVs to deliver a significant amount of aFRR ancillary power, while still satisfying minimum state of charge requirements set by vehicle owners. Utilising both BESS and EVs in aFRR results in substantial grid cost savings and, in some years, potential profits. However, participation in aFRR services results in a higher average cost for imported energy (without taking into account aFRR revenue). This rise is attributed to maintaining sufficient capacity for aFRR provision, where the revenue per unit of energy is generally higher. The combination of vehicle-to-grid and BESS-to-grid without aFRR provision showed the lowest cost of imported energy, since here only day-ahead prices are used to optimise load scheduling. In addition, operating a localised grid with regards to imbalance prices can result in 80-160% portfolio savings for balancing responsible parties (BRPs), due to the concept of passive balancing, where the combination of EV and BESS showed to be most promising. The research contributes to the field by providing an insight and potential framework to leverage flexible assets in both commercial and residential smart grid environments, showcasing a significant step toward sustainable energy management, taking into account the perspective of multiple market parties.

Abbreviations

1SHOT One-shot optimization,

ACE Automatic Control Error,

ACH Air Changes per Hour,

AC Alternating Current,

aFRR Automatic Frequency Restoration Reserve,

ASHP Air-Sourced Heat Pump,

BAR Bid Acceptance Rate,

BEP Balancing Energy Price,

BESS Battery Energy Storage Systems,

BEV Battery Electric Vehicle,

BRPs Balancing Responsible Parties,

BSPs Balancing Service Providers,

CCCV Constant Current-Constant Voltage,

CHP Combined heat and power,

CoP Coefficient of Performance,

DC Direct Current,

DHW Domestic Hot Water,

DoD Depth of Discharge,

EMS Energy Management Systems,

ENTSO-E European Network of Transmission System Operators for Electricity,

ESS Energy Storage Systems,

EU European Union,

EV Electric Vehicle,

FCR Frequency Containment Reserve,

FCEV Fuel Cell Electric Vehicle,

FES Flywheel Energy Storage,

HESS Hybrid Energy Storage Systems,

HP Heat Pump,

IL Interruptible Load,

IP Imbalance Price,

ISP Imbalance Settlement Period,

KW Kilowatt,

KWP Kilowatt peak,

LFC Load Frequency Control,

LFP Lithium Ferrophosphate,

MCS Monte-Carlo Simulation,

mFRRda Manual Frequency Restoration Reserve directly activated,

MPP Maximum Power Point,

PHEV Plug-in Hybrid Electric Vehicle,

PHS Pumped Hydro Storage,

PSB Polysulfide Bromide,

PV SFC Photovoltaic Self-Consumption,

RES Renewable Energy Sources,

RHO Rolling Horizon Optimisation,

SC Smart Charging,

SCES Supercapacitor Energy Storage,

SoC State of Charge,

TSO Transmission System Operator,

UTC Coordinated Universal Time,

V2G Vehicle-to-Grid,

VRB Vanadium Redox Battery

Contents

List of Figures

List of Tables

1

Introduction

The electricity grid is full! Or not? The rapid electrification of the grid poses great challenges for future energy management. Residential heating, transportation and intermittent renewable energy sources (RES) pose an increasingly heavy burden on existing power lines. So much so, that some areas of the Netherlands are no longer able to accept new businesses onto the grid, simply because there is no space; the grid is congested. The grid is in desperate need of efficient power management.

The European Union has set ambitious renewable energy targets under its REPowerEU program, aiming for a 42.5% share of renewable energy by 2030, which would almost double the existing share of renewable energy in the EU (European Commission, 2023a). These targets are part of a broader

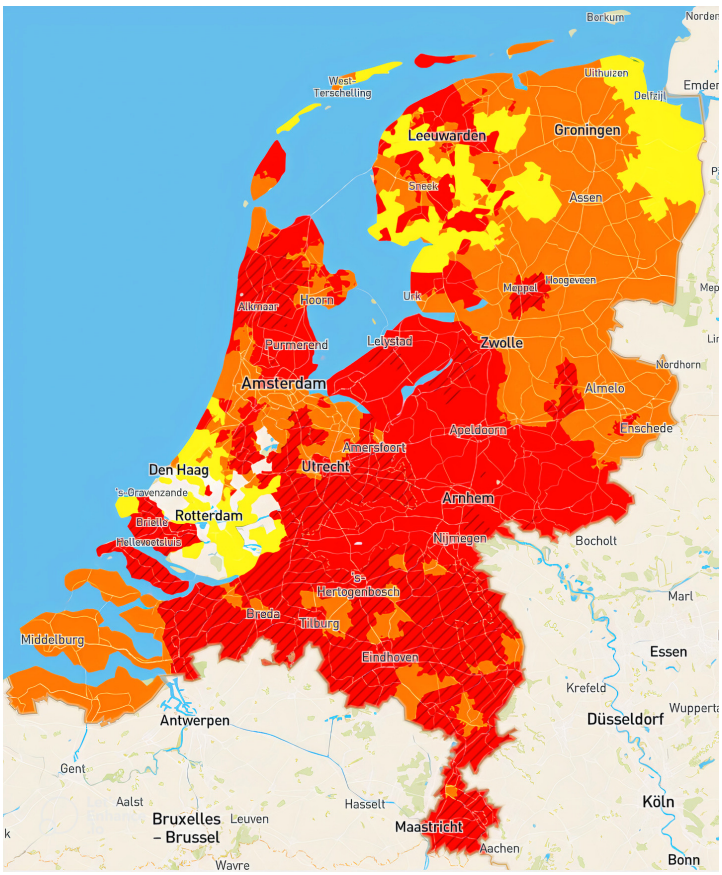

Figure 1.0.1: The national grid capacity map of the Netherlands. Transparent: transport capacity available; Yellow: limited capacity; Orange: none currently available (in research); Red: none available; Red arched: congestion management limits reached. Image reprinted from Netbeheer Nederland, 2023a.

strategy, the European Green Deal, to reduce greenhouse gas emissions by at least 55% from 1990 levels within the same time frame. The push for increased renewable energy production is a direct response to climate change and is facilitated by substantial investments in wind, solar, and other renewable technologies across member states (European Commission, 2023b).

As a result, the penetration of photovoltaic (PV) systems has increased drastically as can be seen in Figure 1.0.2, further increasing grid pressure. Lately, local authorities have been urging rooftop owners to adopt solar energy solutions. Starting in 2024, municipalities will even have the authority to enforce the installation of solar panels on large utility roofs exceeding 250 square meters, which is advised to happen parallel to the creation of effective policies on the electrification of industry, mobility, and heating (SolarPower Europe, 2023). Together with an increase in the total share of EVs among all passenger cars, rising from 1.63% to 7.3% as displayed in Figure 1.0.3, the electrification continues faster than the grid can handle, causing congestion. Recent numbers highlight the congestion issues on the Dutch grid. For instance, in 2023 the Dutch grid operator had 5600 requests for an electricity connection on a waiting list (Netbeheer Nederland, 2024), resulting in significant delays in connecting new businesses and residential developments to the electricity grid. In 2024 this number increased to 9400 requests for regular charging connections, and an additional 10.000 for connections suitable for discharging (Netbeheer Nederland, 2023b). This congestion, largely driven by rapid electrification, has pushed the existing infrastructure to its limits, necessitating immediate and innovative solutions to enhance grid capacity and efficiency. Figure 1.0.1 displays the capacity map of the electricity grid of the Netherlands. The figure serves as a tool for new companies to ascertain whether there is capacity available for constructing new offices or factories. It clearly indicates the amount of stress that is currently placed on the grid, potentially limiting economic growth.

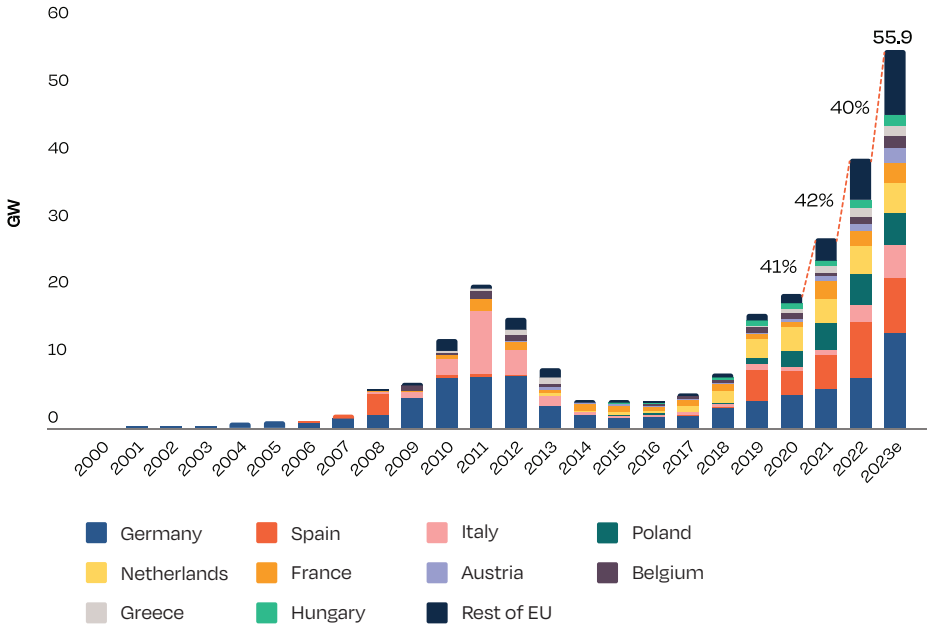

Figure 1.0.2: EU annual PV installed capacity 2000-2023. Reprinted from SolarPower Europe, 2023.

Luckily, the transition in energy production is well on its way, with 48% of all produced energy in the Netherlands being from renewables, see Figure 1.0.4. However, renewable energy production is characterised by intermittency, which refers to the (un)predictable fluctuations in the availability and reliability of renewable energy sources, such as solar and wind power. The increased RES penetration has created a grid imbalance due to a mismatch between generation and consumption profiles, sometimes leading to negative energy prices. Ancillary services are therefore put in place to resolve short- or long-term power imbalances by injecting or subtracting balancing energy from or to flexible energy storage facilities, such as large-scale batteries.

The increase in battery presence within the Dutch grid, shown by battery operators comprising 243

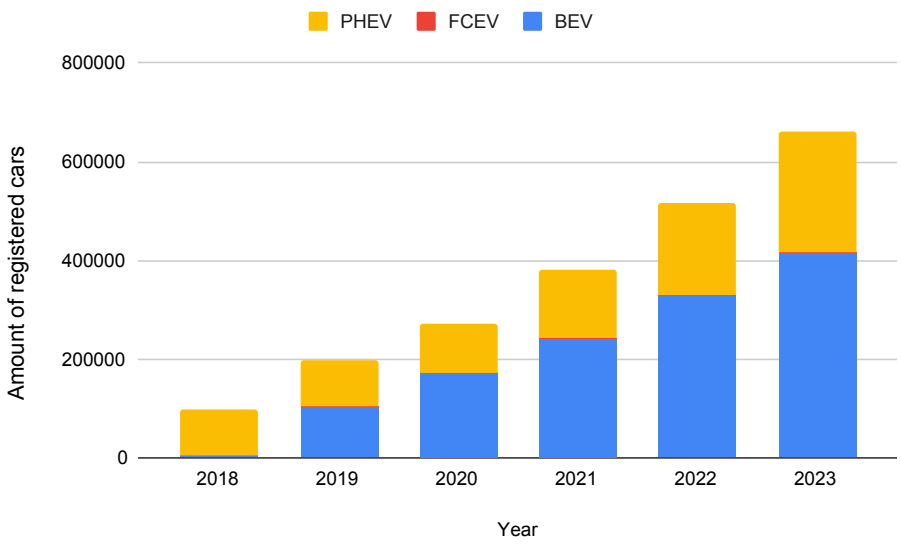

Figure 1.0.3: The amount of registered EV passenger cars in the Netherlands over time. BEV; Battery Electric Vehicle, FCEV; Fuel Cell Electric Vehicle, PHEV; Plug-in Hybrid Electric Vehicle. Data retrieved from Rijksdienst voor Ondernemend Nederland (RVO), 2023.

out of 375 high-voltage connection requests in 2024 (Netbeheer Nederland, 2023b), is likely attributable to initiatives outlined in the National Energy and Climate plan. Notably, the call for the obligation of batteries in large-scale solar parks suggests a direct correlation between policy objectives and increased demand for battery integration (SolarPower Europe, 2023). Furthermore, an increase in RES penetration results in an increase in seasonal intermittency, where the solar yield can be up to 10 times higher during a clear summer's day compared to a bleak winter's day (CBS News, 2024a).

Due to these challenges, the deployment of Energy Management Systems (EMS) become increasingly important. By coordinating the flow of electricity from different sources, an EMS can dynamically match supply with demand patterns. This not only relieves the grid from stress, it also harnesses the full potential of renewable energy sources, possibly turning the challenge of intermittency into a potential for grid resilience. In addition, an EMS can integrate 'smart loads' such as heat pumps and electric vehicles, effectively transforming them from energy consumers to participants in grid stabilisation. This shift not only ensures a reliable energy supply to meet increasing demands but also opens up opportunities for significant cost savings. This paper investigates the effects of different combinations of smart loads and battery storage on the total energy costs and the participation in ancillary services of a localised smart grid. By doing so, we might find that grid congestion can be avoided by a more efficient use of the grid.

This study focuses on the selection and analysis of suitable energy storage solutions for integration into energy management systems, incorporating components like photovoltaics, heat pumps, electric vehicles, and active participation in the automatic frequency restoration reserve (aFRR). We conduct multiple case studies to explore the synergies between smart loads and energy storage systems, examining the effects on energy costs and aFRR participation across different scenarios. These scenarios consider both the presence and absence of stationary Battery Energy Storage Systems (BESS) and electric vehicle (EV) contributions to aFRR. Additionally, this thesis delves into the seasonal and grid configuration impacts on aFRR participation and overall grid activity, with simulations carried out during both winter and summer seasons across various grid configurations including residential, commercial, and mixed nodes. Furthermore, we assess the influence of user behaviour, specifically analysing EV charging schedules and building occupation profiles, to understand their implications on aFRR market participation and the optimization of modern smart grids. This examination aims to highlight critical insights and create a deeper understanding of integrating energy storage solutions within complex energy systems.

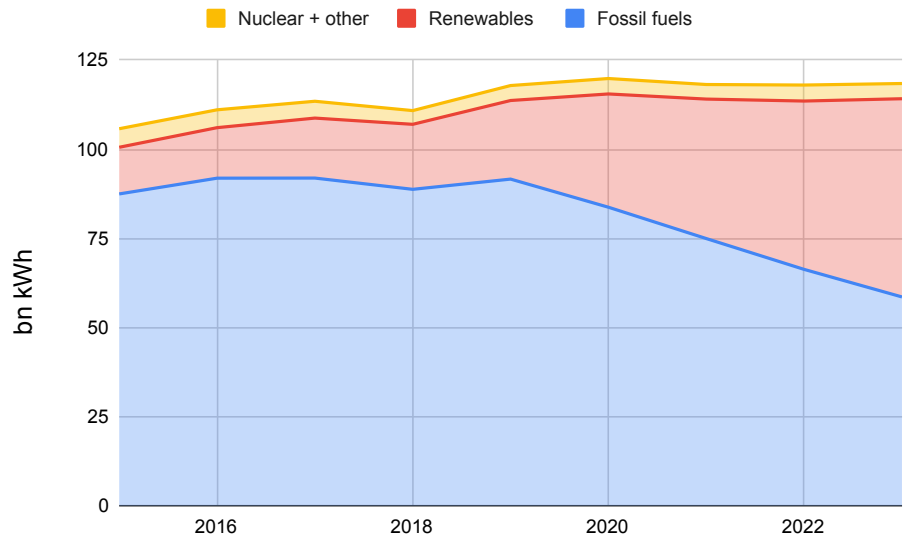

Figure 1.0.4: Dutch electricity production by source. Reprinted from CBS News, 2024b.

1.1. Thesis Organisation

Following the abstract and introduction, this document begins with Chapter 3: Ancillary Market Structure. This chapter provides a comprehensive overview of the ancillary energy market structure, focusing on the key players and their roles, as well as the operational mechanisms of different balancing markets. It highlights how Balancing Responsible Parties manage their energy portfolios to minimise grid imbalances and the financial implications of failing to adhere to their energy programs. The chapter then addresses the specifics of various balancing markets, such as Frequency Containment Reserves, automated Frequency Restoration Reserves, and manual Frequency Restoration Reserves. Next, Chapter 4: Literature Review provides a comprehensive overview of energy storage technologies, including both non-hybrid systems like BESS, PHS, FES, and hybrid systems that combine BESS with SCES. It explores their integration into smart grids to address the challenges posed by renewable energy sources, emphasising the selection of appropriate technologies based on specific grid needs. The chapter also introduces innovative approaches such as using electric vehicles for grid support through Vehicle-to-Grid strategies and the potential of controllable HVAC systems to enhance grid flexibility. In Chapter 5: MIP formulation, the mixed integer programming model is introduced. This model gives the equations and constraints that form both local and nodal power balances, which are needed to simulate the localised smart grid discussed in Chapter 4. The chapter aims to present a detailed view of energy management and distribution within the smart grid and the roles of various grid components. Chapter 6 outlines the data inputs and case studies for the grid model optimisation, focusing on residential, commercial and mixed nodes, each with a distinct set of buildings and chargers. The optimisation uses three input models; a PV, an EV and an HP and a building occupation model. Subsequently, Chapter 7 gives the optimisation results of each case study. It analyses the outcomes of various grid configurations, focusing on the synergy of different asset configurations and their effect on the cost of energy and ancillary market participation. Finally, Chapter 8 will discuss and conclude all findings and present recommendations for future research.

2

Ancillary Market Structure

This chapter provides an overview of the ancillary energy market, focusing on the key roles played by different market entities and the functioning of various balancing markets. We start by examining the roles of Balancing Responsible Parties (BRPs), Balancing Service Providers (BSPs), and the Transmission System Operator (TSO). This section explains how these entities interact to maintain grid balance, with a specific look at how BRPs manage energy imbalances within their portfolios through trading.

Further on, we explore different balancing markets, including Frequency Containment Reserves (FCR), automated Frequency Restoration Reserves (aFRR), and manual Frequency Restoration Reserves (mFRR). Each market is described in terms of its purpose and operation, highlighting how the TSO procures and activates balancing capacity. Extra attention is given to the aFRR market, detailing the process of bid submission, ranking, and activation in response to grid imbalances. The chapter wraps up with a practical look at the methodologies the TSO uses for activating aFRR energy bids, such as the merit order and pro-rata approach. Overall, this chapter aims to provide a clear and concise understanding of how different market players contribute to the stability of the power grid and the operational mechanisms that underpin the ancillary energy market.

2.1. Market Parties

There are three main types of energy market roles: Balancing Responsible Parties (BRPs), Balancing Service Providers and the Transmission System Operator (TSO) (Tennet, 2023d) .

2.1.1. Balancing Responsible Party (BRP)

A BRP collects a portfolio of suppliers and users and is financially responsible for any imbalance present in the portfolio. Since every supplier, user or trader of energy can cause an imbalance on the grid, each party is bound to a BRP. The BRP can keep its portfolio in balance by buying and selling energy from and to other market parties. The BRP communicates these transactions to the local network operator who, in turn, passes it on to the national TSO. The sum of these transactions is called an energy program, or ”E-program”, and is a daily process (Tennet, 2023a). Not adhering to its E-program means a BRP is in imbalance. The BRP is thus defined as the entity that, in principle, bears the imbalance on its connections by measuring the difference between the nomination by Tennet (E-program) and the allocation (measured values by the metering company) (Tennet, 2023d).

This difference is measured in blocks of 15 minutes, which is called an imbalance settlement period (ISP) (TenneT, 2022c). Within an ISP, a BRP can reduce or even solve its portfolio imbalance by trading its imbalance with another BRP. If these imbalances are opposite from each other, BRPs can trade their imbalance without financial consequences and without interference from the TSO (Next Kraftwerke, 2023). This process is visualised in Figure 2.1.1a-2.1.1b. Here, the grid is actually in balance, since the sum of all imbalances is zero meaning no other balancing services need to be used. This is referred to as ”Regulation state 0” (TenneT TSO B.V. (2022)). When imbalances still remain, ancillary power must be activated, as shown in Figure 2.1.3.

Each minute, TenneT publishes the amount of grid imbalance, together with the balancing energy price (BEP) when the grid imbalance is non-zero (Tennet TSO, 2023). Instead of trading its portfolio

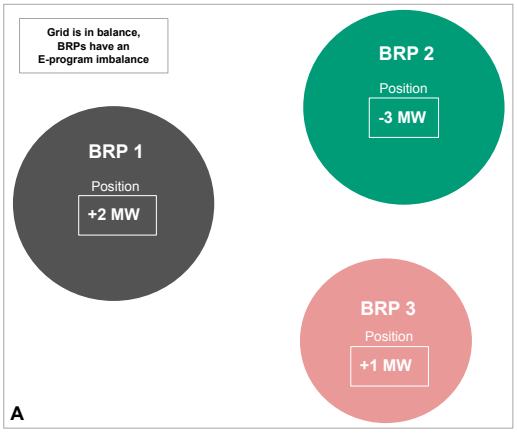

(a) Grid in balance

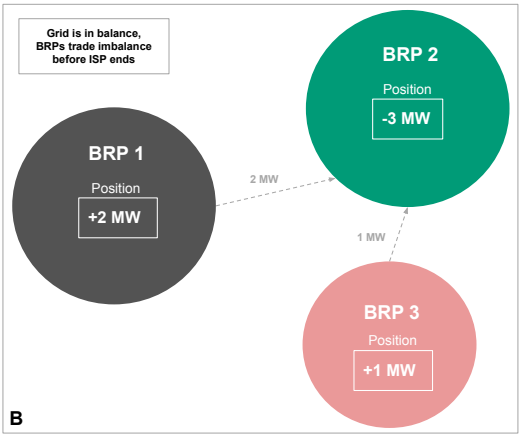

(b) E-program imbalance trading

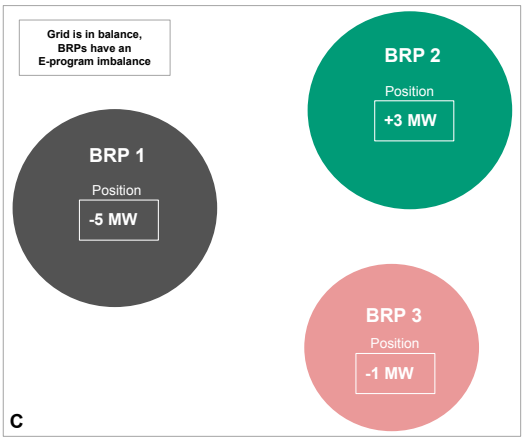

(c) Grid in imbalance

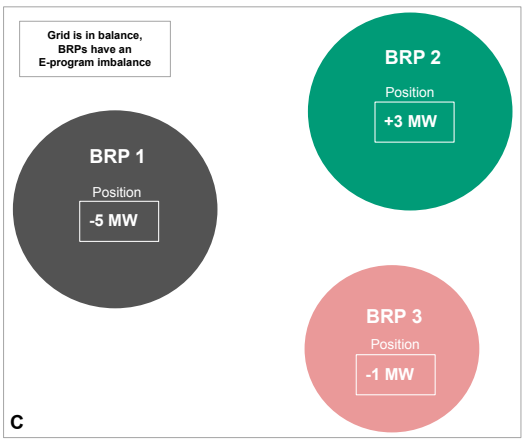

(d) Passive balancing

Figure 2.1.1: Two market situations; A-B: Imbalance Trading, B-C: Passive Balancing

imbalance, a BRP can deliberately keep or create an imbalance in its portfolio opposite from the grid imbalance, hereby reducing the grid frequency deviation. This is called ”passive balancing”, see Figure 2.1.1c-2.1.1d (Tennet, 2023b). For this service, the BRP can be remunerated against the Imbalance Price (IP), which is the highest accepted BEP during the ISP, if the total portfolio imbalance at the end of the ISP was indeed opposite to that of the grid. On the contrary, if the portfolio imbalance is not opposite from the grid imbalance, the BRP needs to pay the product of its total portfolio imbalance times the imbalance price to the TSO, because it is in fact causing a grid imbalance by not adhering to its E-program (TenneT, 2022b). When a BRP introduces flexibility in its portfolio, passive balancing can add up to significant savings (Franz and Röben, 2020).

To determine the IP, Tennet first determines the balancing energy price (BEP) through an automatic Frequency Restoration Reserve (aFRR) (both contracted and voluntary) merit order list, see Figure 2.3.2. To determine the BEP, we need to make a clear distinction between the four regulation states (TenneT TSO B.V. (2022)):

- Regulation state 0: no balancing energy is activated; the grid is in balance.
- Regulation state -1: balancing energy is activated in the downward direction only; the grid is in surplus.
- Regulation state +1: balancing energy is activated in the upward direction only; the grid is in shortage
- When balancing energy is activated in both upward and downward directions, the regulation state is determined by the balance delta:

Balancing Energy Price (Minute Data)

Date	Min	Time	Amount	BEP UP [EUR/MWh]	BEP DOWN [EUR/MWh]
10/30/2023	61	01:00	0	0	0
10/30/2023	62	01:01	0	0	0
10/30/2023	63	01:02	0	0	0
10/30/2023	64	01:03	0	0	0
10/30/2023	65	01:04	0	0	0
10/30/2023	66	01:05	0	0	0
10/30/2023	67	01:06	0	0	0
10/30/2023	68	01:07	0	0	0
10/30/2023	69	01:08	1	88,97	0
10/30/2023	70	01:09	6	88,97	0
10/30/2023	71	01:10	18	101,7	0
10/30/2023	72	01:11	36	106,71	0
10/30/2023	73	01:12	60	107,05	0
10/30/2023	74	01:13	82	107,05	0
10/30/2023	75	01:14	85	107,05	0

Imbalance Price (Per ISP)

Date	ISP	Period	Regulation State	IP UP [EUR/MWh]	IP DOWN [EUR/MWh]
10/30/2023	1	00:00 - 00:15	1	100,98	23,00
10/30/2023	2	00:15 - 00:30	1	105,81	
10/30/2023	3	00:30 - 00:45	1	71,80	
10/30/2023	4	00:45 - 01:00	0		
10/30/2023	5	01:00 - 01:15	1	107,05	
10/30/2023	6	01:15 - 01:30	1	101,7	
10/30/2023	7	01:30 - 01:45	1	101,07	
10/30/2023	8	01:45 - 02:00	1	74,56	

Figure 2.1.2: Example of the determination of the imbalance price from the balancing energy price. The top table indicates the balancing energy price (BEP) as minute data. The bottom table represents the subsequent imbalance price (IP) per ISP arched in red, with the corresponding highest accepted BEP as IP. Data retrieved from Tennet TSO, 2023

- Regulation state 2: the balance delta does not consistently increase or consistently decrease; it fluctuates. Example of balance delta: [+3,-2,+1,-4, +1].
- Regulation state +1: the balance delta either remains the same or increases continuously but never decreases. Example of balance delta: [-2, -1, 0, +1, +1].
- Regulation state -1: the balance delta either remains the same or decreases continuously but never increases. Example of balance delta: [+2, +1, 0, -1, -1]
- Regulation state 0: the balance delta remains constant over time. Example of balance delta: [+1,-1,+1,-1,+1].

2.1.2. Balancing Service Providers (BSP)

When there is an imbalance between supply and demand, the TSO calls upon BSPs to help restore the grid balance. The BSP is the entity that offers balancing power in the form of a power bid against a certain price, independent from any portfolio (Tennet, 2023c). In the aFRR market, bids are placed per ISP and must be available for the full period (TenneT, 2022c). These bids are ranked from lowest to highest price, and are accepted and called according to the grid imbalance through a merit order (explained further in Paragraph 2.3. This merit order is closed on a minute-to-minute basis (TenneT, 2022b). The BSP gets remunerated by the TSO against the balancing energy price for the energy delivered during the ISP (**tennet2022c**).

An example of the IP that comes from the BEP is shown in Figure 2.1.2. A BRP can have a BSP in its portfolio to reduce its portfolio imbalance exposure. In return, the BSP can receive remuneration from the BRP in the form of a contract. In addition, a BSP can operate as a stand-alone entity and provide balancing energy directly to Tennet to either the FCR, aFRR or mFRRda market (TenneT, 2022c).

A positive upward price indicates that Tennet pays the BSP, and a negative upward price (which is practically non-existent (TenneT (2022c)) means the BSP pays Tennet for the delivered balancing energy. For downward bids, a positive price indicates that the BSP pays Tennet and a negative price that Tennet pays the BSP (TenneT, 2022b). Positive downward prices are common. While at first, it seems counterintuitive that a BSP would ever offer a positive price for downward ancillary power, one must realise that downward power can mean two things: using more energy, or producing less. For a gas power plant, the marginal production cost is, for example, 60 EUR/MWh. During regulation state

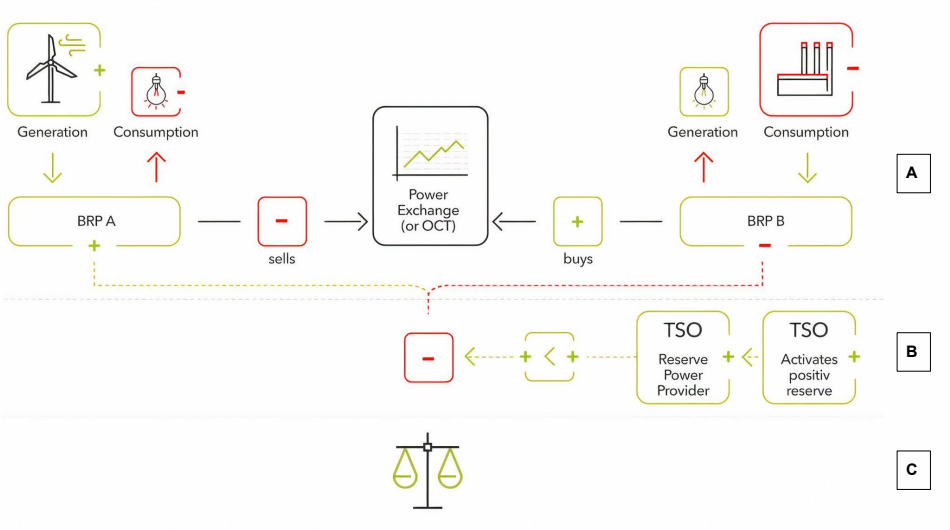

Figure 2.1.3: Process of imbalance trading of BRPs, and subsequent balancing by the TSO. Level A: Imbalance of single BRPs; Level B: Remaining system imbalance; Level C; System in balance. Adapted and Reprinted from Next Kraftwerke, 2023.

-1, the grid is in surplus. If the balancing energy price is 55 EUR/MWh, you are allowed to produce 1 MWh less while paying 55 EUR/MWh, while you save 60 EUR/MWh in production costs therefore profiting 5 euros.

For regulation states 0 and 2, the IP is set equal to the mid-price, which is the average of the lowest price of upward bids and the highest price of downward bids on the merit order list. For regulation states -1 and +1, the balancing energy price is used. Each minute, the BEP is set equal to the highest activated balancing energy bid during that minute. Once an ISP is over, the IP is determined by the highest BEP that occurred during that ISP.

2.2. Balancing Markets

Europe has three distinct balancing markets; FCR, aFRR and mFRRda. Each market has its own characteristics and purpose. FCR is the so-called ”first line of defence” and is activated first in response to a frequency deviation. For FCR, the TSOs across Europe collaboratively ensure that there is enough primary power reserve available (Rancilio et al. (2022)). This joint responsibility is governed by the European Network of Transmission System Operators for Electricity (ENTSO-E) (European Network of Transmission System Operators for Electricity (ENTSO-E), 2023). When, for example, a power plant in the Netherlands suddenly shuts down, Tennet measures the frequency deviation and concludes that FCR power is needed in its area. At this point, all European FCR assets could potentially be automatically activated through the ENTSO-E. If the frequency deviation persists, local aFRR assets will be activated after 30 seconds to restore the full European FCR capacity as soon as possible (TenneT, 2022a). Lastly, mFRRda (previously ”emergency power incident reserve”) is activated during larger and longer duration imbalances and can support the net frequency for hours (TenneT, 2023c).

	mFRRda	**aFRR**	**FCR**
Market Type	Asymmetrical	Asymmetrical	Symmetrical
Market size	954 MW	350 MW	110 MW
Response time	15 minutes	5 minutes	30 seconds
Min. Period	60 minutes	15 minutes	15 min - 4 hours
Min. Cap	1 MW	1 MW	1 MW
Remuneration	Reserved Capacity	Delivered energy + Reserved capacity	Reserved capacity

Table 2.2.1: Comparison of different market characteristics.

2.2.1. FCR - Frequency Containment Reserves

In the FCR ancillary service market (TenneT (2023a)), the daily auctions are divided into 4-hour blocks. If a participant bids a certain capacity, it means that they are committing to provide that capacity for the duration of the 4-hour block if their bid is accepted. Full activation of the contracted FCR lasting 15 minutes (or proportionally longer) is possible when the deviation is less than 200 mHz (TenneT (2022a)).

The term ”capacity market” refers to a system where payments are made for maintaining the available capacity to generate electricity or reduce demand. This is in contrast to an ”energy market” where payments are made for the actual energy produced or saved. The capacity market is designed to ensure that there is sufficient capacity available to meet the maximum demand, whereas the energy market is for the ongoing, routine supply and demand of electricity. The FCR is a capacity market since the focus is on the availability of capacity to respond to frequency deviations. In total, ENTSO-E requires 3000 MW (for both upward and downward reserves) which each local TSO is responsible for contributing (TenneT, 2023a). FCR providers are paid for the capacity they reserve for frequency containment, not for the actual energy activated. However, once activated, the energy delivered is typically compensated in the energy market or imbalance market at the prevailing prices. The FCR market requires BSPs to offer symmetric power bids, which means the offered power should be available in both upward and downward directions (TenneT, 2022a).

2.2.2. aFRR - automated Frequency Restoration Reserves

The aFRR is a market where BSPs offer balancing power to help maintain or restore the balance of the power grid (TenneT (2022c)). When the frequency of the grid deviates from the standard (usually 50 or 60 Hz), aFRR is automatically requested by Tennet and activated by the BSP to restore the frequency to its normal level (TenneT, 2022c). Tennet ensures the availability of the required minimum amount of aFRR by entering into contracts with BSPs. Under these contracts, the BSPs commit to offering at least the agreed volume of aFRR energy in their bids. The contracted aFRR power must be continuously available throughout the contract period, enabling Tennet to correct frequency deviations within 15 minutes. Additionally, prequalified BSPs can voluntarily offer their available aFRR capacity in what are known as ”free bids.” It is important to note that contracted aFRR bids do not receive priority over voluntary bids; the merit order list is established solely based on the price of the bids (TenneT, 2022c).

2.2.2.1. Contracted Energy Bids

Contracted energy bids represent obligations that BSPs must meet. They are required to submit aFRR energy bids for each Imbalance Settlement Period (ISP) of the day for which they have contracted capacity, ensuring the bid volume matches at least the contractual amount for both upward and/or downward adjustments. The deadline for modifying or submitting bids for contracted capacities is no later than 14:45 UTC+01:00 on the day before execution. If a BSP fails to submit an appropriate bid, Tennet reserves the right to place energy bids on behalf of the BSP at a price of 0 €/MWh for upward adjustments and the day-ahead market price for downward adjustments. BSPs receive compensation for the capacity they reserve under these contracts (TenneT, 2022c).

Figure 2.2.1: 200 MWh BEss FCR facility in Belgium. Image: Corsica Sole

Figure 2.2.2: FCR pilot using Honda EVs with bi-directional chargers. Image: Kraftwerke

2.2.2.2. Voluntary Energy Bids

Voluntary energy bids, on the other hand, are not obligatory and are at the discretion of the BSP. The window for submitting changed energy bids closes 2 full ISPs before the start of each ISP where aFRR power is or is not scheduled. The ability to change bids until t-30min of the moment of activation offers flexibility, but means a BSP does not get paid for the reserved capacity, only for the energy delivered. The earnings are thus less certain compared to contracted energy bids. The BSP sends an aFRR energy bid message for the entire day, where different energy bids can be indicated per ISP. An offered volume of 0 MW can only be offered at 0 €/MWh. Voluntary aFRR energy bids are sorted on price and placed on the merit order list together with contracted aFRR bids (TenneT, 2022c).

2.2.3. mFRRda - manual Frequency Restoration Reserves directly activated

mFRRda is a contract from 00:00 - 00:00 and cannot be changed during the day. The contract duration is in principle one calendar day and runs from 00:00 - 00:00. In special situations (e.g. solar eclipse), Tennet may decide to organize an additional auction for a shorter period. Within this contract period, the BSP must keep the contracted power available so that it can supply this power in case of an activation. The mFRRda market has the largest market size among the three markets. However, the longer minimum delivery period of 60 minutes (TenneT (2023c)) and the fixed contract duration of 24 hours may be limiting the asset flexibility.

Figure 2.2.3: Greenhouse facility in the Netherlands that can be used as mFRRda facility. Image: Formsma (2023)

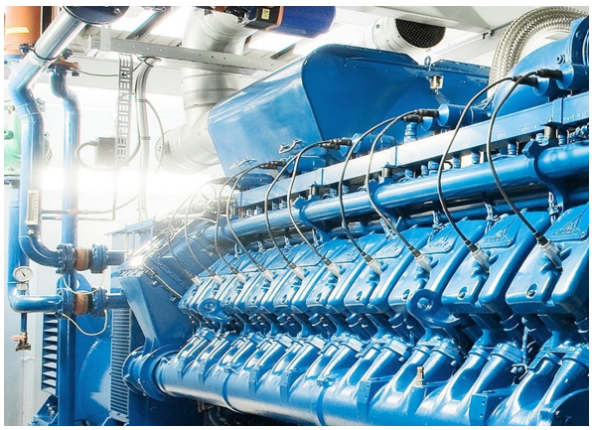

Figure 2.2.4: Combined heat and power (CHP) module, a typical mFRRda facility. Image: Formsma (2023)

2.3. Balancing Capacity Acquisition and Activation

Tennet buys balancing capacity to make sure that the supply and demand of energy can always be brought into equilibrium. As explained, there are three main balancing products; FCR, aFRR and mFRRda. BSPs that are contracted for FCR activate their power automatically based on the grid frequency. When aFRR power is needed, Tennet automatically requests BSPs to activate their power. BSPs must then respond with the requested power within a certain time frame. mFRR is manually activated by Tennet during long-term imbalances. BSPs that participate in FCR are paid a certain amount to have the agreed-upon capacity on standby and do not receive any extra remuneration for actual activation. Figure 2.3.1 shows an overview of this balancing process in time.

To activate aFRR energy bids, Tennet sends aFRR activation volumes, also known as 'delta setpoints', to the BSPs that have submitted these energy bids (TenneT, 2022c). Delta setpoints indicate the demanded aFRR volume, and the total amount of aFRR energy bids activated by the LFC is determined by the balance of the (national) grid balance. There are two ways Tennet may activate aFRR power; via a 'merit order', or via a 'pro-rata' approach. When there are no significant frequency deviations in the Dutch grid, energy bids are activated according to the merit order approach; the necessary adjustment is determined based on the observed system imbalance and activated from the lowest to the highest price. See Figure 2.3.2 for a visualisation. The pro-rata approach is applied only during very large and sudden grid frequency deviations, where the rate of balance delta surpasses a certain threshold set by Tennet. This results in the simultaneous activation of all energy bids to ensure the

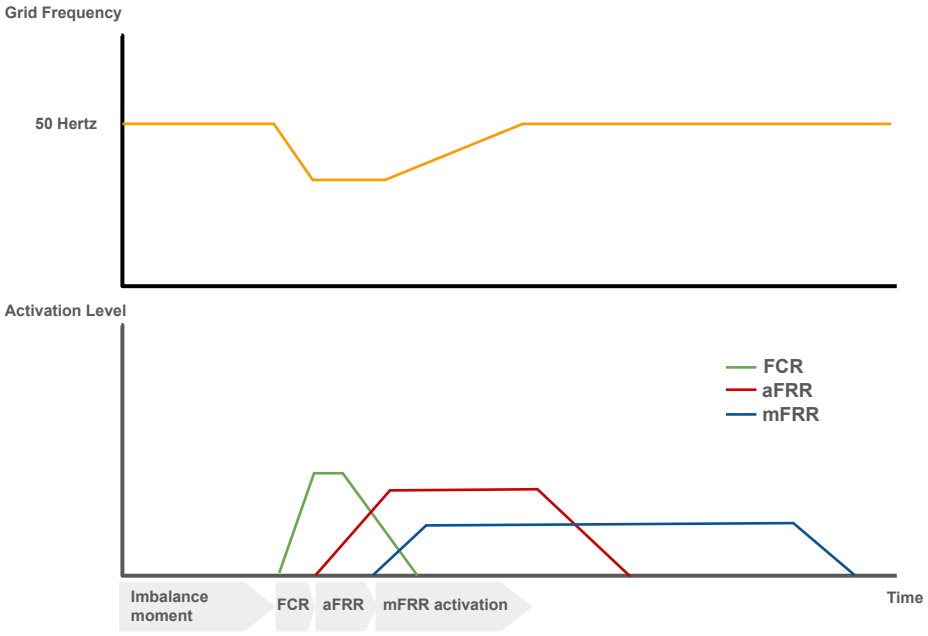

Figure 2.3.1: Overview of the balancing process. Adapted and Reprinted from Tennet (2023e)

maximum possible ramping rate of aFRR assets. This results in a merit-order-wide partial delivery of placed bids, resulting in a high balancing energy price. See Figure 2.3.3 for a visualisation.

Delta setpoints have some properties that are relevant when simulating with aFRR bids:

- Delta setpoints consist are integer and have a stepsize of 1MW
- A delta setpoint will not be more than the volume of the energy bid
- An energy bid can be partially or completely activated in the complete or in part of the ISP to which the energy bid applies
- The change in delta setpoint values will not be faster than the ramp rate of the registered asset. The BSP specifies the ramp rate in its energy bid, which must be at least 20% of the offered capacity, resulting in a maximum ramp rate of 5 minutes.

From the market structure, it becomes evident that one needs either power production assets or introduce the potential for flexibility into the grid to be able to reduce or increase demand at favourable times. Energy storage has proven to be very useful for both scenarios, as it allows for storing excess energy when demand and prices are low and releasing it during high demand and high prices. This enhances grid stability and reliability and enables better integration of renewable energy sources, making energy storage a critical component in dynamic and responsive energy markets.

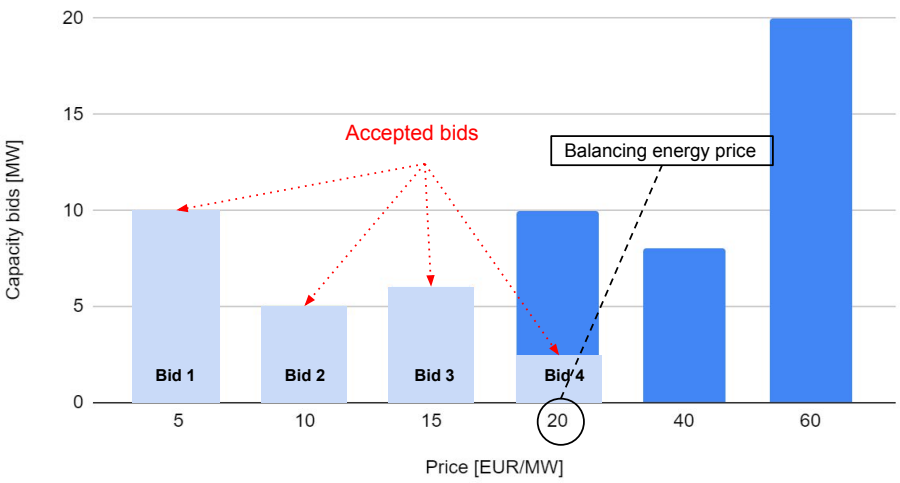

Figure 2.3.2: Regular merit order request example. Bids 1-3 are accepted for their full amount, and bid 4 receives a partial activation request, and sets the balancing energy price.

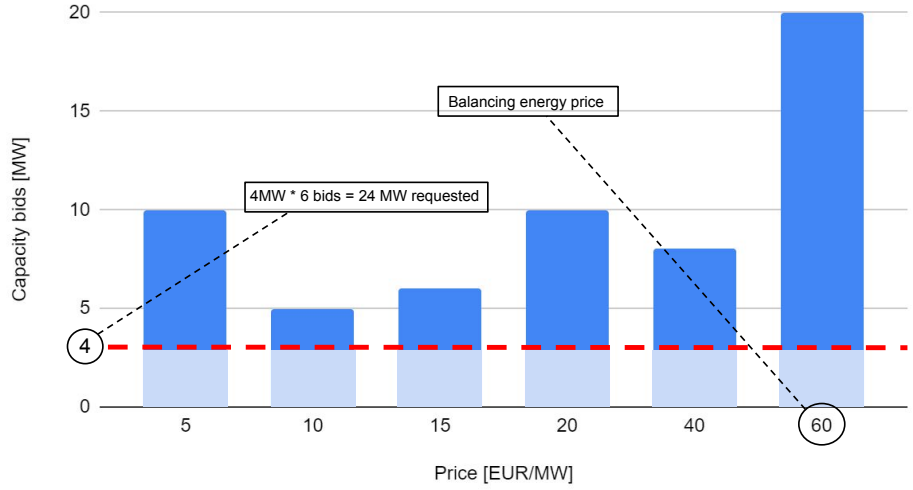

Figure 2.3.3: Pro-rata merit order request example. All bids are accepted in parallel to achieve the maximum ramping rate.

2.4. Passive Balancing

Passive balancing, as introduced in Paragraph 2.1, is the act of deliberately keeping or creating an imbalance in its portfolio opposite from the grid imbalance, hereby reducing the grid frequency deviation. With passive balancing, a BRP can receive remuneration from the TSO, if done correctly.

A BRP is in shortage when it injects less or uses more energy than initially stated in its E-program. A BRP is in surplus when it injects more or uses less than initially stated in its E-program (TenneT, 2022b). The obvious situation where a BRP can earn money is during regulation state +1 (the grid is in shortage), the BRP is in surplus (effectively solving imbalances) and the upward imbalance price is positive. On the contrary to the upward price, the downward price is regularly both positive and negative. During regulation state -1 (the grid is in surplus), a positive downward price indicates that BSPs are willing to pay the TSO money to produce less energy. If during this state a BRP is in shortage, it solves the imbalance but reduces the cash flow to the TSO. Therefore, the TSO sets the direction of payment from the BRP towards the TSO. However, when the downward price is negative, the TSO pays the BSPs for the delivery of balancing energy and wants the imbalance to be solved as quickly as possible, so the direction of payment is set from the TSO to the BRP. In addition, when the BRP is in surplus during regulation state -1 (effectively causing an imbalance), and the downward imbalance price is positive (BSPs pay the TSO), the BRP is rewarded. But, when the downward price is negative

(TSO pays BSP), the direction of payment is towards the TSO. Figure 2.1.2 gives an overview of the direction of payment during different regulation states and BRP positions.

During ISP with	Imbalance position BRP	Imbalance Price	Direction of payment
Regulation state +1	BRP shortage	P_{up} (+)	BRP → TSO
		P_{up} (-)	TSO → BRP
	BRP surplus	P_{up} (+)	TSO → BRP
		P_{up} (-)	BRP → TSO

During ISP with	Imbalance position BRP	Imbalance Price	Direction of payment
Regulation state -1	BRP shortage	P_{down} (+)	BRP → TSO
		P_{down} (-)	TSO → BRP
	BRP surplus	P_{down} (+)	TSO → BRP
		P_{down} (-)	BRP → TSO

Figure 2.4.1: Direction of payment for BRP imbalance positions. Adapted and reprinted from TenneT TSO B.V. (2022)

3

Literature Review

In this chapter, we explore a variety of energy storage technologies and their role in smart grids. We examine non-hybrid systems like BESS, PHS, and FES, alongside Hybrid Energy Storage Systems (HESS) that combine BESS and Supercapacitor Energy Storage (SCES). Our focus is on how these technologies perform across key metrics such as scalability, cycling ability, depth of discharge, efficiency, and application relevance. The discussion moves to the integration of these storage solutions within smart grids, particularly in balancing grids enriched with renewable energy sources. This review aims to provide insights into how different energy storage options can enhance grid stability, efficiency, and cost-effectiveness.

3.1. Energy Storage

This paragraph provides an overview of various non-hybrid energy storage technologies, including Battery Energy Storage Systems (BESS), Pumped Hydro Storage (PHS), and Flywheel Energy Storage (FES). These technologies offer distinct advantages and characteristics that make them suitable for a wide range of applications. Additionally, the chapter explores Hybrid Energy Storage Systems (HESS), which integrate Battery Energy Storage Systems (BESS) and Supercapacitor Energy Storage (SCES). HESS harnesses the strengths of various energy storage technologies to enhance performance, efficiency, and longevity. This paragraph offers a concise overview of these energy storage solutions, providing insights into their capabilities and applicability across diverse scenarios. In this part of the literature review, different energy storage systems will be evaluated based on seven categories. These categories are important in determining the adaptability, performance, and economic viability of energy storage technologies in various applications.

- **Scalability** addresses the adaptability of energy storage systems to the demands of their application, whether it is for residential use or large-scale purposes.
- **Cycling Ability** refers to the number of charge and discharge cycles a storage system can undergo before its capacity diminishes, indicating the system's durability and long-term reliability.
- **Depth of Discharge (DoD)** is a measure of how much energy can be used from a storage system relative to its total capacity, impacting both the efficiency and lifespan of the system.
- **Efficiency** quantifies the proportion of energy that can be retrieved from storage compared to the energy input, highlighting the operational effectiveness of the storage solution.
- **Application** considers the main applications the technology is or can be used for. Qualities that determine this are; response time and energy density. In addition, the practical aspects of maintaining the storage system, influencing its overall cost, are considered.

These categories will form the basis of the comparative analysis, providing a complete overview of each energy storage technology's strengths and limitations within the current energy landscape.

3.1.1. Non-Hybrid Storage Technologies

3.1.1.1. Battery Energy Storage Systems

Battery storage is one of the most common and versatile forms of energy storage. It involves the use of rechargeable batteries, such as lithium-ion, lead-acid, or flow batteries, to store electrical energy. BESS can be deployed at various scales, from residential to utility-scale, and are highly suitable for integrating with PV production, managing EV charging, and providing ancillary services due to their fast response times, high efficiency, and modularity (Killer et al., 2020).

- **Scalability**: Battery systems are highly scalable due to their modularity. You can increase or decrease the power output by adding or removing battery modules. This scalability allows for a high degree of flexibility in terms of adjusting the system's capacity to meet changing demand or supply conditions.
- **Cycling Ability**: Lithium ferrophosphate (LFP) batteries have a cycle life of up to 10.000 cycles (Chen et al., 2009). The ability to partially charge and discharge multiple times per day and still reach a lifetime of around 5-15 years (Behabtu et al., 2020) is advantageous for grid optimisation.
- **Depth of Discharge**: The battery's lifespan is strongly influenced by the DoD. For example, a three-fold improvement of the expected number of equivalent full cycles before the capacity drops below 80% can be seen when going from 100% DoD to 50% DoD cycling in LFP batteries (Guena and Leblanc, 2006). This means that, potentially, a large proportion of the stored energy can be used in critical situations, while a more conservative approach can be implemented in the battery management system during moments of low demand to extend the system's lifetime.
- **Efficiency**: Battery systems have high round-trip efficiencies, as high as 97% (Behabtu et al., 2020), meaning that most of the energy that is stored can be effectively used.
- **Application**: Batteries offer energy management capabilities, such as voltage support, smoothing RES fluctuations, emergency backup power, peak-shaving and load levelling (Luo et al., 2015). Considering the compact size and weight of the system, the complexity of the installation process, and low maintenance, BESS offer an almost plug-and-play structure. Batteries can be monitored remotely and only require yearly maintenance. In addition, BESSs are barely limited by topographic constraints, except for extreme temperatures. Li-Ion BESSs typically have a response time of milliseconds (Behabtu et al., 2020).

In the structure of a lithium-ion battery, which includes an anode, cathode, and electrolyte as illustrated in Figure 3.1.2, the process of charging involves lithium ions moving from the cathode to the anode through the electrolyte. When discharging, these ions move in the opposite direction, from the anode back to the cathode. This movement of lithium ions is essential for converting chemical energy to electrical energy and for the storage of this energy within the battery. The effectiveness and storage capacity of lithium-ion batteries are therefore closely linked to the quality of the active materials used in the anodes and cathodes, as these materials are crucial for housing and managing the lithium ions. Lithium iron phosphate is a popular cathode material due to its relatively low cost, high discharge potential, large specific capacity, good thermal stability and high cycling performance (Toprakci et al., 2010).

Characteristic	Specification
Power Range	0-100 MW[a]
Energy Density	200 - 500 Wh/l[b,c]
Power Density	500 - 2000 W/l[c]
Power costs	900-4000 $/kW[a]
Energy costs	600-3800 $/kWh[a]
Response rate	milliseconds

Table 3.1.1: Specifications of Li-ion BESS. References: [a]Das et al. (2018), [b]Chen et al. (2009), [c]Aneke and Wang (2016).

Figure 3.1.1: Example of 3.9 kWh BESS. Image: Tesla, Inc. (Accessed 2024)

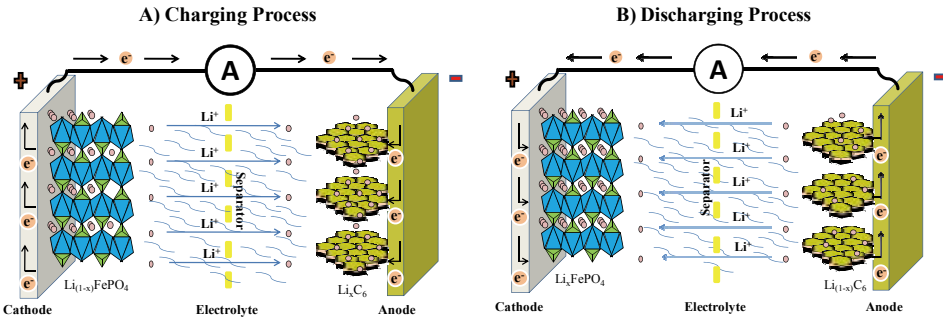

Figure 3.1.2: Schematic overview of the energy management system of one node. Image reprinted from Toprakci et al., 2010.

3.1.1.2. Pumped Hydroelectric Storage (PHS)

Pumped Hydroelectric Storage (PHS) refers to the method of energy storage that involves pumping water from a low reservoir to a higher reservoir using excess electricity and releasing the stored water through turbines to generate electricity during periods of high demand. PHS systems offer high energy capacity and long-duration storage (Behabtu et al., 2020).

- **Scalability** : PHS has a very high power range, making it more suitable for large-scale power management applications. PHS is able to discharge for hours to days. In addition, PHS is very dependent on topographical conditions and requires large land use (Behabtu et al., 2020). PHS plants have long construction times and require high capital investment (Luo et al., 2015).
- **Cycling Ability** : With an average lifetime of 50 years, PHS is meant to be a long-term solution (Behabtu et al., 2020).
- **Depth of Discharge** : PHS systems can achieve a depth of discharge (DoD) of up to 95%, resulting in potential continuous discharge for multiple hours until days (Kaldellis, 2015).
- **Efficiency** : Some PHS systems offer high efficiency of up to 87% (Behabtu et al., 2020).
- **Application** : PHS can be integrated with RESs. However, due to the slow response time, the technique is not suitable to smooth out short-term wind or solar fluctuations, since it typically has a response rate of minutes (Behabtu et al., 2020). PHS can be used in applications such as; load levelling (balancing fluctuations associated with electricity demand), seasonal energy storage and standing reserve (Luo et al., 2015).

Characteristic	Specification
Power Range	100-5000 MW[a]
Energy Density	0.5 - 1.5 Wh/L[a]
Power Density	0.5 - 1.5 W/L[a]
Power costs	2500 - 4300 $/kW[a]
Energy costs	5-100 $/kWh[b]
Response rate	Minutes

Table 3.1.2: Specifications of PHS. References: [a]Luo et al. (2015), [b]Chen et al. (2009).

Figure 3.1.3: Example of a 152 MW pumped hydroelectric storage facility Koepchenwerk, Germany. Image reprinted from Entura (2016)

3.1.1.3. Flywheel Energy Storage (FES)

Flywheel Energy Storage (FES) systems store energy in a rotating mass (flywheel) by converting electricity into kinetic energy. The stored energy can be converted back to electricity when needed. Flywheels offer rapid response times and high cycling capabilities, making them suitable for providing short-term grid stabilisation and frequency regulation services.

- **Scalability** : FES systems can be connected modularly to scale up both power and capacity. However, flywheels are often not used as a standalone backup facility due to their high self-discharge rate but interoperate with other energy storage types such as batteries or diesel generators (Luo et al., 2015).
- **Cycling Ability**: Flywheels can undergo a large number of cycles without significant degradation. The typical lifetime is around 15 years (Behabtu et al., 2020). This makes them well-suited for applications that require frequent charge-discharge cycles, such as grid frequency regulation.
- **Depth of Discharge**: Flywheels have no DoD effects giving freedom to charge/discharge cycle management. The DoD typically lies around 75-80% (Kaldellis, 2015).
- **Efficiency** : The round-trip efficiency of FES systems can be high, often in the range of 90-95%. Energy losses in FES systems primarily come from mechanical friction and air resistance. With a daily self-discharge rate of up to 100% (compared to 0.3% for lithium batteries), FES is meant for short-term energy storage only. This characteristic makes it difficult to use FES for day-ahead ancillary services since the energy delivered is often charged hours before the actual moment of delivery.
- **Application** : Flywheels can provide services like frequency regulation, voltage support, and smoothing power fluctuations. They are mainly used for wind energy storage purposes (Behabtu et al., 2020). FES is particularly good at providing rapid short-term power, due to their ability to quickly discharge their stored energy. FES can react to changes in power demand within milliseconds, faster than most other forms of energy storage. This makes flywheels excellent for applications requiring immediate response. Once installed, they require minimal maintenance (Luo et al., 2015).

Characteristic	Specification
Energy Density	5 - 100 Wh/kg[a]
Power Density	1000-2000 W/l[b]
Power Cost	250-350 $/kWh[b]
Energy Cost	1000-5000 $/kWh[b]
Response rate	seconds[c]
Discharge duration	15 s - 15 min[d]

Table 3.1.3: Specifications of flywheel energy storage systems. References: [a]Hadjipaschalis et al. (2009), [b]Chen et al. (2009), [c]Luo et al. (2015), [d]International Renewable Energy Agency (2012).

Figure 3.1.4: Example of 300 kW flywheel energy storage system. Image reprinted from “ABB Brochure” (Publication date unavailable)

3.1.2. Hybrid Storage Technology

3.1.2.1. Battery Energy Storage and Supercapacitor

Integrating batteries with supercapacitors can enhance the performance of a BESS in terms of power density and rapid charge/discharge capabilities. Firstly, let us look at the characteristics of Supercapacitor Energy Storage (SCES) only. Supercapacitors can provide short-duration high-power bursts,

complementing the energy storage capacity of batteries. SCES systems have a long lifetime, high cycle efficiency, high power density, and a very fast response time. In addition, SCES is not negatively affected by DoD and requires almost no maintenance. However, SCES has a high self-discharge rate (5-40% per day) (Behabtu et al., 2020), making the technology suitable for short-term energy storage only. The fusion of BESS and SCES results in a combination known as Hybrid Energy Storage Systems (HESS). HESS offers three primary advantages, as explained by Bocklisch (2015). HESS separates energy and power by introducing two distinct energy storage components, ES1 and ES2. ES1 is engineered to manage peak power demands (SCES), while ES2 is designed to accommodate more typical power requirements (BESS), thus enhancing cost-effectiveness. Secondly, HESS optimises overall system efficiency by fine-tuning ES2's operation at high-efficiency operating points and mitigating dynamic losses. Lastly, HESS extends the longevity and operational effectiveness of the storage system by optimising ES2's operation and reducing the dynamic stresses it encounters.

- **Scalability** : Hybrid systems demonstrate scalability similar to that of battery-only systems. The system's power capacity can be increased or decreased by adding or removing battery modules or supercapacitor units, enabling straightforward adaptation to different demand or supply conditions.
- **Cycling Ability** : Supercapacitors play a crucial role in extending the operational life of BESSs by sharing the load during high-power demand periods, thereby mitigating BESS ageing, as emphasised by Baek et al. (2021).
- **Depth of Discharge (DoD)** : As discussed earlier, the DoD significantly influences the lifespan of the battery component in hybrid systems. By incorporating supercapacitors, the strain on batteries can be reduced during high-power events, ultimately increasing their lifespan. Consequently, the overall DoD of the BESS decreases. In addition, the DoD of supercapacitors has no impact on the system's lifetime, resulting in an overall increase in hybrid system longevity.
- **Efficiency**: The overall round-trip efficiency of a hybrid system depends on the efficiencies of its individual components and how they are integrated. Batteries typically boast high round-trip efficiencies, reaching up to 97%, and can store energy for extended periods with minimal self-discharge. Supercapacitors also offer high efficiencies, up to 98% (Behabtu et al., 2020), but are characterised by a relatively high self-discharge rate.
- **Application**: A Hybrid Energy Storage System (HESS) consisting of BESS and SCES components has proven to be well-suited for seamless integration with RES and other load-dependent systems, catering to short-term, mid-term, and long-term energy storage requirements. Both BESS and SCES components require minimal maintenance, simplifying their practical implementation and ongoing operation. In addition, both technologies offer nearly instantaneous response characteristics, enabling swift charge/discharge cycles and high-power output in response to dynamic demand changes.

Characteristic	Specification
Power Range	0 - 0.3 MW
Energy Density	10-30 Wh/L
Power Density	100,000+ W/L
Power Cost	100-300 $/kW[a]
Energy Cost	300-2000 $/kWh[a]
Response rate	Milliseconds[b]
Discharge duration	Milliseconds - 1 h[b]

Table 3.1.4: Specifications of Supercapacitor. References: [a]Chen et al. (2009), [b]Luo et al. (2015).

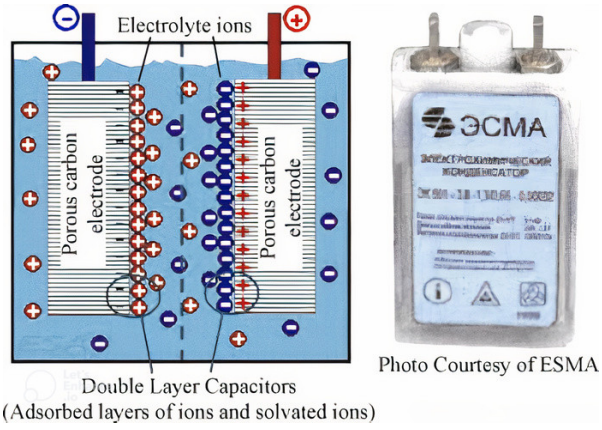

Figure 3.1.5: Schematic overview of a supercapacitor (left) and an example of a supercapacitor module (right). Image reprinted from Chen et al. (2009)

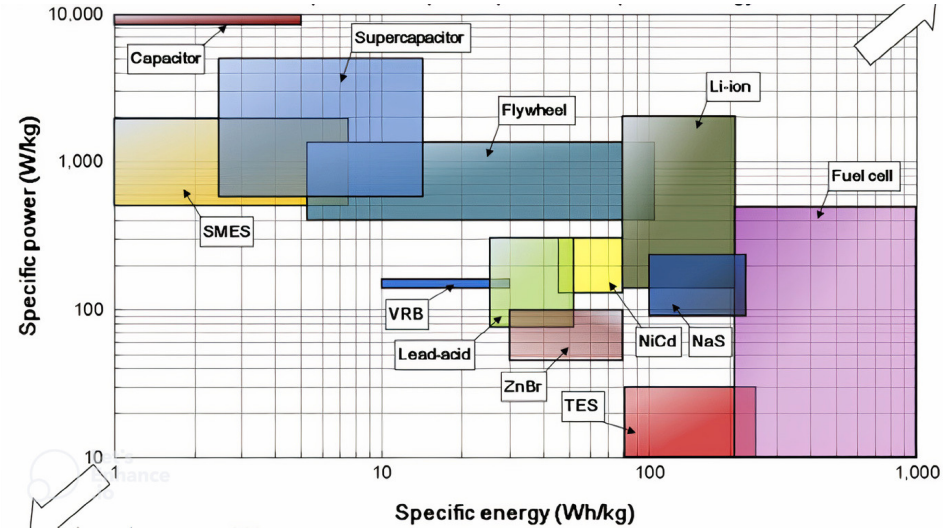

Figure 3.1.6: Comparison of energy and power densities of different ESS technologies. Image adapted and reprinted from Luo et al. (2015)

Figure 3.1.6 compares the energy and power density of different energy storage technologies. In the figure, the top right corner indicates high power densities and high energy density, making the technologies present here suitable for applications with limited space. The bottom left corner displays the opposite, technologies with low power and energy density, thus having a relatively high volume. The lithium-ion battery features the highest energy and power density compared to other energy storage technologies (except fuel cells), making it widely used in portable devices and showing promise in transportation and other small-scale energy storage applications (Luo et al., 2015).

3.2. Energy Storage in Smart Grids

The ongoing energy transition poses new challenges to power grid balance due to the increasing integration of renewable energy sources (RES), which results in a supply and demand mismatch. To address this imbalance and provide ancillary services, such as frequency control, energy storage systems (ESS) are being incorporated into energy management systems (EMSs), which are systems that are designed to monitor, control, and optimise the operation of various energy resources and loads within a power grid or energy system.

ESSs play a crucial role in providing flexibility in EMSs, particularly in RES-integrated grids. Extensive literature has explored various types of ESS for their suitability, as shown by studies such as those by Luo et al. (2015), Killer et al. (2020), Bocklisch (2015), Behabtu et al. (2020), Worku (2022), Traore et al. (2017), Alsharif et al. (2021), and Akram et al. (2019). Selecting the correct ESS technology is highly dependent on the specific application requirements, such as response time, power rating, operational duration and self-discharge (Luo et al., 2015). For applications demanding fast response times at the millisecond level, such as maintaining power quality, technologies like flywheels (Suzuki et al., 2005), conventional batteries, supercapacitors (Author(s), 2007,Seo et al., 2011), certain flow batteries (VRB, PSB) (Shigematsu et al., 2002) and hydrogen fuel cells (Krishnan et al., 2013, Yıldız et al., 2022) are found suitable. These technologies are capable of protecting against short-duration voltage drops in renewable energy systems, for example, stabilising wind turbine or PV power output fluctuations, while some technologies (flywheels, supercapacitors) show limitations in providing long-term solutions. Li-Ion battery ESSs exhibit high power and energy density, fast response time, flexibility, and high efficiency (Luo et al., 2015, Killer et al., 2020, Behabtu et al., 2020, Worku, 2022). However, BESSs may experience reduced battery lifetime due to cycle depth of discharge (DoD). Li-ion batteries surpass Pb-acid batteries in terms of energy density, depth of discharge, and round-trip efficiency, but, relative to Pb-acid batteries, they are currently more expensive (Rezaei Mozafar et al., 2022). However, Li-ion prices are dropping significantly according to Rezaei Mozafar et al. (2022),Berckmans et al. (2017),Ziegler and Trancik (2021),Cole et al. (2016) and Schmidt et al. (2017) and are expected to be the most cost-efficient in most applications, in particular with < 4 hour discharge periods and < 300 an-

nual cycles (Schmidt et al., 2019). A potential solution to reduce degradation is the adoption of Hybrid Energy Storage Systems (HESSs), which combine multiple energy storage technologies, improving the total system efficiency, reducing the system cost and extending the lifespan (Hajiaghasi et al., 2019). Combining a supercapacitor (SC) with a BESS to handle peak loads and power fluctuations in smart grids can mitigate battery stress and improve longevity (Bocklisch, 2015, Hajiaghasi et al., 2021, Kumar and Pahariya, 2017, Lei et al., 2023, Ni et al., 2021, Singh and Lather, 2020, Torkashvand et al., 2020). Grid simulations by Traore et al. (2017) and Bandyopadhyay et al. (2020) indicate that SC-BESS HESS systems outperform BESS-only solutions in terms of efficiency, uncertainty management, and frequency response in high RES penetration systems. Although HESS offers advantages such as fast response times (in milliseconds) and reduced degradation, the simulation in this study operates with five-minute time steps and does not account for efficiency degradation. Consequently, the benefits of SCES-BESS-HESS over traditional BESS may not be visible. As a result, the simulation will incorporate Lithium BESS only instead.

3.2.1. BESS in Smart Grids

Research from Liao et al. (2018) showed the potential of purely using BESS to cover RES intermittency, however, did not consider the effect of residential loads present on the grid. The benefits of optimally sizing a complete smart grid (RES, loads and storage), such as better reliability and cost-effectiveness, are introduced in Okhuegbe et al. (2019). Research from Zhuo and Savkin (2019), Worighi et al. (2019) and Bandyopadhyay et al. (2020) included multiple residential loads and showed that optimising the size of PV systems and BESS can maximize self-sufficiency, relieve the grid, and leverage cost-effective tariff incentives. One drawback however is that the research only considered the widely adopted BESS technology. Investigating the integration of different ESS types in residential smart grids is advised in Worighi et al. (2019) and further researched by authors in Traore et al. (2017) and Akram et al. (2019), where the ability of SC/Battery HESS to cover high-frequency loads showed benefits over traditional battery-only storage. In addition, the studies conducted by Hajiaghasi et al. (2021), Lei et al. (2023), and Ni et al. (2021) have determined that HESSs exhibit superior overall performance and longer lifespan compared to BESSs in islanded microgrids with high renewable energy source (RES) penetration. However, it is worth noting that these studies primarily focused on only having the ESS as a controllable asset, with all other RES in- and output and loads fixed. Given the electrification of the grid (IEA, 2023), it is essential to consider a more complete EMS in simulations that represent real-life scenarios.

3.2.2. Electric Vehicles as Energy Storage System

An emerging area of research is exploring the use of Electric Vehicles (EVs) as an innovative form of energy storage or controllable load (Alsharif et al., 2021). These approaches, respectively, Vehicle-to-Grid (V2G) and load-shifting, can further enhance grid flexibility, dampen peak loads and reduce operational costs. The research from Rassaei et al. (2015) and Rassaei et al. (2018) demonstrated the benefits of controllable EVs with the use of day-ahead planning, however, this time only EVs were considered as flexible loads, and no RES was integrated into the EMS. Through the integration of ESS, RES, EVs, and building loads, studies from Fanti et al. (2017) and Tushar et al. (2018) demonstrated the optimisation of a more advanced EMS. This research revealed the potential synergy between EVs and ESS in day-ahead planning, leading to reduced energy costs and enhanced microgrid (and smart grid) resilience. Importantly, the case studies in Fanti et al. (2017) underscored the considerable benefits obtained by combining RESs, ESSs, and EVs in district grid management, surpassing the advantages of considering EVs or ESS individually.

3.2.3. Controllable HVAC Systems

Furthermore, controllable HVAC systems, such as AC units and HPs, are an emerging component in controllable grid management. However, the studies mentioned earlier do not account for the inclusion of these HVAC systems, leading to incomplete research. To optimise grid management effectively, it is crucial to integrate controllable HVAC systems with RESs, ESSs, and EVs. The research conducted by Wakui et al. (2019) and Coppitters et al. (2021) highlighted the potential of incorporating HPs with RES and ESS. Additionally, the works by Yan et al. (2019) and Blonsky et al. (2021) demonstrated the potential of including HPs alongside RES, ESS, and EVs to effectively mitigate peak demand. In addition, work from Huang et al. (2019) conducted various case studies including PV, EV, HP and

ESS while focusing on maximising self-consumption of a building cluster in Sweden while ensuring the profitability of the system. The integration of ESS, heat pump control, and EVs demonstrated a stepwise increase in self-consumption. Additionally, there was a slight decrease in the levelized cost of electricity attributed to EV integration, advocating for the complete integration of smart loads alongside RES production. These findings are supported by the study conducted by Yousefi et al. (2021), which showed a 34% decrease in electricity cost by integrating PV, EV, HPs and a BESS into a home energy management system. A similar study conducted by Stamatellos et al. (2022) focused on the interaction of a rooftop PV system, accompanied by an HP, BESS and a number of EVs. The results showed a significant increase in self-consumption, which was highly dependent on the amount of EVs present, indicating the importance of EV fleet simulation. However, these studies neglected the significant aspect of participating in ancillary services, which could have positive effects on cost-effectiveness.

3.2.4. Ancillary Services

Works from Nelson and Johnson (2020), Imani et al. (2018), and Tabar et al. (2019) explored the impact of prosumer participation in ancillary services (FCR or demand response incentive programs) within microgrids integrating ESS and RES. Their collective objective was to minimise costs or maximise microgrid revenue. In all instances, the implementation of demand response programs led to a reduction in total operational costs. However, the absence of other flexible loads, such as EVs or HPs, represents a limitation in their research. A more comprehensive analysis was carried out in Vermeer et al. (2022) and Gomez-Gonzalez et al. (2021). Both studies included ESS, RES, EV, FCR, and PV-self consumption (PV SFC) in a power and sizing optimisation, aiming to minimise costs. The results revealed significant cost savings when incorporating FCR and PV SFC into the system, preferring HESS over BESS. One drawback, however, is the absence of HPs as flexible loads. In Zhou et al. (2023), authors showed that HPs together with ESS, RES and EV, considering a temperature comfort range, show excellent capability in providing the flexibility needed for demand response. The study however does not include any other study cases where the trade-off between smart loads and ESS is investigated in terms of total grid cost-efficiency, and only FCR is considered as an ancillary service.

In Papakonstantinou et al. (2024), Mohamed et al. (2023), Maeyaert et al. (2020) a BESS participates in multiple energy markets (FCR, aFRR, mFRRda), investigating the potential of stacked revenue. Here Papakonstantinou et al. (2024) incorporates state-of-charge supervision and regulation via a local controller to avoid provision of scheduled power beyond the battery's SoC limits. While this protects the battery, aFRR and FCR power output throttling may result in market penalties due to the deviation from scheduled ancillary power and must be avoided at all times. Each study shows a significant increase in revenue indicating the BESS's potential to operate in multiple energy markets. However, the grid simulated by Mohamed et al. (2023) does not contain any other smart loads or RES and Mohamed et al. (2023) and Maeyaert et al. (2020) only consider PV power, indicating a research gap in the current literature.

3.3. Contributions

Study	Opt. Control	Opt. C_E	Opt. $C_{Anc.}$	V2G	EV Anc.	PV Self.	BESS	BESS Anc.	Smart HPs	aFRR
Rassaei et al. (2015)	✓			✓						
Lei et al. (2023)	✓						✓			
Traore et al. (2017)	✓					✓	✓			
Akram et al. (2019)	✓					✓	✓			
Ni et al. (2021)	✓					✓	✓			
Liao et al. (2018)	✓	✓				✓	✓			
Zhuo and Savkin (2019)	✓	✓				✓	✓			
Worighi et al. (2019)	✓	✓				✓	✓			
Bandyopadhyay et al. (2020)	✓	✓				✓	✓			
Hajiaghasi et al. (2021)	✓	✓				✓	✓			
Rassaei et al. (2018)	✓	✓		✓						
Fanti et al. (2017)	✓	✓		✓		✓	✓			
Tushar et al. (2018)	✓	✓		✓		✓	✓			
Wakui et al. (2019)	✓	✓				✓	✓		✓	
Coppitters et al. (2021)	✓	✓				✓	✓		✓	
Yan et al. (2019)	✓	✓		✓		✓	✓		✓	
Blonsky et al. (2021)	✓	✓		✓		✓	✓		✓	
Mohamed et al. (2023)	✓	✓	✓				✓	✓		✓
Maeyaert et al. (2020)	✓	✓	✓			✓	✓	✓		✓
Papakonstantinou et al. (2024)	✓	✓	✓			✓	✓	✓		✓
Imani et al. (2018)	✓	✓	✓			✓	✓	✓		
Tabar et al. (2019)	✓	✓	✓			✓	✓	✓		
Gomez-Gonzalez et al. (2021)	✓	✓	✓			✓	✓	✓		
Nelson and Johnson (2020)	✓	✓	✓			✓	✓	✓		
Zhou et al. (2023)	✓	✓	✓	✓		✓	✓		✓	
Vermeer et al. (2022)	✓	✓	✓	✓	✓	✓	✓	✓		
Proposed	✓	✓	✓	✓	✓	✓	✓	✓	✓	✓

Table 3.3.1: Summary of Related Studies in Smart Grid Literature

The benefits of integrating ESS in EMSs that contain RES are intensively researched in the literature. The findings of this thesis can contribute to the optimisation of modern smart grids, aiming to establish a resilient and flexible power grid. The first focus will lie on selecting an appropriate storage solution to be used in an EMS that incorporates RES, HPs, EVs, and aFRR participation. Secondly, the study will conduct multiple case studies to examine the synergy between smart loads and ESS on energy costs and aFRR participation. Initially, the power control will be analysed both with and without aFRR participation to assess effects such as potential grid activity increase and its impact on grid limits.

Moreover, the investigation will delve into aFRR participation levels with and without the presence of a stationary BESS. In scenarios without a stationary BESS, the aFRR potential of EVs will become evident.

When a BESS is present, the study will explore the synergy between BESS and EVs regarding aFRR participation by simulating scenarios with and without EV aFRR participation. These diverse cases will consider two additional influencing factors: seasonality and grid configuration. To address the seasonal effects on variables such as PV production and EV battery performance, each case will undergo simulation during both winter and summer. By doing so, the study aims to gain valuable insights into how aFRR participation and overall grid activity vary across different seasons. The study will examine various grid configurations, including residential, commercial, and mixed setups. Simulating each case for each grid type will highlight how user behaviour influences grid performance. By analysing EV charging schedules and building occupation profiles, the study aims to understand their effects on participation in the aFRR market.

Table 3.3.1 gives a summary of related studies about smart grids and/or ancillary services. The studies are compared based on ten different categories; Optimal control, Energy cost optimisation, ancillary revenue optimisation (either demand response or FCR), EV smart charging (including V2G), EV ancillary service participation, PV self-consumption, BESS self-consumption, BESS ancillary service participation, presence of smart heat pumps and aFRR ancillary service participation. The proposed method in this thesis offers valuable insights into optimal control and participation in aFRR of a state-of-the-art smart grid.

In all, the contributions of this study can be summarised into the following points:

- Demonstrating the flexibility of localised smart grids, which integrate flexible heat pumps, solar power, controllable electric vehicles, and battery energy storage systems, to enhance national grid stability and reduce operational costs through effective participation in the automatic frequency restoration reserve (aFRR) market.
- Compare the usability of flexible loads versus stationary battery energy storage in load shifting and aFRR participation.
- Establishing the influence of seasonal variations and different grid types on the effectiveness of aFRR market participation, providing key insights into how smart grid capabilities can be optimised year-round and across various urban and residential settings.
- Showcasing the potential of passive balancing in a localised smart grid containing flexible heat pumps, solar power, bi-directional electric vehicles and battery energy storage to enhance BRP portfolio efficiency. This contribution underscores how passive strategies can leverage favourable imbalance prices to reduce portfolio imbalances, suggesting further research into this area.

The general research question then yields: to what extent can localised smart grids, integrating flexible heat pumps, solar power, controllable bi-directional electric vehicles, and battery energy storage systems, be used to reduce local grid costs and enhance national grid stability by participating in the aFRR market?

Having outlined the key contributions of this study in optimising modern smart grids through flexible solutions and strategic participation in energy markets, the following chapter delves into the methodology to achieve these results. This involves a detailed Mixed Integer Programming (MIP) problem formulation, which serves as the basis of our analysis and creates the possibility simulate a localised grid. The MIP framework is needed to simulate the local and nodal power balances within localised

smart grids through the use of Python. By using two levels of optimisation strategies, each with a different time frame, this formulation not only predicts optimal energy distribution and aFRR participation but also adapts to real-time variations, ensuring that the smart grid operates efficiently under both planned and unexpected conditions.

4

Problem Formulation

In this chapter, we focus on two critical elements of the grid model: the local and nodal power balances. First, the two levels of optimisation are discussed: the One-shot and Rolling Horizon optimisation. The second section details the local power balance, addressing the equations and functionalities of flexible loads such as Battery Energy Storage Systems (BESS), Electric Vehicles (EVs), and Photovoltaic (PV) systems. This includes their roles in the grid and their specific contributions to Automatic Frequency Restoration Reserve (aFRR) services. In this problem formulation, both V2G and (upward) EV aFRR power represent power output from the EV. However, V2G refers to the power directed into the node for local use, whereas aFRR power leaves the node to be supplied to the grid. To prevent any confusion, we will henceforth use 'Vehicle-to-Node (V2N)' to denote V2G power.

The latter part of the chapter shifts to the nodal power balance, examining the interaction between fixed loads, the AC side of bi-directional inverters, and Heat Pumps (HPs). The framework for this analysis follows the one presented in Vermeer et al. (2022), with some modifications. Notably, we have chosen not to include energy storage degradation in this model, or any degradation for that matter, as it is beyond the scope of this research.

Through these sections, the chapter aims to provide a thorough and clear presentation of the key aspects of energy management and distribution within the smart grid, emphasizing the crucial roles played by different components in maintaining grid balance and efficiency.

4.1. Two Level Optimisation

This model works with a two-level optimisation; one-shot and rolling horizon optimisation (RHO). The one-shot optimisation allocates power based on the power profile predictions of the building, EV and RES models of the next day, using perfect knowledge and day-ahead prices. Subsequently, the rolling horizon optimisation is a more realistic scenario where the profiles deviate from the predicted values. The RHO uses the one-shot optimisation data, which is the optimal power scheduling plan based on a single dataset without uncertainties. This initial optimisation is designed to be efficient until there is a deviation from the expected one-shot data. When such a deviation occurs, it acts as a signal for the RHO to initiate a re-optimisation process. This process involves updating the original optimisation in response to the new, previously unaccounted-for conditions, thereby ensuring the system remains at peak efficiency despite the change in circumstances.

4.1.1. One-Shot Optimisation

In the first level, the one-shot optimisation, the optimisation runs a full day where all EV arrival and departure times, building's occupation and energy usage profiles and weather data are fixed and known to the model. The model knows the exact power request of the node for the full day together with the day-ahead energy prices. This way the optimisation finds the optimal strategy to allocate and buy energy in line with the objective function. The optimisation window T is the length over which the model optimises the grid simulation, which, in this case, is 24 hours from 00:00 to 00:00 (D+1).

In the one-shot optimisation, aFRR power is scheduled for the next day based on the imbalance price. Since balancing energy prices are normally published in real-time, and the imbalance price is

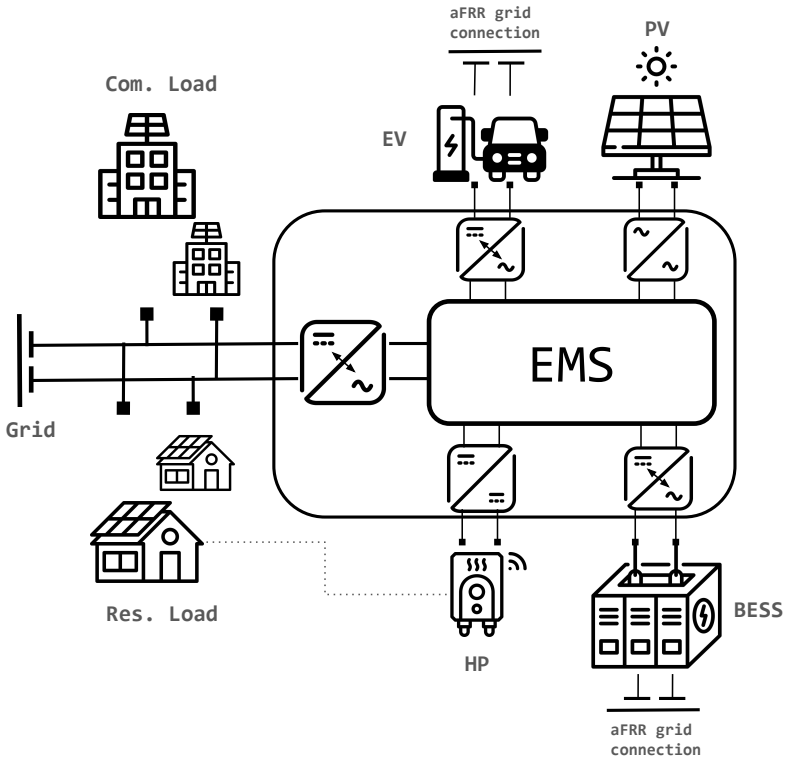

Figure 4.0.1: Schematic overview of the energy management system of one node. Dotted line: data connection.

determined after an ISP ends, an assumption of perfect price prediction is made. Since the imbalance price indicates the presence of a grid shortage or an imbalance, the model knows the exact moments of imbalance one day ahead. In all, this deterministic approach ensures that the most cost-effective and efficient energy management strategies are known upfront. However, it also means that the capacity of the model to adapt to unforeseen changes in energy demand or supply throughout the day is not taken into account at this stage, which limits its applicability in dynamic or uncertain environments. For that, we use the RHO optimisation.

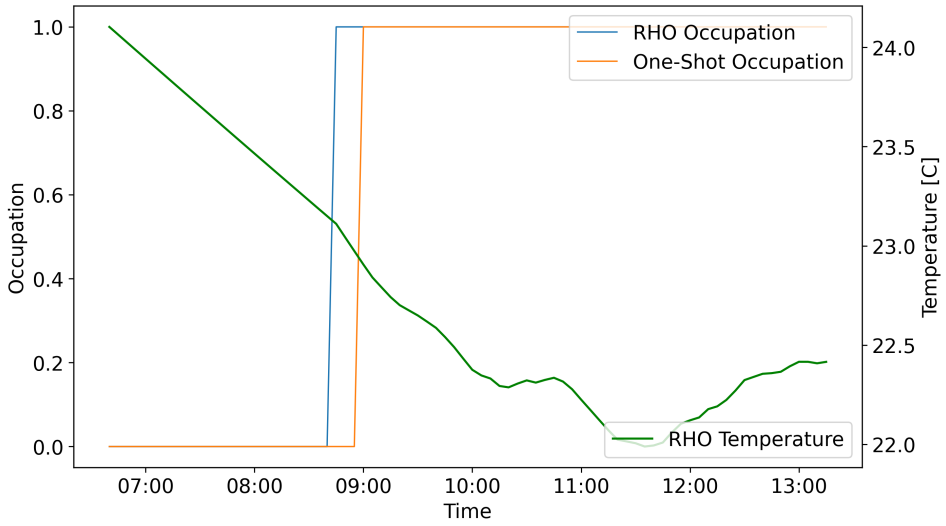

Figure 4.1.1: One-shot and rolling horizon building occupation profile example.

4.1.2. Rolling Horizon Optimisation

Once the one-shot optimisation is completed, the rolling horizon optimisation starts. At the beginning of the day, the RHO uses the prediction of the one-shot optimisation until the end of the optimisation horizon T. Figure 4.1.2) shows this process visually. However, this second level uses real-time control instead of day-ahead scheduling. The RHO input data is similar to that of the one-shot, but instead, it can use ”real” EV and building occupancy profiles. The profiles in the RHO are taken from the one-shot and subjected to uncertainties, which scatter for example EV arrival and building occupancy times. This results in a model that needs to react to unexpected events, just like in real life. Any deviation from the predicted profiles causes a re-optimisation from that moment until the end of the re-optimisation horizon, again using the one-shot prediction data. An example of the difference in building occupation is shown in Figure 4.1.1.

The following five situations trigger a re-optimisation;

- A new day starts: The system resets and prepares for the day’s energy demands and supply, taking into account the updated forecasts and schedules.
- New EV arrival: The system re-optimises to integrate the energy requirements of the newly arrived EV into the grid load profile, ensuring optimal charging strategies.
- An EV joins smart charging: The EV participation in smart charging (when $SoC_{EV}(i,t) > SoC_{SC}$) allows for more flexible and efficient energy management, adapting to grid needs and EV owner preferences.
- An EV arrives later in RHO than scheduled in one-shot optimisation: when an EV is originally scheduled to arrive at a certain time step but is not present at that time step in the RHO, the optimisation removes the scheduled EV from the optimisation horizon and waits until the ’real’ EV arrives, and re-optimises once it does.
- An occupant enters a building: The system adjusts the energy consumption of the building to accommodate the presence of the occupant, optimising comfort and energy efficiency.
- An occupant leaves the building: Energy consumption patterns are modified to reflect the reduced demand, optimising energy usage and cost.
- A scheduled aFRR bid changes: The system updates its strategies to align with the new aFRR bid, ensuring no aFRR power is either drawn or given when it is not called.
- Any arrival/departure instances of EVs or occupants based on the one-shot prediction.

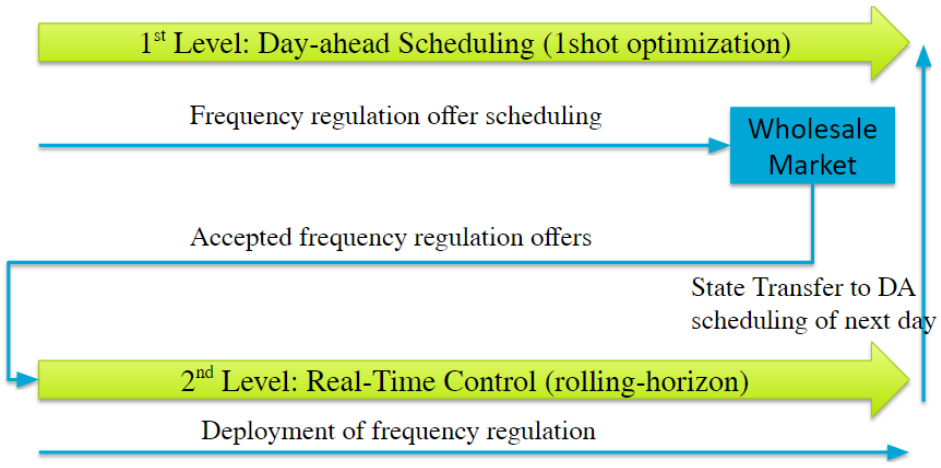

Figure 4.1.2: One-shot and rolling horizon optimisation schematic. Reprinted from N. Damianakis (2023, October). Coordinated power control in future distribution grids [PowerPoint slides]. Electrical Sustainable Energy Department, DC Systems, Energy Conversion & Storage, Delft University of Technology.

Almost all variables in the RHO are being calculated in real-time, depending on the energy requirements, independent from the one-shot predicted variables. Except for the aFRR power provision bids, which are planned and fixed in the one-shot optimisation for the next day. The RHO must adhere to exactly those values of variables to avoid market penalties and are therefore used as fixed input values in the RHO. However, due to the BAR explained in Paragraph 4.5.1, the values can still be differentiated from the initially planned values to account for real-life market situations. Table 4.1.1 contains all constraints that are either active or non-active between the one-shot and rolling horizon optimisation.

	One-Shot	RHO
Active Constraints	(1)-(50),(54),(55),(57),(58), (67)-(75)	(1)-(52),(54),(55),(57)-(75)
Non-active Constraints	(51)-(53),(56),(59)-(66)	(53), (56)

Table 4.1.1: Overview of active and non-active equations for both one-shot and rolling horizon optimisation (RHO).

4.2. Local Power Balance and Constraints

All loads are connected to individual (bi-directional) AC/DC converters that connect the load to the node or grid. Equation (4.1) shows the power balance of each converter per node. Here both $P_{\text{BESS}}(n,t)$ and $P_{\text{EV}}(n,i,t)$ exclude aFRR power, T denotes the optimisation horizon, $T_a^{n,j}$ the arrival time a of an EV at charger i in node n, $T_d^{n,j}$ the departure time and b the building number.

$$P_{\text{con}}(n,b,i,t) = P_{PV}(n,b,t) - P_{EV}(n,i,t) - P_{BESS}(n,t) \quad \forall t \in T \tag{4.1}$$

Each converter is modelled using individual efficiencies η_x, where X denotes EV or BESS. Both EV and BESS are able to draw from and deliver power to the node, resulting in a distinction between positive and negative power respectively (4.2)-(4.3). Here, i represents an i^{th} load in a certain node. The grid power is dynamically constrained by $P_{\text{grid}}^{+,max}$ and $P_{\text{grid}}^{-,max}$, which represent the maximum available power for import and export respectively, to allow for power curtailment for each n^{th} node (4.4)-(4.5).

$$P_{EV}(n,i,t) = \eta_{EV} P_{EV}^{+}(n,i,t) - \frac{1}{\eta_{EV}} P_{EV}^{-}(n,i,t) \quad \forall t \in T \tag{4.2}$$

$$P_{BESS}(n,t) = \eta_{BESS} P_{BESS}^{+}(n,t) - \frac{1}{\eta_{BESS}} P_{BESS}^{-}(n,t) \quad \forall t \in T \tag{4.3}$$

$$P_{\text{grid}}^{-}(n,t) \leq P_{\text{grid}}^{-,max}(n,t) \quad \forall t \in T \tag{4.4}$$

$$P_{\text{grid}}^{+}(n,t) \leq P_{\text{grid}}^{+,max}(n,t) \quad \forall t \in T \tag{4.5}$$

4.2.1. PV Constraints

To enable PV curtailing, Equation (4.6) is introduced for each building b. It is assumed that the efficiencies of all systems remain constant over their lifetime. The PV panels are able to be curtailed during negative energy prices to avoid unnecessary costs. Each building has a unique azimuth and tilt angle, leading to variations in PV production. This variability, including maximum power point (MPP) tracking, module efficiency and climate conditions are modelled in the PV model presented in Damianakis et al. (2023). In this research, 90 summer and winter profiles are created using various tilt angles and orientations. Each rooftop contains 12 modules with rated power according to Table 5.3.1. Subsequently, for the simulations in the research, the power output of these profiles is randomly selected from the database and are able to be curtailed according to Equation (4.6).

$$0 \leq P_{PV}(n,b,t) \leq P_{\text{PV}}^{\text{max}}(n,b,t) \quad \forall t \in T \tag{4.6}$$

4.2.2. Battery Model

The BESS is limited by the maximum amount of power that can be drawn from its batteries. This depends on two variables; the C-rate and the capacity. Since the majority of deployed residential and commercial scale, (<100kWh) stationary BESS are between 0.5C and 2C (European Commission, Joint Research Centre, 2018), the C-rate is limited to a maximum of 0.5C. In addition, BESS producers indicate a cycle life based on a maximum C-rate and DoD (Tesla, 2023, Panasonic, 2021). Based on the insights from Vermeer et al. (2022) and Gomez-Gonzalez et al. (2021), it is evident that a high C-rate diminishes the lifespan of a battery. This understanding allows for more accurate cost estimations by adhering to the manufacturer's recommended C-rate, which aligns with the promised or indicated product lifetime by the factory. Both the BESS and EV use the same $LiFePO_4$ battery types, so the equations for their battery operation are assumed to be consistent.

$$P_{\text{EV}}^{\text{rated}}(n,i) \leq 2E_{\text{EV}}^{\text{rated}}(n,i) \tag{4.7}$$

$$P_{\text{EV}}^{+}(n,i,t) \leq P_{\text{EV}}^{\text{char,max}}(n,i,t) \quad \forall t \in [T_a^{n,i} : T_d^{n,i}] \tag{4.8}$$

$$P_{\text{EV}}^{\text{char,max}}(n,i,t) \leq P_{\text{EV}}^{\text{op}}(n,i) \quad \forall t \in [T_a^{n,i} : T_d^{n,i}] \tag{4.9}$$

$$P_{\text{EV}}^{\text{char,max}}(n,i,t) \leq \frac{P_{\text{EV}}^{\text{op}}(n,i)}{(1-D_{\text{ch}})}\left(\frac{E_{\text{EV}}(n,i,t)}{E_{\text{EV}}^{\text{rated}}(n,i)} - 1\right) \quad \forall t \in [T_a^{n,i} : T_d^{n,i}] \tag{4.10}$$

$$P_{\text{EV}}^{\text{char,max}}(n,i,t) \leq \left(\frac{1}{16}\frac{E_{\text{EV}}(n,i,t)}{E_{\text{EV}}^{\text{rated}}(n,i)} + \frac{151}{160}\right)P_{\text{EV}}^{\text{op}}(n,i) \quad \forall t \in [T_a^{n,i} : T_d^{n,i}] \tag{4.11}$$

$$P_{\text{EV}}^{-}(n,i,t) \leq P_{\text{EV}}^{\text{dis,max}}(n,i,t) \quad \forall t \in [T_a^{n,i} : T_d^{n,i}] \tag{4.12}$$

$$P_{\text{EV}}^{\text{dis,max}}(n,i,t) \leq P_{\text{EV}}^{\text{op}}(n,i) \quad \forall t \in [T_a^{n,i} : T_d^{n,i}] \tag{4.13}$$

$$P_{\text{EV}}^{\text{dis,max}}(n,i,t) \leq \frac{P_{\text{EV}}^{\text{op}}(n,i)E_{\text{EV}}(n,i,t)}{D_{\text{dis}}E_{\text{EV}}^{\text{rated}}(n,i)} \quad \forall t \in [T_a^{n,i} : T_d^{n,i}] \tag{4.14}$$

$$P_{\text{BESS}}^{\text{rated}}(n) \leq 2E_{\text{BESS}}^{\text{rated}}(n) \tag{4.15}$$

$$P_{\text{BESS}}^{+}(n,t) \leq P_{\text{BESS}}^{\text{char,max}}(n,t) \quad \forall t \in T \tag{4.16}$$

$$P_{\text{BESS}}^{\text{char,max}}(n,t) \leq P_{\text{BESS}}^{\text{op}}(n) \quad \forall t \in T \tag{4.17}$$

$$P_{\text{BESS}}^{\text{char,max}}(n,t) \leq \frac{P_{\text{BESS}}^{\text{op}}(n)}{(1-D_{\text{ch}})}\left(\frac{E_{\text{BESS}}(n,t)}{E_{\text{BESS}}^{\text{rated}}(n)} - 1\right) \quad \forall t \in T \tag{4.18}$$

$$P_{\text{BESS}}^{\text{char,max}}(n,t) \leq \left(\frac{1}{16}\frac{E_{\text{BESS}}(n,t)}{E_{\text{BESS}}^{\text{rated}}(n)} + \frac{151}{160}\right)P_{\text{BESS}}^{\text{op}}(n) \quad \forall t \in T \tag{4.19}$$

$$P_{\text{BESS}}^{-}(n,t) \leq P_{\text{BESS}}^{\text{dis,max}}(n,t) \quad \forall t \in T \tag{4.20}$$

$$P_{\text{BESS}}^{\text{dis,max}}(n,t) \leq P_{\text{BESS}}^{\text{op}}(n) \quad \forall t \in T \tag{4.21}$$

$$P_{\text{BESS}}^{\text{dis,max}}(n,t) \leq \frac{P_{\text{BESS}}^{\text{op}}(n)E_{\text{BESS}}(n,t)}{D_{\text{dis}}E_{\text{BESS}}^{\text{rated}}(n)} \quad \forall t \in T \tag{4.22}$$

The C-rate is modelled using Equation (4.7) and (4.15) for EV and BESS respectively. Research from Vermeer et al. (2022) state that the maximum charging and discharging power ($P_{\text{EV}}^{\text{char,max}}$, $P_{\text{BESS}}^{\text{char,max}}$

and $P_{\text{EV}}^{\text{dis,max}}$, $P_{\text{BESS}}^{\text{dis,max}}$ respectively) depend on the SoC of the battery, where $P_{\text{EV}}^{\text{dis,max}}$ represents Vehicle to Grid (V2N) power.

The SoC dependency divides the charging and discharging regions into three sections; precharge region (low SoC), constant current (CC) region and constant voltage (CV) region (high SoC) (Vermeer et al., 2022). The charging profiles follow a linearized version of the CC/CV charging method, which is widely adopted and is used to protect battery performance and cycle life (Shen et al., 2012), which are stated in Equation (4.11) and (4.19) for the CV region for EV and BESS respectively, and Equation (4.10) and (4.18) for the precharge region.

The converter's constant operational power limit $P_{\text{EV}}^{\text{op}}(n,i)$ and $P_{\text{BESS}}^{\text{op}}(n)$ will determine the maximum charging (4.8)-(4.9), (4.16)-(4.17) and discharging (4.12)-(4.13), (4.20)-(4.21) power from the batteries to ensure the converter operates within safe and stable boundaries. The CC region for discharging is limited by the lower SoC limit; D_{dis} respectively. Work from Damianakis (2024) introduces a linear power increase during the charging CC region because of a gradual increase in voltage, see Equation (4.11) and (4.19). As explained, aFRR power is scheduled in the one-shot optimisation for the next day. According to Equation 4.29, $P_{\text{EV}}^{-,aFRR}$ and $P_{\text{BESS}}^{-,aFRR}$ are bounded by the SoC in the CC region. Since the SoC in the one-shot is not identical to the SoC in the RHO, downward aFRR power is limited to $P_{\text{EV}}^{+,\text{aFRR}}(n,i,t) \leq min(P_{\text{EV}}^{\text{char,max}}(n,i))$ and $P_{\text{BESS}}^{+,\text{aFRR}}(n,t) \leq min(P_{\text{BESS}}^{\text{char,max}}(n))$ to avoid overcharging due to SoC deviations between the two levels of optimisation. From Equation (4.10)-(4.11) and (4.14) it can be seen that, at 100% SoC ($E_{\text{EV}} = E_{\text{EV}}^{\text{rated}}$), the maximum charging power $P_{\text{EV}}^{\text{char,max}} = 0$. At 0% SoC ($E_{\text{EV}} = 0$), the maximum discharging power $P_{\text{EV}}^{\text{dis,max}} = 0$, which coincides with logic (same for the BESS). The charging and discharging profiles are plotted in Figure 4.2.1.

Since both EV and BESS will provide ancillary services, power is reserved to ensure power delivery to both the node and the grid. Therefore, Equation (4.23) and (4.24) splits the available power into two parts; P_{EV}^{op} and P_{EV}^{aFRR}. Here P_{EV}^{rated} represents the rated power of the converter, P_{EV}^{op} the available operational power to be scheduled and P_{EV}^{aFRR} the scheduled ancillary power, as for BESS. The efficiencies and bounds used in the optimisation are given in Table 5.3.1.

$$P_{\text{EV}}(n,i,t) + |P_{\text{EV}}^{\text{aFRR}}(n,i,t))| \leq P_{\text{EV}}^{rated}(n,i) \quad \forall t \in [T_a^{n,i} : T_d^{n,i}] \tag{4.23}$$

$$P_{\text{BESS}}^{\text{op}}(n,t) + |P_{\text{BESS}}^{\text{aFRR}}(n,t))| \leq P_{\text{BESS}}^{rated}(n) \quad \forall t \in T \tag{4.24}$$

The total P_{x}^{aFRR} is composed of two components: $P_{\text{x}}^{+,aFRR}$ for downward regulation and $P_{\text{x}}^{-,aFRR}$ for upward regulation, as detailed in Equation (4.25)-(4.27) for EV and Equation (4.28)-(4.30) for BESS.

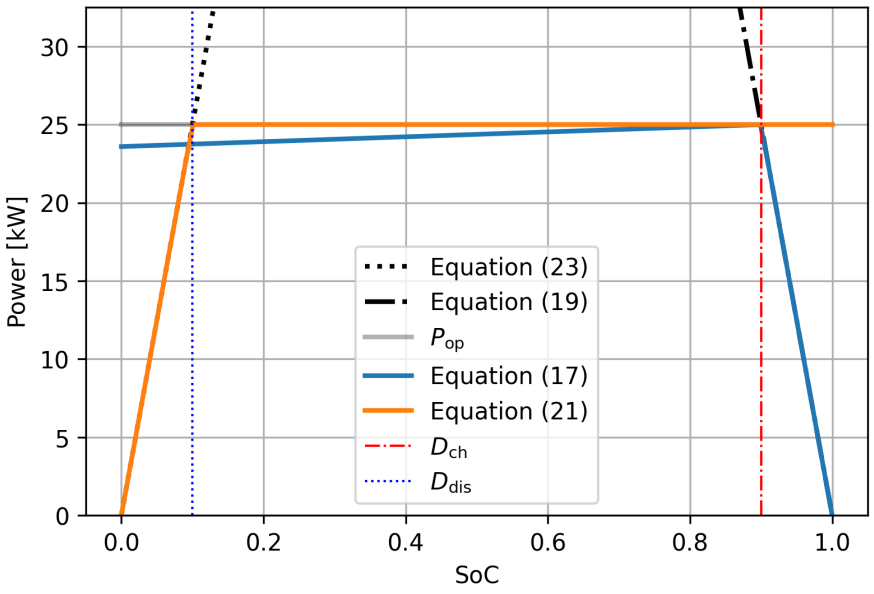

Figure 4.2.1: Graphic representation of charging power P_{x}^{+} (blue) and discharging power P_{x}^{-} (orange). $D_{\text{dis}} = 0.1$, $D_{\text{ch}} = 0.9$, and $P_{\text{x}}^{\text{op}} = 25kW$

Each EV and BESS is interpreted as a stand-alone ancillary service facility which can not deliver both up- and downward power at the same time.

$$P_{\text{EV}}^{\text{aFRR}}(n,i,t) = P_{\text{EV}}^{+,\text{aFRR}}(n,i,t) - P_{\text{EV}}^{-,\text{aFRR}}(n,i,t) \quad \forall t \in [T_a^{n,i} : T_d^{n,i}] \tag{4.25}$$

$$P_{\text{EV}}^{+,\text{aFRR}}(n,i,t) \leq P_{\text{EV}}^{\text{char,max}}(n,i,t) \quad \forall t \in [T_a^{n,i} : T_d^{n,i}] \tag{4.26}$$

$$P_{\text{EV}}^{-,\text{aFRR}}(n,i,t) \leq P_{\text{EV}}^{\text{dis,max}}(n,i,t) \quad \forall t \in [T_a^{n,i} : T_d^{n,i}] \tag{4.27}$$

$$P_{\text{BESS}}^{\text{aFRR}}(n,t) = P_{\text{BESS}}^{+,\text{aFRR}}(n,t) - P_{\text{BESS}}^{-,\text{aFRR}}(n,t) \quad \forall t \in T \tag{4.28}$$

$$P_{\text{BESS}}^{+,\text{aFRR}}(n,t) \leq P_{\text{BESS}}^{\text{char,max}}(n,t) \quad \forall t \in T \tag{4.29}$$

$$P_{\text{BESS}}^{-,\text{aFRR}}(n,t) \leq P_{\text{BESS}}^{\text{dis,max}}(n,t) \quad \forall t \in T \tag{4.30}$$

4.3. Node Power Balance

Equation (4.31) shows the node level power balance. The loads are divided into three groups; P_{con} , P_{load} and P_{HP}. Both P_{con} and P_{HP} are considered flexible, while P_{load} represents the node's required power from other appliances, which is considered non-flexible. The maximum import and export power is limited by the maximum grid power P_{grid}.

$$P_{\text{grid}}^{+}(n,t) - P_{\text{grid}}^{-}(n,t) \leq \sum_{b=1}^{B}\sum_{i=1}^{I} P_{\text{con}}(n,b,i,t) - \sum_{b=1}^{B}(P_{\text{load}}(n,b,t) + P_{\text{HP}}(n,b,t)) \quad \forall t \in T \tag{4.31}$$

Ancillary power is modelled outside the node's power balance. To understand this, the difference between self-consumption and ancillary power must be noted. While self-consumption involves using energy generated or stored within the same system for local needs, ancillary power represents external services provided to the grid. $P_{\text{x}}^{-,aFRR}$ directly leaves the node and is not able to be used by any load inside the node. In addition, $P_{\text{x}}^{+,aFRR}$ must directly come from the grid since otherwise it would be seen as self-consumption from either a PV or EV source. In the energy balance, however, the sourced $P_{\text{x}}^{+,aFRR}$ can later be used for local purposes. The maximum allowable grid input and output for each node n is defined in Equation (4.32)-(4.33).

$$P_{\text{EV}}^{\text{aFRR}}(n,i,t) + P_{\text{BESS}}^{\text{aFRR}}(n,t) + P_{\text{grid}}^{+}(n,t) - P_{\text{grid}}^{-}(n,t) \leq P_{\text{grid}}^{+,max}(n) \quad \forall t \in T \tag{4.32}$$

$$-P_{\text{EV}}^{\text{aFRR}}(n,i,t) - P_{\text{BESS}}^{\text{aFRR}}(n,t) - P_{\text{grid}}^{+}(n,t) + P_{\text{grid}}^{-}(n,t) \leq P_{\text{grid}}^{-,max}(n) \quad \forall t \in T \tag{4.33}$$

4.3.1. Heating Model

The temperature inside a building needs to stay within an allowable range to avoid uncomfortable situations, see Equation (4.34). Depending on this temperature, P_{HP} can increase or decrease to heat or cool the building, which results in a variable power output, or interruptible load (IL). Reducing P_{HP} during high retail energy prices while staying within the acceptable temperature window can reduce energy costs. The authors in Zhou et al. (2023) propose Equation (4.35) to regulate the HP power output, where P_{HP} and $P_{\text{HP}}^{\text{rated}}$ represent the operating power and rated power of HP b at time slot t and $x(b,t)$ a state quantity, indicating whether HP b is active or not. The decision for the state quantity to be either 0 or 1 depends on the building climate at time t.

$$Te_{min} \leq Te(b,t) \leq Te_{max} \tag{4.34}$$

$$P_{\text{HP}}^{\text{op}}(b,t) = x(b,t)P_{\text{HP}}^{\text{rated}}(b) \tag{4.35}$$

$$0 \leq P_{\text{HP}}^{\text{rated}}(b) \leq P_{\text{HP}}^{\max} \tag{4.36}$$

Equation (4.37) calculates the heat loss for each building i, comprising two components: Q^{con}, the conductive heat loss, and Q^{vol}, the volumetric heat loss. The latter is determined by the volume, air change rate (r_b), and the occupancy (N) of building b at a given time t. This formula takes into account the heat capacity (C_{air}) of air and its density (ρ_{air}), multiplied by the temperature difference between the building and the ambient environment. Equation (4.39) represents the total heat balance, with Q^{HP} the heat pump energy influx and Q^{sun} the total heating due to solar irradiation. Finally, Equation (4.40) represents the required power output based on the Coefficient of Performance (CoP) of the heat pump.

$$Q^{loss}(b,t) = (Q^{con}(b,t) + Q^{vol}(b,t))(Te(b,t) - Te_{amb}(b,t)) \tag{4.37}$$

$$Q^{vol}(b,t) = V_b C_p \rho r_b N(b,t) \tag{4.38}$$

$$Q^{tot}(b,t) = Q^{\text{HP}}(b,t) + Q^{\text{sun}}(b,t) - Q^{\text{loss}}(b,t) \tag{4.39}$$

$$Q^{HP}(b,t) = CoPP_{\text{HP}}^{\text{op}}(b,t) \tag{4.40}$$

4.4. Energy Balance and Constraints

Both the EV and BESS are subjected to certain energy limitations to ensure realistic energy capacity modelling. During operation, the available capacity $E_{\text{x}}(i,t)$ will change with each time step Δt. The capacity and SoC over time for each i^{th} EV and BESS is modelled according to Equations (4.41)-(4.44) for EV and Equations (4.45)-(4.47) for BESS.

$$SoC_{\text{EV}}(n,i,t) = \frac{E_{\text{x}}(n,i,t)}{E_{\text{x}}^{\text{lim}}(n,i,t)} \quad \forall t \in [T_a^{n,i} : T_d^{n,i}] \tag{4.41}$$

$$0 \leq SoC_{\text{EV}}(n,i,t) \leq 1 \quad \forall t \in [T_a^{n,i} : T_d^{n,i}] \tag{4.42}$$

$$E_{\text{EV}}(n,i,t) = \begin{cases} E_{\text{EV}}^{\text{init}}(n,i,t), & \text{for } t = 1, \\ E_{\text{EV}}^{\text{end}}(n,i,t), & \text{for } t = T_d^{n,i}. \end{cases} \tag{4.43}$$

$$\begin{aligned} E_{\text{EV}}(n,i,t) = & E_{\text{EV}}(n,i,t-1) + \Delta t \cdot \Big(\eta_{\text{EV}} \cdot P_{\text{EV}}^{+}(n,i,t) + \eta_{\text{EV}} \cdot P_{\text{EV}}^{+,\text{aFRR}}(n,i,t) \\ & - \frac{1}{\eta_{\text{EV}}} \cdot P_{\text{EV}}^{-}(n,i,t) - \frac{1}{\eta_{\text{EV}}} \cdot P_{\text{EV}}^{-,\text{aFRR}}(n,i,t) \Big) \quad \forall t \in [T_a^{n,i} : T_d^{n,i}] \end{aligned} \tag{4.44}$$

$$SoC_{\text{BESS}}(n,t) = \frac{E_{\text{BESS}}(n,t)}{E_{\text{BESS}}^{\text{lim}}(n,t)} \quad \forall t \in T \tag{4.45}$$

$$0 \leq SoC_{\text{BESS}}(n,t) \leq 1 \quad \forall t \in T \tag{4.46}$$

$$\begin{aligned} E_{\text{BESS}}(n,t) = & E_{\text{BESS}}(n,t-1) + \Delta t \cdot \Big(\eta_{\text{BESS}} \cdot P_{\text{BESS}}^{+}(n,t) + \eta_{\text{BESS}} \cdot P_{\text{BESS}}^{+,\text{aFRR}}(n,t) \\ & - \frac{1}{\eta_{\text{BESS}}} \cdot P_{\text{BESS}}^{-}(n,t) - \frac{1}{\eta_{\text{BESS}}} \cdot P_{\text{BESS}}^{-,\text{aFRR}}(n,t) \Big) \quad \text{for } t > 1 \end{aligned} \tag{4.47}$$

An EV is considered available if it is connected and satisfies the SoC requirements to participate in smart charging (SC), which means both V2N and aFRR services. In addition, Equation (4.48) shows a minimum departure SoC as a soft constraint to ensure enough usable energy for SC participants

at departure. A difference should be noted between $E_{\text{EV}}^{\text{dep}}$, which is the requested departure energy amount by the user, and $E_{\text{EV}}^{\text{end}}$, which is the actual amount of energy in the battery at departure.

$$E_{\text{EV}}^{\text{end}}(n,i,t) \geq E_{\text{EV}}^{\text{dep}}(n,i,t) \quad \text{for } t > T_d^{n,i} \tag{4.48}$$

The EVs behave according to a predefined connect range in the one-shot which is fixed, see Equation (4.49). The RHO uses the same range with an added uncertainty δ for a more realistic scenario where users do not arrive at a fixed instance every day, see Equation (4.50). To avoid scheduling aFRR power at a time instance where the EV might not be connected the next day, Equation (4.51) is introduced to account for the maximum time deviation K.

$$t_{\text{EV,sched}}^{\text{connect}} = T_a^{n,i} : T_d^{n,i} \tag{4.49}$$

$$t_{\text{EV,rho}}^{\text{connect}} = t_{\text{arr}} + \delta : t_{\text{dep}} + \delta \quad \text{for} \quad -K \leq \delta \leq K \tag{4.50}$$

$$t_{\text{EV,rho}}^{\text{aFRR}} = t_{\text{arr}} + K : t_{\text{dep}} - K \tag{4.51}$$

The BESS in this study is sized according to the proportions identified in the study by Vermeer et al. (2022), which determined an optimal BESS size for a specific microgrid configuration, see Table 5.3.1. The scaling was approximately based on the total kilowatt peak (kWp) of photovoltaic installations and the number of electric vehicles (EVs) present in the microgrid.

4.5. Bidding Model and Constraints

Some ancillary services require symmetrical power provision. While in the EU only FCR requires symmetrical bidding and aFRR does not ENTSOE (2023), Equation (4.52) and (4.55) can be implemented for cases that do require symmetrical bidding. The model schedules ancillary power an amount of time T (one day) ahead in a one-shot simulation, indicating perfect knowledge of the aFRR market prices, see (4.53) and (4.56). Here, $t+t1 : t+t2$ represents the time frame for which the ancillary power is reserved in the rolling horizon optimisation (RHO). In addition, equations (4.54) and (4.57) are used in the one-shot optimisation to ensure constant power delivery throughout the bidding interval, where $n = \left\lfloor \frac{ISP}{\Delta t} \right\rfloor$, using the floor function to avoid non-integer values, represents one timestep of length Δt in the simulation. Downward aFRR power is only scheduled when the downward imbalance price lies below zero, meaning the asset receives remuneration for increasing consumption (charge).

$$P_{\text{EV}}^{\text{-,aFRR}}(n,i,t) = P_{\text{EV}}^{\text{+,aFRR}}(n,i,t) \quad \forall t \in [T_a^{n,i} : T_d^{n,i}] \tag{4.52}$$

$$P_{\text{EV}}^{\text{aFRR}}(n,i,t+t_1 : t+t_2) = P_{\text{EV},sched}^{\text{aFRR}}(n,i,t_1 : t_2) \quad \forall t \in [T_a^{n,i} : T_d^{n,i}] \tag{4.53}$$

$$\forall k \in \{0,1,\dots,n\}, \quad P_{\text{EV},sched}^{aFRR}(n,i,t) = P_{\text{EV},sched}^{aFRR}(n,i,t+k) \quad \forall t \in [T_a^{n,i} : T_d^{n,i}] \tag{4.54}$$

$$P_{\text{BESS}}^{\text{-,aFRR}}(n,t) = P_{\text{BESS}}^{\text{+,aFRR}}(n,t) \quad \forall t \in T \tag{4.55}$$

$$P_{\text{BESS}}^{\text{aFRR}}(n,t+t_1 : t+t_2) = P_{\text{BESS},sched}^{\text{aFRR}}(n,t_1 : t_2) \quad \forall t \in T \tag{4.56}$$

$$\forall k \in \{0,1,\dots,n\}, \quad P_{\text{BESS},sched}^{aFRR}(n,t) = P_{\text{BESS},sched}^{aFRR}(n,t+k) \quad \forall t \in T \tag{4.57}$$

4.5.1. Bid Acceptance Rate (BAR)

When aFRR power is called by the TSO during a certain ISP, it is not uniform throughout the full delivery period. For example, an upward power request from the TSO can be positive during the first ten minutes of an ISP and zero during the last five. Therefore we introduce aFRR acceptance rates for upward and downward power requests, denoted as α^{up} and α^{down}. These rates represent the chance that scheduled aFRR power is actually called during a time step in the simulation. By using these rates, we approach a more realistic version of the potential voluntary aFRR earnings. Calculated from 2023 Tennet aFRR data (Tennet TSO, 2023), the average activation percentage per ISP during regulation state 1 is 71% and regulation state -1 is 41%. Given the initial states of $P^{+,\text{aFRR}}_{EV,sched}(i,t)$ and $P^{-,\text{aFRR}}_{EV,sched}(i,t)$ for EV and $P^{+,\text{aFRR}}_{BESS,sched}(i,t)$ and $P^{-,\text{aFRR}}_{BESS,sched}(i,t)$ for BESS, the conditional probabilities for each time step t are expressed in Equation (4.58)-(4.61) and (4.62)-(4.65) respectively.

$$P(P^{+,\text{aFRR}}_{\text{EV}}(i,t) = P^{+,\text{aFRR}}_{\text{EV},sched}(i,t) \mid P^{+,\text{aFRR}}_{\text{EV},sched}(i,t)) = \alpha_{\text{up}} \quad \forall t \in [T_a^{n,i} : T_d^{n,i}] \tag{4.58}$$

$$P(P^{+,\text{aFRR}}_{\text{EV}}(i,t) = 0 \mid P^{+,\text{aFRR}}_{\text{EV},sched}(i,t)) = 1 - \alpha_{\text{up}} \quad \forall t \in [T_a^{n,i} : T_d^{n,i}] \tag{4.59}$$

$$P(P^{-,\text{aFRR}}_{\text{EV}}(i,t) = P^{-,\text{aFRR}}_{\text{EV},sched}(i,t) \mid P^{-,\text{aFRR}}_{\text{EV},sched}(i,t)) = \alpha_{\text{down}} \quad \forall t \in [T_a^{n,i} : T_d^{n,i}] \tag{4.60}$$

$$P(P^{-,\text{aFRR}}_{\text{EV}}(i,t) = 0 \mid P^{-,\text{aFRR}}_{\text{EV},sched}(i,t)) = 1 - \alpha_{\text{down}} \quad \forall t \in [T_a^{n,i} : T_d^{n,i}] \tag{4.61}$$

$$P(P^{+,\text{aFRR}}_{\text{BESS}}(n,t) = P^{+,\text{aFRR}}_{\text{BESS},sched}(n,t) \mid P^{+,\text{aFRR}}_{\text{BESS},sched}(n,t)) = \alpha_{\text{up}} \quad \forall t \in T \tag{4.62}$$

$$P(P^{+,\text{aFRR}}_{\text{BESS}}(n,t) = 0 \mid P^{+,\text{aFRR}}_{\text{BESS},sched}(n,t)) = 1 - \alpha_{\text{up}} \quad \forall t \in T \tag{4.63}$$

$$P(P^{-,\text{aFRR}}_{\text{BESS}}(n,t) = P^{-,\text{aFRR}}_{\text{BESS},sched}(n,t) \mid P^{-,\text{aFRR}}_{\text{BESS},sched}(n,t)) = \alpha_{\text{down}} \quad \forall t \in T \tag{4.64}$$

$$P(P^{-,\text{aFRR}}_{\text{BESS}}(n,t) = 0 \mid P^{-,\text{aFRR}}_{\text{BESS},sched}(n,t)) = 1 - \alpha_{\text{down}} \quad \forall t \in T \tag{4.65}$$

Where:

- $P^{+,\text{aFRR}}_{\text{x},sched}(t)$ and $P^{-,\text{aFRR}}_{\text{x},sched}(t)$ represent the initial states of upward and downward ancillary frequency response reserve for system X at time t, with X being either BESS or EV.
- α_{up} and α_{down} are the probabilities that $P^{+,\text{aFRR}}_{\text{x}}(t)$ and $P^{-,\text{aFRR}}_{\text{x}}(t)$ respectively, remain equal to $P^{+,\text{aFRR}}_{\text{x},sched}(t)$ and $P^{-,\text{aFRR}}_{\text{x},sched}(t)$.
- $1 - \alpha_{\text{up}}$ and $1 - \alpha_{\text{down}}$ are the probabilities that $P^{+,\text{aFRR}}_{\text{x}}(t)$ and $P^{-,\text{aFRR}}_{\text{x}}(t)$ respectively, change to 0.

4.6. Objective Function

The model's primary goal is to minimize the total energy costs. This is formulated in Equation (4.66), which breaks down into three key components: penalties costs (P_{EV}, P_{PV}, P_{HP}), grid energy costs (C_{grid}), and aFRR earnings (C_{aFRR}). The penalties are detailed in Equations (4.67)-(4.69). In these equations, O denotes the occupancy of a building i at time t and p_{ev}, p_{pv}, p_{hp} the individually assigned penalties. With the penalties inside the objective function, they function as soft constraints. By increasing or decreasing the weight of each penalty, the model can be adjusted for different objectives. For example, p_{ev} and p_{pv} can be increased until no EV departs with a less-than-requested SoC, and all produced PV power is used. λ_{buy} and λ_{sell} represent the day-ahead prices for purchasing and selling energy, respectively. Similarly, λ_{down} and λ_{up} are the prices associated with aFRR. The term ΔTe indicates the temperature variation from the acceptable range in the buildings. Lastly, Equations (4.70), (4.72) and

$$C_{\text{tot}}(n) = \min(P_{\text{EV}}(n) + P_{\text{PV}}(n) + P_{\text{HP}}(n) + C_{\text{grid}}(n) - C_{\text{aFRR}}(n)) \tag{4.66}$$

$$P_{\mathrm{EV}}(n) = p_{\mathrm{ev}} \times \sum_{i=1}^{I} \left(E_{\mathrm{EV}}^{\mathrm{dep}}(n,i,t) - E_{\mathrm{EV}}^{\mathrm{end}}(n,i,t) \right), \quad \text{for} \quad t = T_d^{n,i} \tag{4.67}$$

$$P_{\mathrm{PV}}(n) = p_{\mathrm{pv}} \times \sum_{b=1}^{B} \sum_{t=1}^{T} \Delta t \left(P_{\mathrm{PV}}^{\mathrm{max}}(n,b,t) - P_{\mathrm{PV}}(n,b,t) \right), \quad \forall t \in T \tag{4.68}$$

$$P_{\mathrm{HP}}(n) = p_{\mathrm{hp}} \times \sum_{b=1}^{B} \sum_{t=1}^{T} \Delta t \left(\Delta Te(n,b,t) \times \mathrm{O}(n,b,t) \right), \quad \forall t \in T \tag{4.69}$$

$$P_{\mathrm{tot}} = \sum_{n=1}^{N} P_{\mathrm{EV}}(n) + P_{\mathrm{HP}}(n) + P_{\mathrm{PV}}(n) \quad \forall t \in T \tag{4.70}$$

$$C_{\mathrm{grid}}(n) = \sum_{t=1}^{T} \Delta t \left(P_{\mathrm{grid}}^{+}(n,t) \times \lambda_{\mathrm{buy}}(t) \right) - P_{\mathrm{grid}}^{-}(n,t) \times \lambda_{\mathrm{sell}}(t) \Big), \quad \forall t \in T \tag{4.71}$$

$$C_{\mathrm{grid,\ tot}} = \sum_{n=1}^{N} C_{\mathrm{grid}}(n) \tag{4.72}$$

$$C_{\mathrm{aFRR}}(n) = \sum_{t=1}^{T} \Delta t \left((P_{\mathrm{EV}}^{+,\mathrm{aFRR}} + P_{\mathrm{BESS}}^{+,\mathrm{aFRR}}) \times \lambda_{\mathrm{down}}(t) + (P_{\mathrm{EV}}^{-,\mathrm{aFRR}} + P_{\mathrm{BESS}}^{-,\mathrm{aFRR}}) \times \lambda_{\mathrm{up}}(t) \right), \quad \forall t \in T \tag{4.73}$$

5

Data Inputs and Case Studies

This chapter delves into how data inputs and case studies operate within a smart grid optimization framework. We begin by explaining the input models, which simulate different types of buildings and their energy setups. Then, we discuss a two-step optimisation process: one-shot and rolling horizon optimisation, which helps manage energy use effectively. We also explore the complexities of pricing structures and present six case studies that investigate various synergies of smart grid operations. Finally, we address the assumptions of the model used to approach real-world scenarios.

5.1. Input models

The optimisation process simulates three distinct nodes in parallel: a residential, commercial, and mixed node. Each node is composed of five buildings, with the residential node containing exclusively residential buildings, the commercial node exclusively commercial buildings, and the mixed-use node a mix of both. Each building contains a unique generation profile of 12 PV modules. Similarly, the nodes are equipped with chargers that correspond to their type: residential nodes feature home chargers, commercial nodes are equipped with public and semi-public chargers, and mixed-use nodes contain a randomly assigned mix of all charger types. Each building and charger type follows a specific occupation and power profile simulated in external models.

	Node 1	Node 2	Node 3
Residential Build.	5	0	2
Commercial Build.	0	3	3
Public Chr.	0	2	2
Semi-public Chr.	0	2	0
Home Chr.	4	2	3
BESS	1	1	1

Table 5.1.1: Number of buildings per node.

5.1.1. HP and Building model

This optimisation uses three input models; a PV, EV and HP and a building model. The models for heat pumps and buildings in this study are based on the design presented in Damianakis et al. (2023). This design includes a simulator for managing power consumption and building temperature, suitable for both residential and commercial buildings. The simulator operates with air-sourced heat pumps (ASHPs) for space heating and domestic hot water (DHW) management. It incorporates variables like building occupancy schedules, HP specifications, insulation quality, and weather data. The simulator's goal is to maintain indoor temperatures within a comfortable range (typically 21°C to 23°C) while occupied, effectively calculating the energy consumption of the heat pumps. To add variety to the simulation, over 200 distinct HP consumption profiles for residential and commercial buildings were generated. These profiles are based on a standard HP-rated power of 3 kW and are randomised by altering building occupancy schedules. Additionally, normal distributions were introduced to simulate

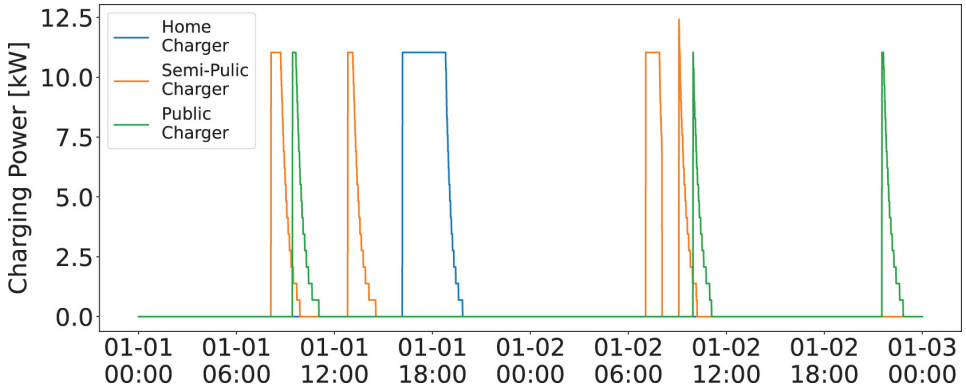

Figure 5.1.2: Typical EV Charging Profiles of Home, Semi-Public & Public Chargers (2 days duration). Reprinted from Damianakis et al. (2023).

the daily routines of occupants, such as the times of leaving and returning to their residences, typically around 08:00 and 14:00. This method allows for a more realistic representation of energy consumption patterns in daily life. Figure 5.1.1 shows the HP power consumption profile and building temperature for both winter (heating) and summer (cooling) days. These profiles depicted in Figure 5.1.1 represent uncontrolled HPs, where no building occupation profiles are considered. The temperature always stays within the comfort range (21°-23°), except for hours when the building is not occupied (08:00-14:00).

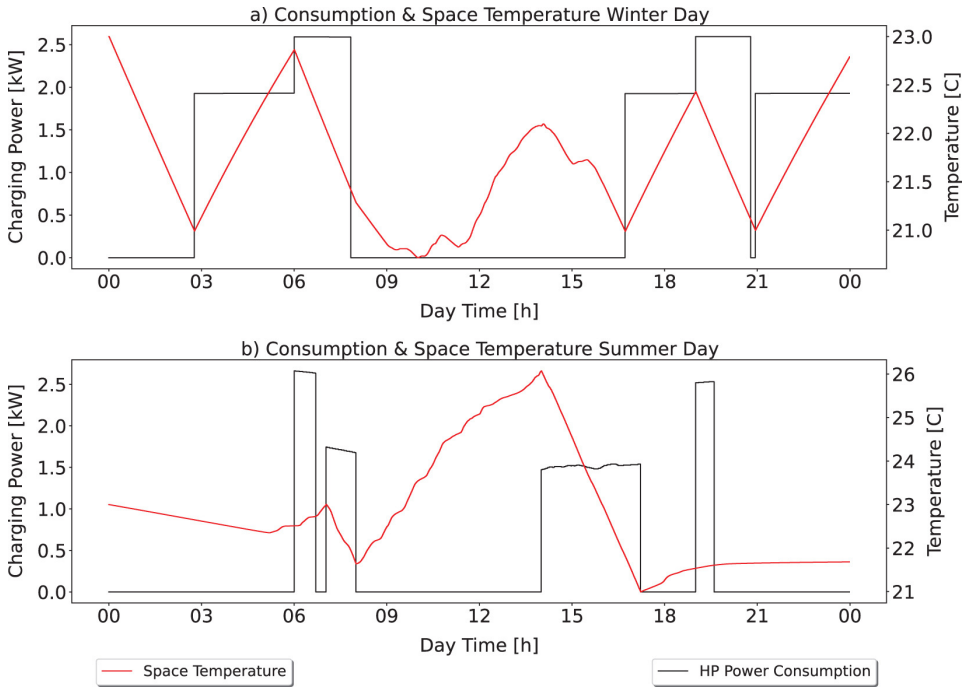

Figure 5.1.1: Power Consumption & Space Temperature at Residential Buildings. Reprinted from Damianakis et al. (2023).

5.1.2. EV model

The EV model used in this thesis is taken from the extensive research from Damianakis et al. (2023). In this model, a Monte-Carlo Simulation (MCS) is used to create 200 weekly profiles for electric vehicles (EVs) at three different charging locations: Home, Semi-Public, and Public. These profiles are then randomly distributed across the chargers in the grid simulation. The EV pool includes models such as 'Kona, I3, I-Pace, and Model 3' with a rated power of 11 kW, 'Model X and Model S' at 16 kW, and the 'Zoe' at 22 kW. All bi-directional chargers are assumed to be capable of providing a maximum power of 22 kW in both directions. Home Chargers are characterised by a lower frequency of use but with higher energy requests compared to Semi-Public and Public chargers, see Figure (5.1.2).

The model also differentiates between weekday and weekend charging patterns. For example, an EV is typically charged three times during weekdays and once at weekends at a home charger. Additionally, the Constant Current-Constant Voltage (CC-CV) charging phase is incorporated into the model using a linear approximation using Equation (4.8)-(4.10) and (4.14).

Seasonal variations in EV charging are also taken into account, with a 30% increase in energy consumption during winter, as displayed in Equation (5.1) and (5.2), with $SoC^{win}_{\text{EV,arr}}$ and E^{win}_{dep} the arrival SoC and requested energy respectively (Damianakis et al., 2023).

$$SoC^{win}_{\text{EV,arr}} = 1.3SoC^{sum}_{\text{EV,arr}} - 0.3SoC^{sum}_{\text{EV,arr}} \tag{5.1}$$

$$E^{win}_{dep} = (SoC_{\text{EV,dep}} - SoC^{win}_{\text{EV,arr}})E^{\text{rated}}_{\text{EV}} \tag{5.2}$$

This adjustment is based on data analysis from 7500 EVs, indicating higher energy consumption in summer due to various factors such as minimal temperature adjustments inside the EV, pre-cooling capabilities while plugged in, optimal tyre pressure, and battery operations within their preferred conditions. The model focuses on the Netherlands, where winters are typically harsher than summers, affecting energy consumption due to the difference in ambient and interior EV temperatures. This impacts the heating and cooling coefficients of performance (COPs) and, subsequently, the power consumption.

5.1.3. PV Model

The upcoming section details a model for solar photovoltaic (PV) systems, based on the work done by Damianakis et al. (2023). This model calculates the solar angle of incidence to estimate the potential solar power on different surfaces. In the model, a basic sky model estimates diffuse solar irradiance, leaving out the effects of shading from surrounding structures. The temperature of the PV modules is influenced by a mix of factors: the ambient temperature, the wind's speed, and the total solar irradiance, which includes direct, diffuse, and reflected sunlight. These factors collectively determine the module's operational temperature, which influences the output efficiency. Module efficiency dips as temperatures climb, which is factored into the model using temperature coefficients. These adjust the power output at the maximum power point (MPP) and the module efficiency according to the solar irradiance level. To reflect the variety of rooftop angles and orientations within a grid, the model generates multiple PV generation profiles. These profiles are designed to capture the variation in solar power generation between summer and winter, acknowledging the impact of seasonal changes.

5.1.4. Grid Constraints

In the localised grid, a total of fifteen buildings are distributed across three nodes, with the constraint that no node consists of more than five buildings, to manage the load distribution effectively. The maximum grid input and output constraints are based on the type of electrical connections available, as explained in Table 5.1.2. A 1-phase connection typically supports lower power requirements, such as those found in residential settings with basic appliances and possibly a small number of solar panels. The 3-phase connections, however, is suitable for higher power demands, such as residential buildings with additional high-power devices, small businesses, and commercial locations with significantly higher energy needs. In the simulation, eight Standard Residential buildings require a 3 x 25 amps connection to support common household appliances along with solar panels and electric vehicle charging. The two Heavy Residential buildings, with a 3 x 35 amps connection, can support additional high-power devices like saunas or hot tubs. The inclusion of two Small Commercial buildings at 3 x 50 amps and three Heavy-Small Commercial buildings at 3 x 63 amps reflects the mix of commercial activities that demand a stronger energy infrastructure, such as offices and stores.

All nodes combined request a peak power output close to 400 kW at the standard grid voltage of 230V. The maximum grid power constraints are put at 400 kW distributed evenly across the nodes (in both directions) and must ensure that the total power draw does not exceed the grid capacity while simultaneously meeting the requirements of residential and commercial users. This balance is critical in preventing overloads and ensuring that all connected loads have reliable access to electricity for their needs.

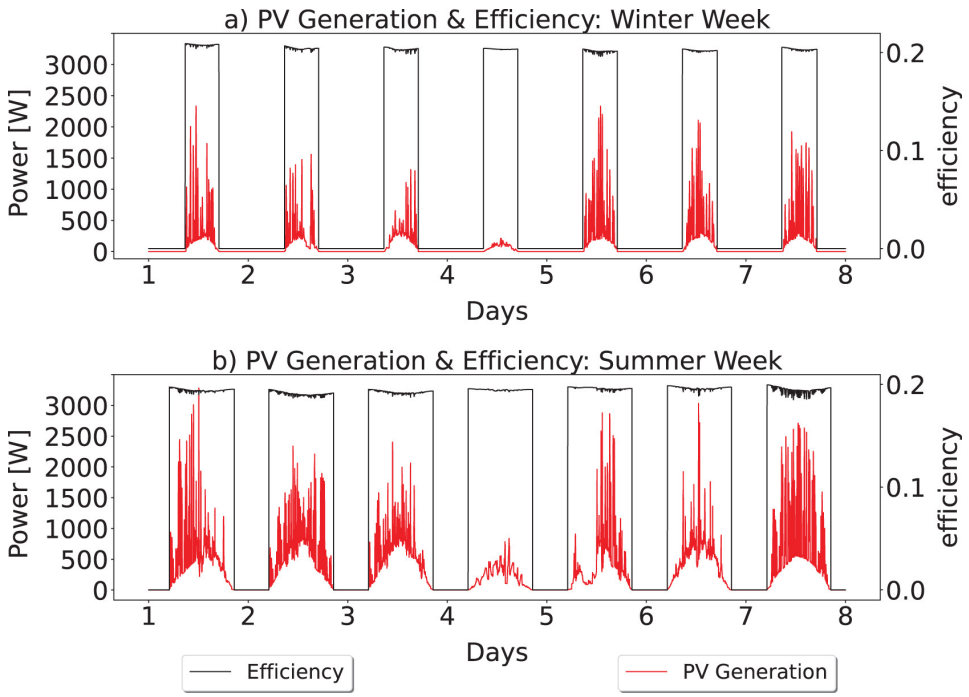

Figure 5.1.3: PV Rooftop 3 kW-rated Power & efficiency for (a) Winter & (b) Summer (tiltangle = 30°, azimuth = 180°). Reprinted from Damianakis, Mouli, Bauer, & Yu (2023) Damianakis et al. (2023).

Type	Elements	Size
Garage box	Garage door, lighting	1 x 10 Amps
Small Residential	Washing machine, oven, lighting, a small amount of solar panels	1 x 35 Amps
Standard Residential	Solar panels, induction cooking, heat pump, EV charger	3 x 25 Amps
Heavy Residential	Standard Residential + heavy loads (sauna or bubble bath etc.)	3 x 35 Amps
Small Commercial	Regular store	3 x 50 Amps
Heavy-Small Commercial	Office	3 x 63 Amps
Heavy Commercial	Business with heavy loads (public pools, tennis clubs, large saunas)	3 x 80 Amps

Table 5.1.2: Grid Connections by Type and Loads. Data retrieved from Enexis Netbeheer (n.d.)

5.1.5. Optimisation Penalties

The penalties p_{ev}, p_{pv}, p_{hp} can be adjusted for different objectives. Each penalty is assigned in its own way, see Table 5.1.3. There are three objective of this optimisation; EV SoC satisfaction, thermal comfort and PV self-consummation. Each penalty is increased until the sums P_{ev}, P_{pv}, P_{hp} are zero. p_{ev} is assigned per percent the SoC_{end} differs from the predetermined SoC_{dep}, for $SoC_{end} < 0.98$. In addition, the model takes into account the special situation when it is not possible to charge the required energy, even at $P_{\text{EV}}^{\text{char,max}}$ during the full connection period. Both thermal comfort and EV SoC satisfaction arise from the importance of avoiding any discomfort for the consumer; cars must be charged so nobody arrives late to work and the building environment must be comfortable. In addition, 100% PV self-consumption is desired for two reasons; the future regulatory framework of PV feed-in

prices is uncertain and PV self-consumption relieves grid pressure.

Penalty	Unit	Value
p_{ev}	10	$[EUR/(1\% * \Delta SoC]$
p_{hp}	10	$[EUR/(1°C * \Delta t)]$
p_{pv}	10^5	$[EUR/(kW * \Delta t)]$

Table 5.1.3: Optimisation parameters: Penalties.

5.1.6. Price Model

The pricing structures for the day-ahead market and imbalance prices are complex. Figure 5.3.1 illustrates the causal framework within the imbalance market, noting that the process of balancing imbalances with neighbouring countries, known as imbalance netting, is not included in this research. While the primary emphasis is on imbalance and day-ahead prices, it is crucial to recognize that intraday prices play a significant role for Balance Responsible Parties (BRPs) in acquiring last-minute energy for their consumers.

The relation between day-ahead, intraday, and imbalance prices is intricate. The day-ahead price impacts the intraday market and, subsequently, influences imbalance prices. In this study, day-ahead prices are used for the one-shot optimisation of the model. The model anticipates the events of the next day and schedules aFRR power based on the imbalance prices, which are presumed to be perfectly predicted for the purposes of the simulation. Data for both prices are taken from the Tennet historic price database “Tennet” (n.d.).

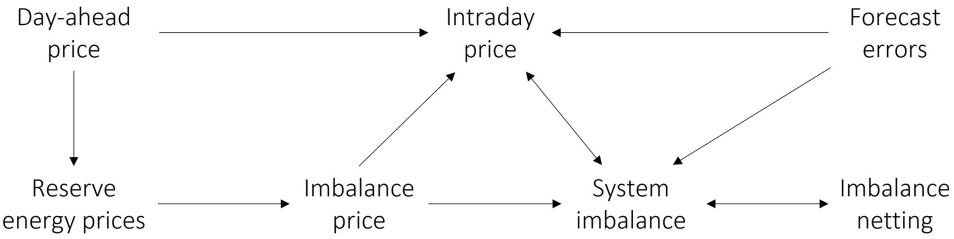

Figure 5.1.4: Visual representation of the causal effects in the imbalance market. Reprinted from Eicke et al. (2021).

5.2. Case Studies

To investigate the synergy of different loads, six case studies are conducted. Each case study investigates a unique aspect of the localised smart grid, focusing on the aFRR capabilities of the EVs and BESSs and how they affect the total grid costs. In each case study, some constraints are either removed or added. Since only BSPs can offer ancillary power, each aFRR providing assets is considered as a stand-alone facility. The objective in Case 0-5 is to minimise the grid costs, therefore maximising the aFRR revenue, ignoring any effects of passive balancing. The equations stated per case are considered as separate instances, where all other equations according to Table 4.1.1 are active. Constraining variables to zero is dominant over all other variables regarding a specific EV or BESS.

5.2.1. Case 0: No BESS, No aFRR, No V2N

This scenario represents a basic grid setup without any advanced energy management strategies. It lacks battery energy storage systems, aFRR services, and V2N capabilities. As a baseline for comparison, it allows observation of grid performance in the absence of these technologies. The combination of Equations (5.3)-(5.5) are only active in Case 0.

$$P_{\text{EV}}^{\text{-,aFRR}}(i,t) = P_{\text{EV}}^{\text{+,aFRR}}(i,t) = 0 \quad \forall t \in T \tag{5.3}$$

$$P_{\text{BESS}}^{\text{-,aFRR}}(n,t) = P_{\text{BESS}}^{\text{+,aFRR}}(n,t) = 0 \quad \forall t \in T \tag{5.4}$$

$$P_{EV}^{-}(i,t) = P_{BESS}^{+}(n,t) = P_{BESS}^{-}(n,t) = 0 \quad \forall t \in T \tag{5.5}$$

5.2.2. Case 1: No BESS, No aFRR, With V2N

In this setup, the grid does not have BESS or aFRR but utilises V2N technology. This case assesses the effectiveness of V2N in node load management and its capacity to compensate for the lack of BESS and aFRR. The constraints displayed in Equation (5.6)-(5.8) are active in Case 1.

$$P_{\text{EV}}^{\text{-,aFRR}}(i,t) = P_{\text{EV}}^{\text{+,aFRR}}(i,t) = 0 \quad \forall t \in T \tag{5.6}$$

$$P_{\text{BESS}}^{\text{-,aFRR}}(n,t) = P_{\text{BESS}}^{\text{+,aFRR}}(n,t) = 0 \quad \forall t \in T \tag{5.7}$$

$$P_{BESS}^{+}(n,t) = P_{BESS}^{-}(n,t) = 0 \quad \forall t \in T \tag{5.8}$$

5.2.3. Case 2: BESS (Self-consumption), V2N, No aFRR

This scenario involves BESS focused on self-consumption, combined with V2N but without aFRR services. The key observations include the collective impact of BESS and V2N on grid stability and energy cost reduction. In Case 2, only Equation (5.10) is active and different from the MIP formulation given in chapter 4.

$$P_{\text{EV}}^{\text{-,aFRR}}(i,t) = P_{\text{EV}}^{\text{+,aFRR}}(i,t) = 0 \quad \forall t \in T \tag{5.9}$$

$$P_{\text{BESS}}^{\text{-,aFRR}}(n,t) = P_{\text{BESS}}^{\text{+,aFRR}}(n,t) = 0 \quad \forall t \in T \tag{5.10}$$

5.2.4. Case 3: No BESS, With V2N and EV aFRR

Without BESS, this setup utilises EVs for aFRR and V2N. It highlights the capability of EVs in grid management through aFRR and V2N, especially in the absence of BESS. Equations (5.11)-(5.12) are active in Case 3.

$$P_{\text{BESS}}^{\text{-,aFRR}}(n,t) = P_{\text{BESS}}^{\text{+,aFRR}}(n,t) = 0 \quad \forall t \in T \tag{5.11}$$

$$P_{BESS}^{+}(i,t) = P_{BESS}^{-}(i,t) = 0 \quad \forall t \in T \tag{5.12}$$

5.2.5. Case 4: BESS (Self-consumption), V2N, Combined aFRR

This setup combines BESS for self-consumption, aFRR services, and V2N capabilities. It demonstrates the combined effect of all three technologies on cost-effectiveness. In Case 4 no constraints different from the list of equations in Table 4.1.1 are active.

5.2.6. Case 5: BESS (Self-consumption) and aFRR, no EV

Involving aFRR activities and self-consumption from BESS only, this case focuses on the potential of the technology in passive balancing, ancillary services and the impact on the overall cost of energy. Equation (5.13) is active in Case 5 to enable BESS and EV to charge, but disable to discharge into the node.

$$P_{\text{EV}}^{\text{-,aFRR}}(i,t) = P_{\text{EV}}^{\text{+,aFRR}}(i,t) = P_{EV}^{-}(i,t) = 0 \tag{5.13}$$

Case	BESS: B2N	BESS: aFRR	EV: V2N	EV: aFRR
Case 0				
Case 1			✓	
Case 2	✓		✓	
Case 3			✓	✓
Case 4	✓	✓	✓	✓
Case 5	✓	✓		

Table 5.2.1: Technologies and applications used in each case study

5.3. Passive Balancing Case

Post optimisation, using the same objective Equation (4.66), the grid position for Case X relative to the base case (Case 0) is determined for each node at each timestep. In this scenario, the power that was initially allocated for aFRR is considered as standard imported and exported energy, leading to the elimination of the BSP player from the simulation. Consequently, this situation explores the impact of passive balancing on a BRP portfolio, under the assumption of perfect imbalance price prediction. Looking back at Paragraph 2.4, Case 0 acts as the E-program, and Case X demonstrates the effect of introducing flexibility in the localised controlled grid on a BRP's portfolio. This relative position is determined by the net energy injections or withdrawals (imports minus exports) and adjustments from BESS and EV aFRR downward or upward power. A positive position value for Case X indicates a portfolio surplus (more energy is either injected or less is withdrawn than Case 0), while a negative position value indicates a portfolio shortage (less energy is injected or more is withdrawn than Case 0). From Equation (4.66) it can be seen that, within the optimisation, only $P_{\mathrm{x}}^{-,\mathrm{aFRR}}$ and $P_{\mathrm{x}}^{+,\mathrm{aFRR}}$ consider the imbalance prices. However, since the day-ahead price is linked to the imbalance price Eicke et al. (2021), both aFRR as self-consumption cases (Case 3,4,5 and Case 1,2 respectively) can influence the dynamics of passive balancing since the performance of passive balancing is directly linked to the imbalance price.

$$\begin{aligned}\Delta P_{\mathrm{x}}(n,t) = P_0^+(n,t) - P_0^-(n,t) + P_{0,\mathrm{x}}^{\mathrm{aFRR}}(n,t) \\ - (P_{\mathrm{X}}^+(n,t) - P_{\mathrm{X}}^-(n,t) + P_{\mathrm{X,x}}^{\mathrm{aFRR}}(n,t))\end{aligned} \tag{5.14}$$

Equation (5.14) calculates the relative position differences for each node by comparing its energy balance in Case X with the base case (Case 0). The energy balance is determined by net imports (P^+) minus exports (P^-) adjusted for BESS and EV activity ($P_{\mathrm{x}}^{\mathrm{aFRR}}$). Where n is the node index, and t is the time index, x can represent EV, BESS, or the sum of both contributions and X indicates the case number. The function stores these differences for each node, reflecting how the node's position has changed from the base case. Each case is simulated for the same calendar day, which results in identical base loads, EV arrivals and PV production.

$$C_{\mathrm{passive}}(n,t) = \sum_{t=1}^{T} \Delta t(\Delta P_{\mathrm{x}}(n,t) \times \lambda_{\mathrm{down}}(t) + \Delta P_{\mathrm{x}}(n,t) \times \lambda_{\mathrm{up}}(t)\big), \quad \forall i,t \tag{5.15}$$

Equation (5.15) assesses the financial implications of the calculated position differences based on the imbalance prices. It multiplies the position differences by the corresponding imbalance prices, considering the direction of payments (earnings or losses) as defined by the market rules. The financial impact is modelled as zero if both upward and downward imbalance prices are zero or when both prices are non-zero, reflecting regulation state 0 and 2 respectively. During these regulation states, the TSO uses the mid-price in some instances to reimburse or charge the BRP for its portfolio imbalance. Since the model does not schedule ancillary power during these regulation states, the effects are considered to be negligible.

$$C_{\text{grid,passive}}(n,t) = \sum_{t=1}^{T_{\text{sim}}} \Delta t \Big((P^{+}_{\text{grid}}(n,t) + P_{\text{x}}^{+,\text{aFRR}}(n,t)) \times \lambda_{\text{buy}}(n,t) - (P^{-}_{\text{grid}}(n,t) + P_{\text{x}}^{-,\text{aFRR}}(n,t)) \times \lambda_{\text{sell}}(n,t) \Big), \quad \forall t \tag{5.16}$$

$$C_{\text{aFRR}} = 0 \tag{5.17}$$

In addition, the cost Equation (4.71) needs to be updated to add the downward and upward power to the cost of imported power and exported power respectively. In the passive balancing case, the scheduled downward aFRR power is treated as regular imported power which has to be bought against the electricity prices of that time step, see Equation (5.16). The scheduled upward power is modelled against two scenarios; upward power is sold against a feed-in tariff, similar to PV production, or upward power is sold against 0 EUR/MWh to see the effect of passive balancing without feed-in tariff price uncertainties. In both cases, $C_{\text{aFRR}} = 0$.

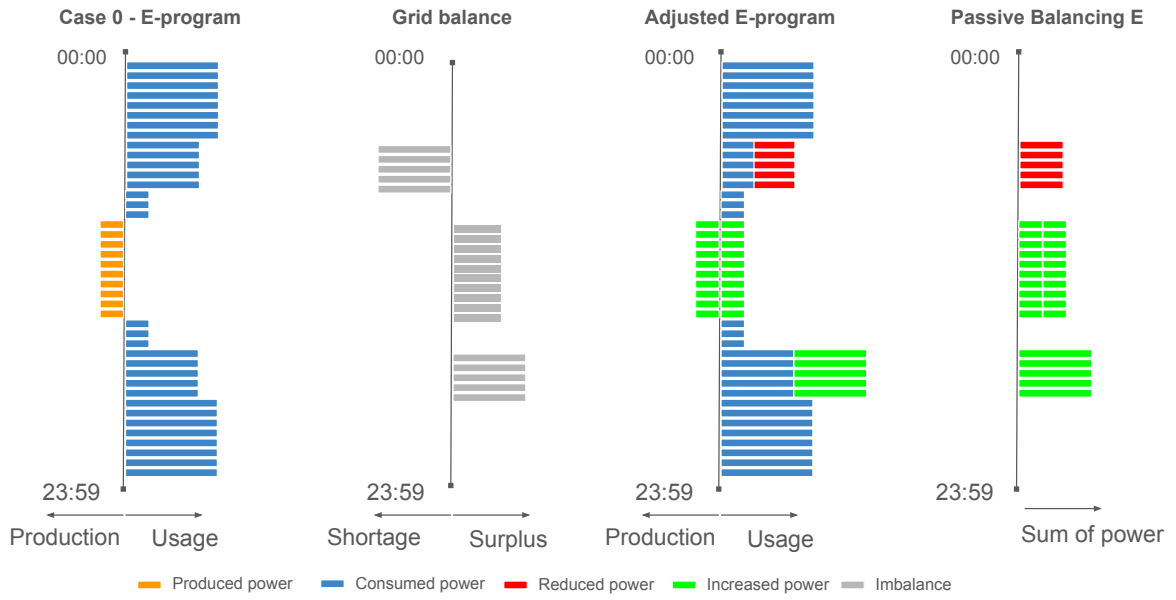

Figure 5.3.1: Visual representation of the passive balancing process. From left to right: base case containing originally scheduled E-program (D-1), grid imbalance position (D), adjusted E-program (D) , total passive balanced power (D).

Variable	Symbol	Value
Building Thermal Capacity	C_b	4.755 kWh/K
Building Volume	V_b	585 m^3
Air Specific Capacity	C_{air}	0.279 Wh/kgK
Air Density	ρ_{air}	1.225 kg/m^3
Air Change Rate	r_b	0.3 kg/h^{-1}
HP Flow Water Rate	$\dot{m}_{wat}$	0.8 kg/s
Water Specific Capacity	C_{water}	1.16 Wh/kgK
HP Rated Power	P_{HP}^{rated}	3 kW
Coefficient of Performance HP	CoP	3
BESS/EV converter efficiency	η_{con}	97% (Vermeer et al., 2022)
BESS charge/discharge efficiency	η_{BESS}	98% (Vermeer et al., 2022)
EV charge/discharge efficiency	η_{EV}	98% (Vermeer et al., 2022)
PV converter efficiency	η_{PV}	98% (Mouli et al., 2017)
Upper and lower SoC limit of CC-region	$D_{\text{ch}}, D_{\text{dis}}$	0.9, 0.1
Rated Capacity BESS	$E_{\text{BESS}}^{\text{rated}}$	50 kWh
Maximum time deviation EV	K_{EV}	0 min
Maximum time Deviation Occupation	K_O	15 min
Simulation Duration	T	One Day (00:00 - 00:00)
Nodes	N	3
Buildings	B	15
Grid Voltage	V	230 V
Maximum Grid Power (total)	$P_{\text{grid}}^{-,\text{max}}, P_{\text{grid}}^{+,\text{max}}$	400 kW
Bid Acceptance Rates	α^{up}, α^{down}	1

Table 5.3.1: Parameters Overview for Building, HP, PV, Battery, and Simulation

6

Results & Discussion

This chapter presents the findings of the MIP problem which is simulated for the cases described in Paragraph 5.2 for four different years and two seasons; 2018,2019,2020,2023, Summer and Winter respectively. Due to a combination of the Covid-19 pandemic and the turbulent situation in Eastern Europe, 2021 and 2022 have been excluded from the simulation, as the market price data is non-representative of typical situations. The analysis done in this chapter aims to provide insight into the performance on the aFRR market of different flexible assets within a localised smart grid. Firstly, the nodal power flows are presented, visually showcasing the difference in grid activity between cases. After an introduction to the DAM and aFRR imbalance prices, the quantitative results of grid costs and asset aFRR activity are discussed per case, together with the effect of passive balancing on grid savings. Lastly, we focus on BESS specifics and how each case shows different BESS behaviour.

6.1. Node Power Flow

The power flows shown in Figure 6.1.1 represent all imported, exported and produced power inside the node for Case 1, which does not include BESS and EV aFRR participation but does include flexible HPs and the potential to deliver V2N power. In Case 1, as depicted in Figure 6.1.1, V2N power is activated

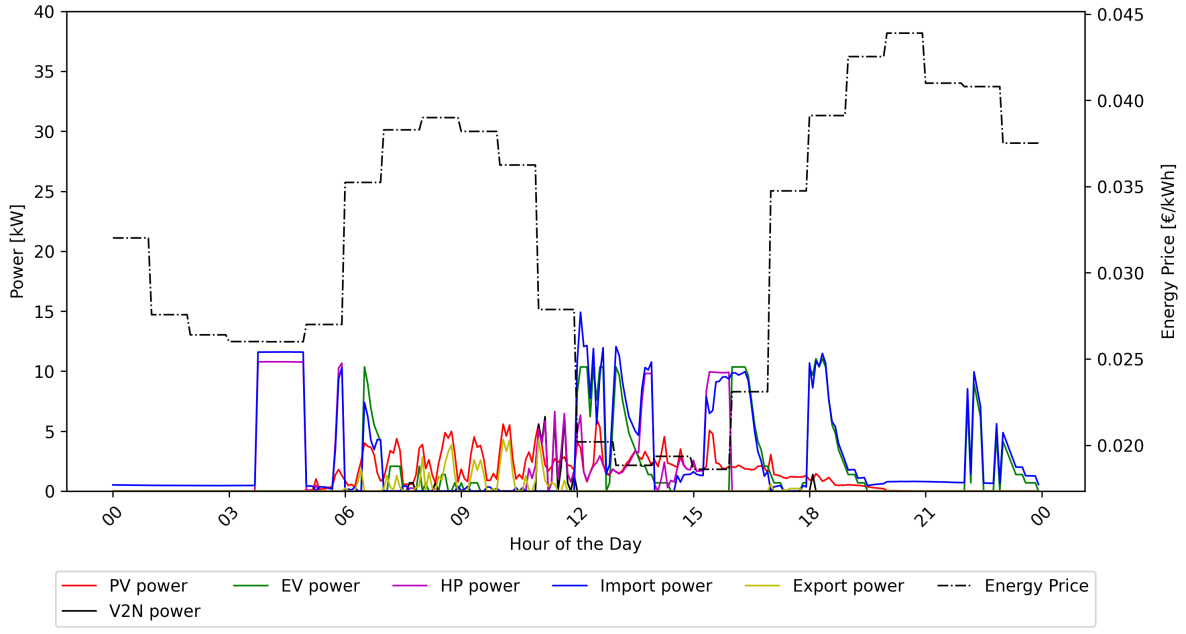

Figure 6.1.1: Nodal Power Flow and Day-Ahead Energy Price for Case 1, Summer, 2020 and Node 2: Commercial Node. For other years, see AppendixA.1

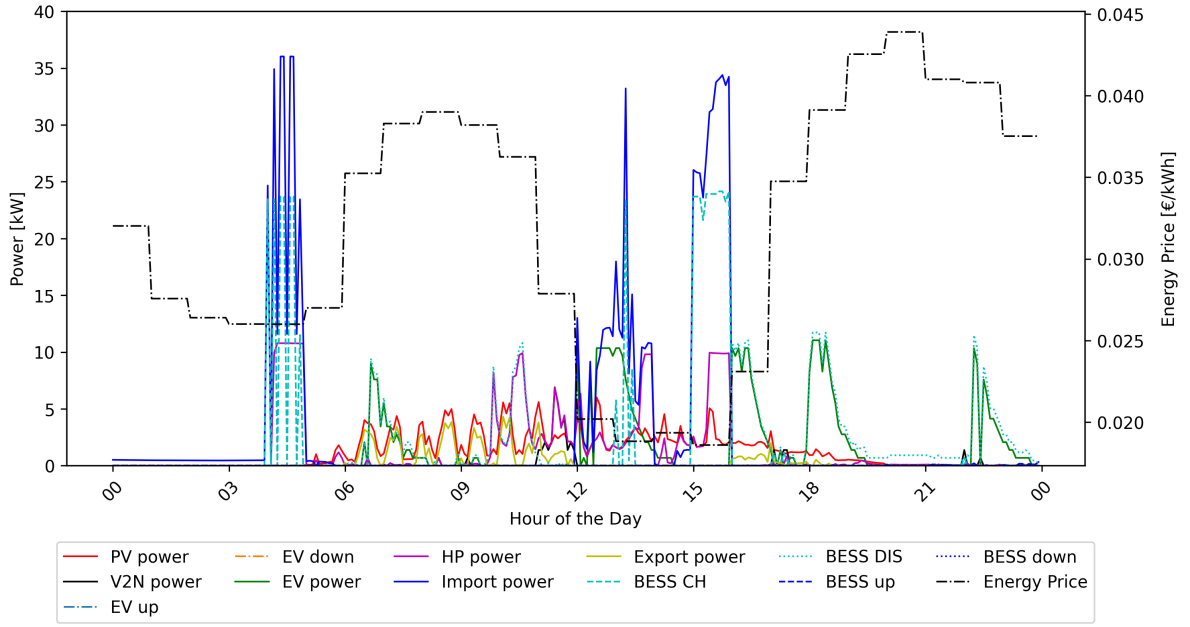

Figure 6.1.2: Nodal Power Flow and Day-Ahead Energy Price for Case 2 Summer 2020 Node 2: Commercial Node. For other years, see AppendixA.1

just before 12:00, which helps the HPs avoid using power against high DAM prices. However, V2N is heavily depending on the node type and day-ahead prices and, thus is not always present in each node. In addition, Figure 6.1.1 shows how the climate control of commercial buildings can be scheduled —note the periods between 03:00-06:00 and 12:00-15:00— to avoid high energy prices while ensuring user comfort, since $P_{\text{HP}} = 0$. In this context, the buildings act as thermal energy storage systems, with the distinction that they must maintain indoor temperatures within a specific comfort range, a constraint not typically present in conventional thermal storage systems. Furthermore, the power flows of Case 1 show that, once the sun has set and no PV power is being produced, power has to be imported against high energy prices.

Introducing B2N in Case 2 (see Figure 6.1.2) shows much higher nodal peak demand than Case 1 due to the clustering of power flows around low energy prices. Looking at the 16:00 timestamp in Figure 6.1.2 simultaneous charging of the BESS and turning on HPs have increased the nodal peak demand by 350% compared to Case 1 at the same time instance. Introducing energy storage, looking at the period between 18:00 and 00:00, both building base load and EV charging can be covered by the BESS, eliminating the need to import energy during high market prices.

Figure 6.1.3 introduces Case 4 which allows aFRR power from both EVs and BESS. Comparing Case 2 with Case 4 shows a grid with more activity between 18:00 and 03:00. Incorporating aFRR provision introduces the potential for an additional revenue stream during periods when grid loads for non-aFRR scenarios are minimal. In some instances, however, this results in the unavailability of the BESS to deliver B2N power to, for example, charge an EV. As a result, power must be imported against unfavourable energy prices as can be seen at 18:00 in Figure 6.1.3, eventually contributing to an increase in the cost of imported energy for Case 4 compared to non-aFRR cases.

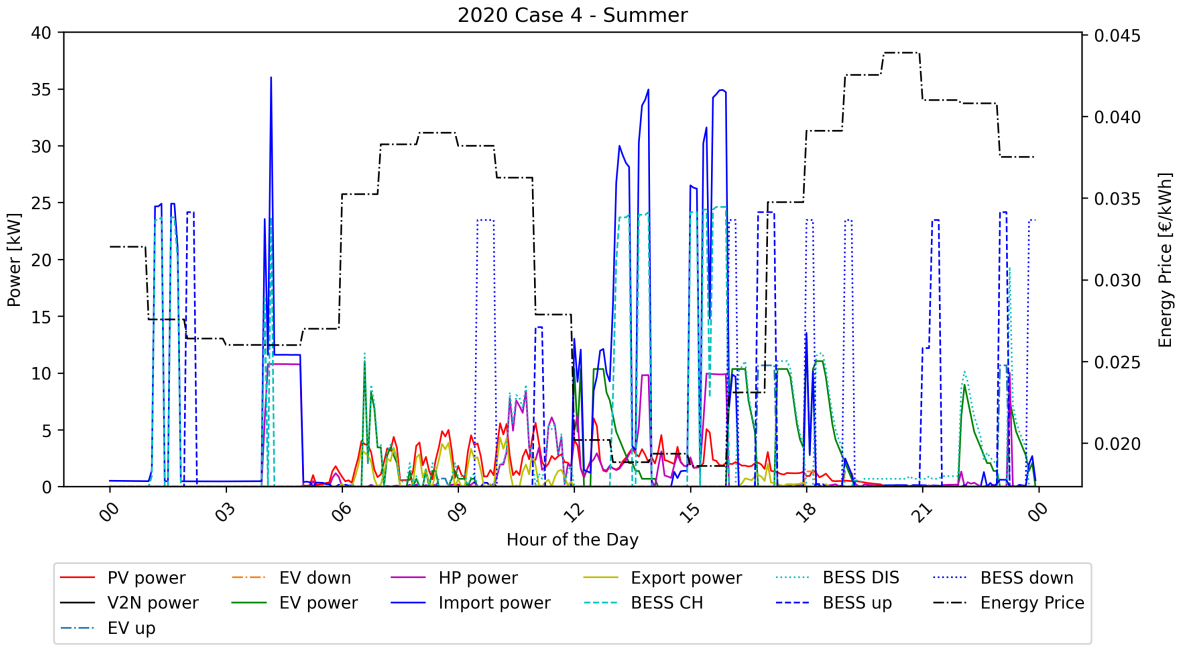

Figure 6.1.3: Nodal Power Flow and Day-Ahead Energy Price for Case 4 Summer 2020 Node 2: Commercial Node. For a version with BESS and EV power flows only, see Figure A.1.1 in the Appendix. For other years, see Appendix Chapter A.1

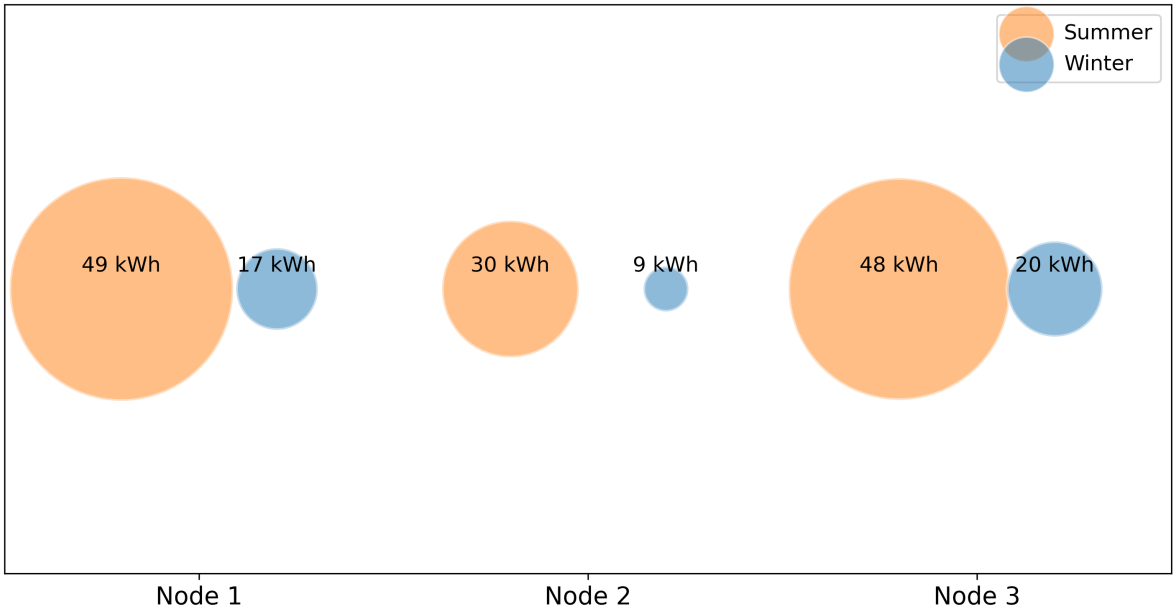

Figure 6.1.4: Total produced photovoltaic energy per node and season, uniform for all years.

Figure 6.1.4 presents a proportional area chart illustrating the photovoltaic energy production for each node, comparing summer and winter seasons. Given the geographical positioning of the Netherlands, there are notable climatic variations between seasons. These variations lead to decreased PV energy input and increased energy consumption by heat pumps and electric vehicles during winter. Consequently, there is an average increase of 72% in energy imports during the winter days compared to summer, see Figure 6.1.5.

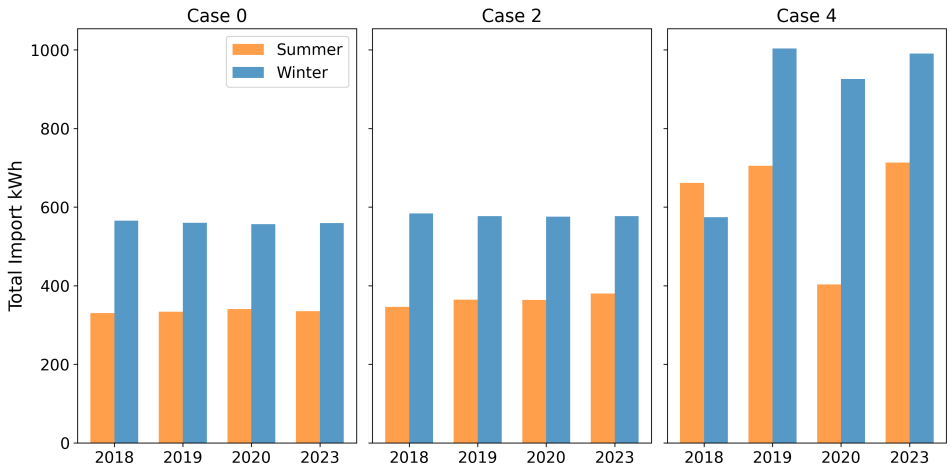

Figure 6.1.5: Sum of imported energy over all nodes, per case, year and season.

Figure 6.1.6 and 6.1.7 show the power flows for Node 3 for Summer and Winter respectively. Notably, the day-ahead prices for winter are much higher than summer for this simulated day. Because Node 3 is a mixed node, EV charging sessions are spread out more throughout the day. As a result, Node 3 consistently outperforms the other nodes in aFRR participation (aggregated upward and downward). Between 14:00-17:00 and 14:00-19:00 in Figure 6.1.6 and 6.1.7 respectively, this EV activity is visible. In addition, from the nodal power flows it is visible that most PV production is exported during high energy prices, avoiding PV self-consumption to, for example, charge BESS.

Figure 6.1.9 shows the day-ahead price distribution for both seasons. Each box plot shows the distribution of the price data for one day. Notably, the average price for 2023 lies much higher and is more spread out than for the years 2018-2020, which is expected to have an impact on grid costs, which will be discussed in Paragraph 6.2. The imbalance prices, both upward and downward, are presented in Figure 6.1.10 and 6.1.8 respectively, where imbalance prices of 0 EUR/kWh are not included in the box plots. In addition, imbalance prices are constant per ISP. The price distributions for both upward and downward adjustments reveal a significant increase in outliers in the imbalance price compared to day-ahead prices. This is primarily attributed to the mechanics of the merit order system, as introduced

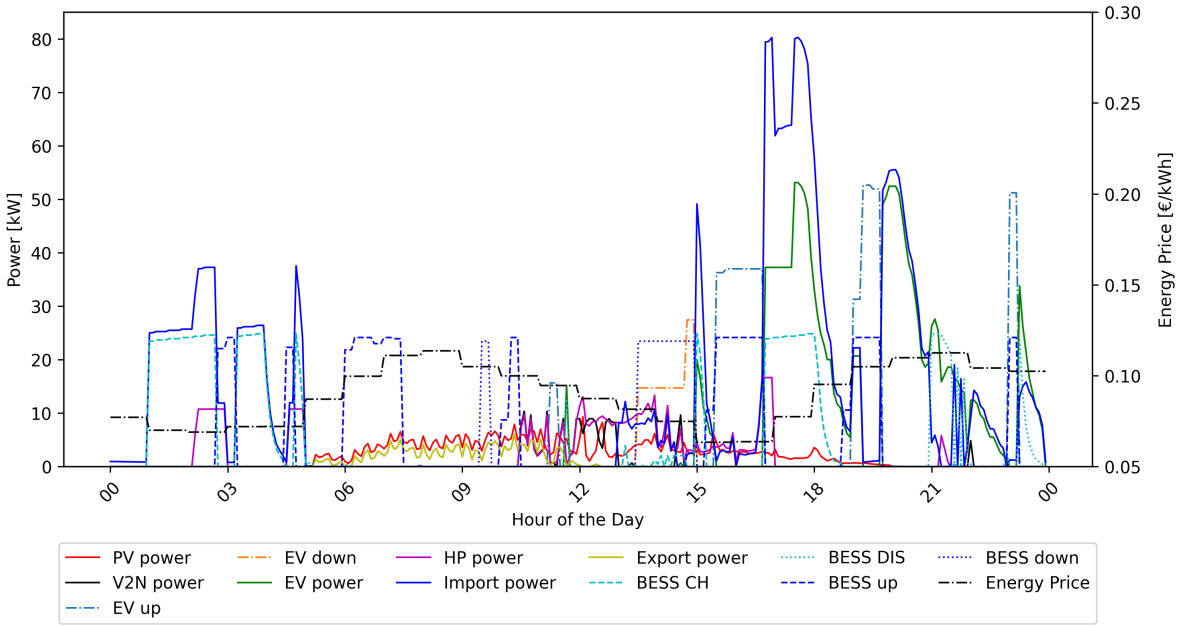

Figure 6.1.6: Nodal power flows and day-ahead energy price for case 4 summer 2023 node 3: mixed node. For a version with BESS and EV power flows only, see Figure A.1.2 in the Appendix. For other years, see AppendixA.1

earlier in Section 2.3. With a set limit price for balancing energy at 15,000 MW/h (ENTSO-E, 2024), prices can escalate dramatically during periods of significant imbalance and low availability of balancing energy. While both the imbalance and day-ahead markets operate on an auction basis where energy providers are free to set their prices, the nature of their bids can vary greatly due to differing motivations. The day-ahead market, where prices are determined through competitive bidding, reflects the expected hourly value of electricity based on supply and demand forecasts (TenneT, 2023b). This market tends to be more stable as it is not influenced by real-time events but is auctioned one day before deployment.

In contrast, the imbalance market adjusts for real-time discrepancies between forecasted and actual electricity generation and consumption, leading to more unpredictable and often higher risks. This unpredictability needs more immediate adjustments, resulting in more pronounced price fluctuations. Additionally, some BSPs in the imbalance market may not aim primarily to profit from selling imbalance energy. Instead, their strategies can include measures like temporarily shutting down operations, such as a factory, which only becomes cost-effective at higher prices. This scenario further contributes to the potential for extreme pricing, as these BSPs set their price thresholds based on the costs saved by reducing their energy consumption rather than the market demand alone. Moreover, the imbalance market is sensitive to sudden shifts in renewable energy output, unexpected power plant outages, or unanticipated demand spikes. These factors increase price volatility, contributing to the higher incidence of outliers observed in this market. In essence, while both markets use similar auction mechanisms, the critical need for real-time adjustments and the different motivations of participants in the imbalance market result in a setting where more extreme prices are more likely, compared to the forecast-driven, more stable day-ahead market. In the simulated data, certain outliers exceed the average day-ahead prices by over sevenfold, indicating the potential for substantial aFRR revenue within a short time frame. Although seasonal variations exist, the one-day simulation horizon limits conclusive observations, necessitating an examination of long-term price profiles.

The distribution of the downward imbalance prices has a considerable impact on potential aFRR earnings. As stated in Paragraph 4.5, scheduling of downward aFRR power occurs only when the downward price is negative. Therefore, looking at Figure 6.1.8, it can already be concluded that no downward aFRR power is scheduled for the winter day of 2023, resulting in zero downward aFRR revenue.

Figure 6.1.5 illustrates the cumulative imported energy over all nodes across Case 0, Case 2, and Case 4. The baseline scenario, Case 0, demonstrates minimal variance across the years, despite notable differences in energy costs. Since Case 0 only contains smart charging and heat pumps as

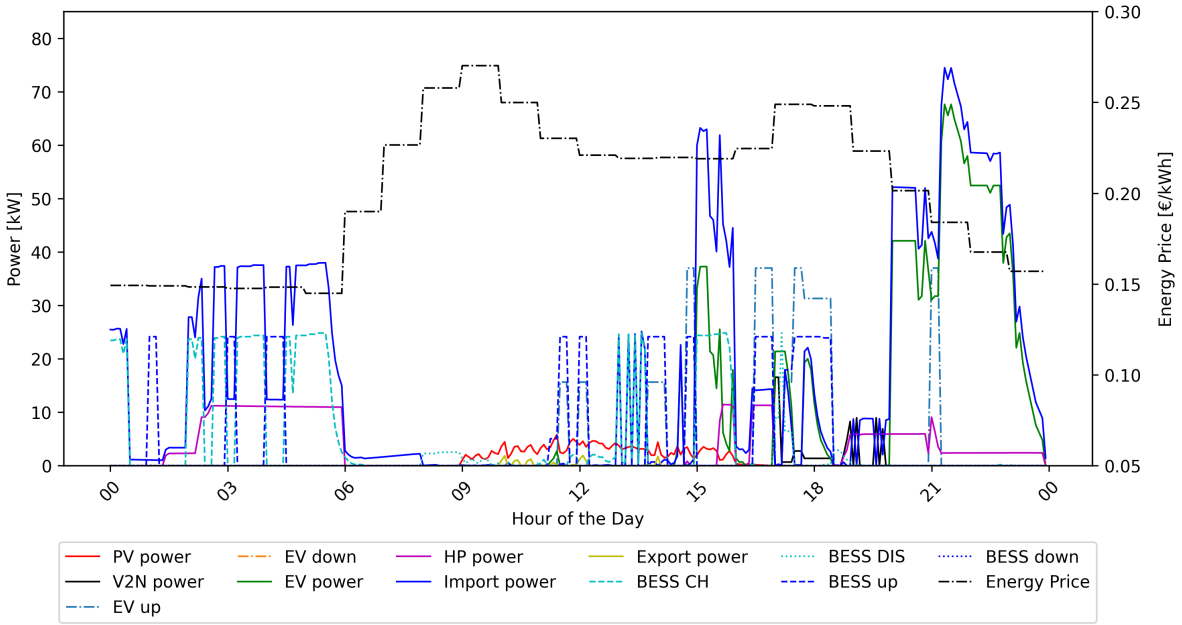

Figure 6.1.7: Nodal Power Flows and Day-Ahead Energy Price for Case 4 Winter 2023 Node 3: Mixed Node. For a version with BESS and EV power flows only, see Figure A.1.3 in the Appendix. For other years, see AppendixA.1

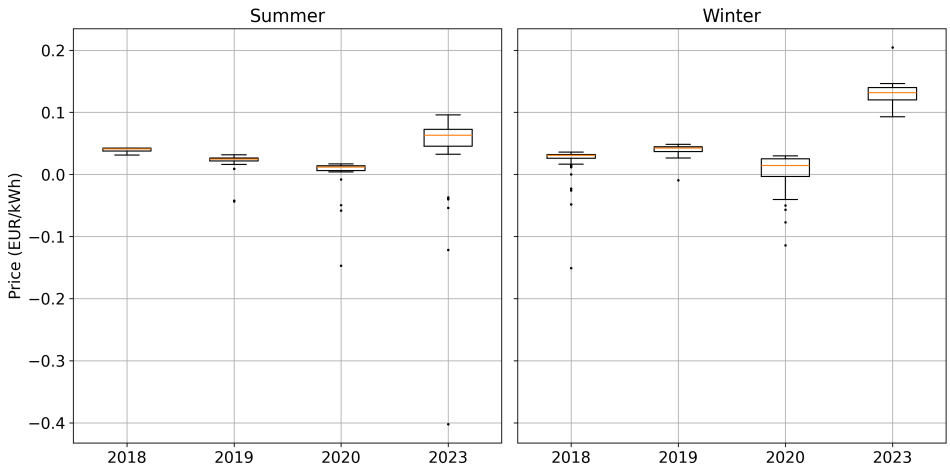

Figure 6.1.8: Distribution of downward imbalance prices for one simulated day. The box shows the interquartile range (IQR), the line inside the box indicates the median, the whiskers extend to points within 1.5 IQRs from the quartiles, and outliers are plotted as individual points. Data retrieved from Tennet TSO (2023)

flexible assets, there is little capacity to react to price fluctuations, resulting in consistent energy usage throughout the years. Case 2 only shows a slight increase in total imported energy. Case 4 however has both BESS and EVs that are able to react to price fluctuations, both imbalance and day-ahead, by charging and discharging into the node and from aFRR, resulting in more fluctuations and a higher amount of total imported energy throughout the years. In addition, wintertime energy demands are significantly higher due to lower PV energy production, higher building heat losses and higher EV energy requirements. Given the observations in the power flows and energy prices, we now turn our attention towards the financial implications, particularly concerning grid costs.

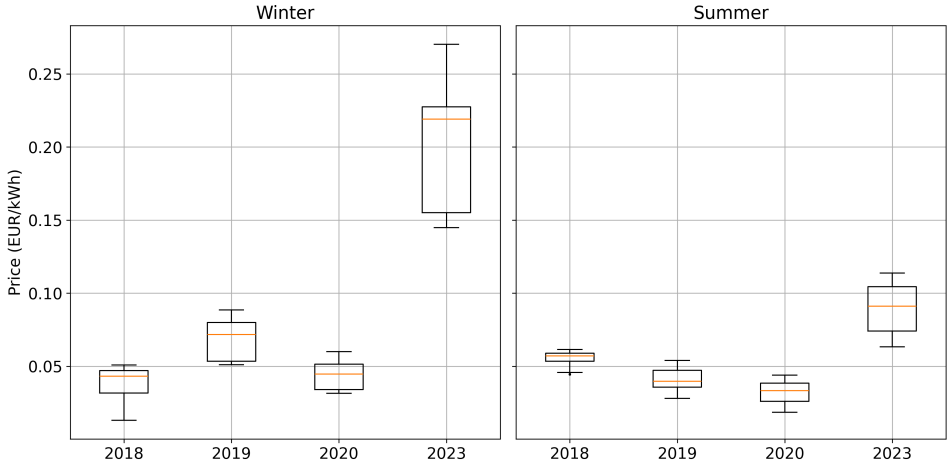

Figure 6.1.9: Distribution of day-ahead prices for one day per year and season. The box shows the interquartile range (IQR), the line inside the box indicates the median, the whiskers extend to points within 1.5 IQRs from the quartiles, and outliers are plotted as individual points. Data retrieved from Tennet TSO (2023)

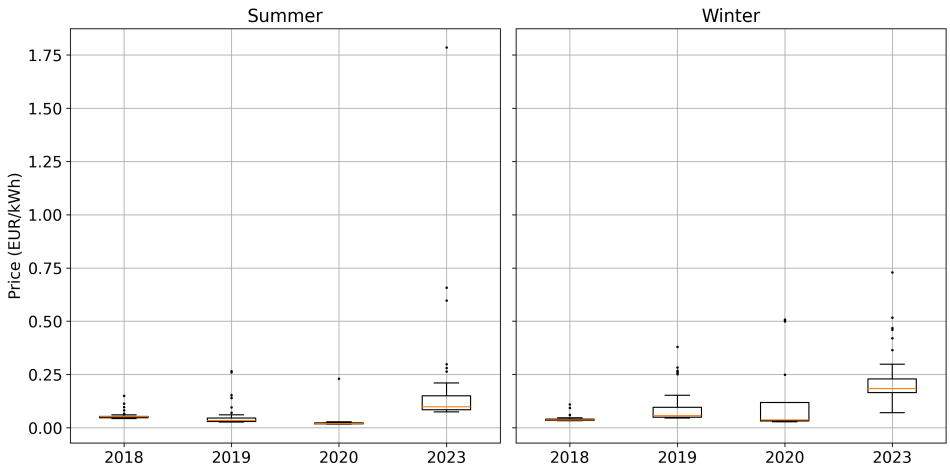

Figure 6.1.10: Distribution of upward imbalance price for one simulated day per year and season. The box shows the interquartile range (IQR), the line inside the box indicates the median, the whiskers extend to points within 1.5 IQRs from the quartiles, and outliers are plotted as individual points. One data point was removed for clarity: Value=1.6, Summer 2023. Data retrieved from Tennet TSO (2023)

6.2. Grid Costs

Given the objective function shown in 4.6, the model strives towards minimising grid costs. In Figure 6.2.1 we see the cost of imported energy across the three distinct nodes across two different seasons for the year 2023. It is important to note that the imported energy does not include downward aFRR power, since this is remunerated against the (negative) downward imbalance price. The total cost of imported energy is thus calculated by the summation of the imported energy multiplied by the day-ahead energy price, divided by the total imported energy of that node. Interestingly, Case 2 (B2N and V2N without aFRR) shows the lowest costs of imported energy due to purely optimising based on the day-ahead prices. Also, by focusing solely on minimising grid costs using day-ahead prices—essentially practice load-shifting—the addition of a BESS helps even out the average cost of imported energy for each node. Meanwhile, in other scenarios, we see more noticeable cost variations among the nodes. Secondly, due to the low amount of V2N activity, Case 1 barely shows any difference from Case 0 throughout both seasons. Incorporating aFRR in Cases 3, 4, and 5 leads to a considerable rise in the average cost of imported energy when compared to Case 2. This increase can be attributed to the BESS being charged against higher day-ahead prices. However, the additional expenses incurred are offset by the revenue generated from providing aFRR services, due to imbalance prices being higher than the day-ahead prices. Due to the one-day simulation, we focus on the differences between cases and avoid making hard conclusions based on seasonal variations. However, the increase in the cost of imported energy in winter can be attributed to the increased cost of energy in 2023, as shown in Figure 6.1.9. Consistently throughout each simulated year, Case 2 proved to produce the lowest cost of imported energy, see Appendix A.2. In addition, in all years except 2018, the cost of imported energy was higher in winter than in summer, which is in line with the findings in Figure 6.1.9.

The increase in aFRR provision becomes visible in Figure 6.2.2, which shows the aggregated grid costs over all nodes, including aFRR revenue, for each case, year and season. Cases 0 and 1, as we might expect given the average cost of imported energy, show minimal variation in their total grid costs due to the absence of additional revenue streams like aFRR. The most notable variation between these two cases is a slight reduction of 2.17% in Case 1 during the summer day of 2018, as stated in Table 6.2.1.

Shifting the focus to Case 2, there is a clear reduction in grid costs, marked by a significant 28.25% drop during the summer of 2020. This trend of cost reduction is continued in Case 3 with the introduction of EV aFRR provision, with a significant 230.86% cost decrease in the summer of 2023, thus resulting in a profit as indicated by the negative grid costs in Figure (6.2.2). This highlights the potential impact of including EV aFRR in strategies aimed at reducing localised grid costs.

Case 4 however, jumps out by reversing grid costs into profits in most cases, particularly in 2023 with a 650.21% decrease when compared to Case 0 of the same year and season. Similarly, Case 5 reveals significant reductions in grid costs, peaking at a 414.23% decrease in the summer of 2023. This

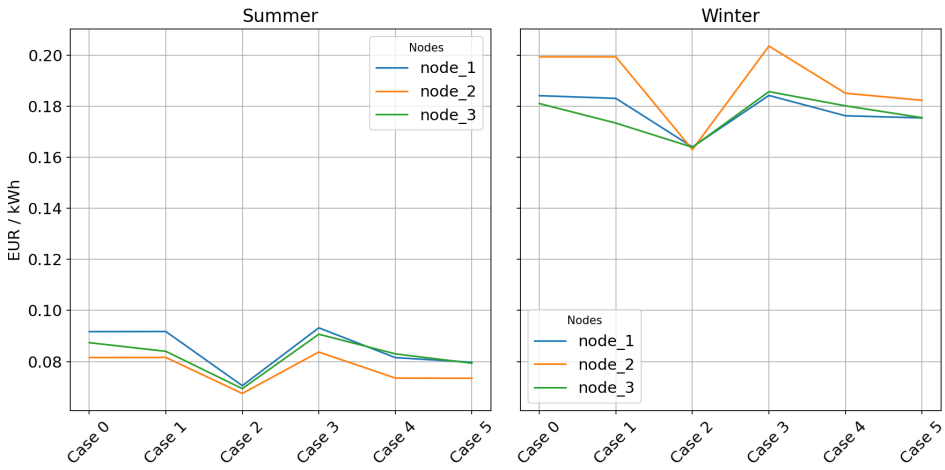

Figure 6.2.1: Cost of imported energy for each case, and season in 2023. aFRR imported power is not considered as the energy that is paid for against the DAM price, thus not part of the cost of imported energy. See data for other years in Appendix A.2.

Table 6.2.1: Grid Cost Differences in Percentage for Each Case Compared to Case 0 of that year

Case - Season	**2018**	**2019**	**2020**	**2023**
Case 0 - Summer	0.00%	0.00%	0.00%	0.00%
- Winter	0.00%	0.00%	0.00%	0.00%
Case 1 - Summer	-2.17%	0.02%	0.00%	-0.67%
- Winter	-0.43%	-0.78%	-0.25%	-1.12%
Case 2 - Summer	-8.90%	-17.67%	-28.25%	-17.97%
- Winter	-21.29%	-10.22%	-10.31%	-9.61%
Case 3 - Summer	-14.31%	-102.03%	-128.22%	-230.86%
- Winter	-29.25%	-53.10%	-147.19%	-28.14%
Case 4 - Summer	-56.55%	-280.42%	-377.43%	-650.21%
- Winter	-99.27%	-199.52%	-573.86%	-89.79%
Case 5 - Summer	-41.70%	-176.22%	-253.00%	-414.23%
- Winter	-70.78%	-147.63%	-444.35%	-58.17%

clearly shows how strategic scheduling of BESS aFRR and B2N provisions can potentially transform grid operational costs.

To better differentiate between summer and winter effects, extending the simulation duration would reduce sensitivity to price fluctuations. This, in turn, could provide clearer insights into seasonal variations. Additionally, such an increase could help identify patterns of grid cost savings across different cases and years, whether they occur mainly in summer or winter, thus offering a more comprehensive understanding of the seasonal differences.

Figure 6.2.2 demonstrates that including aFRR in localised grid management systems, particularly when combining BESS and EV technologies, is crucial not only for reducing grid costs but also for creating opportunities for profit under the right conditions. In Paragraph 6.3, we will take a closer look at the aFRR participation per individual asset and node.

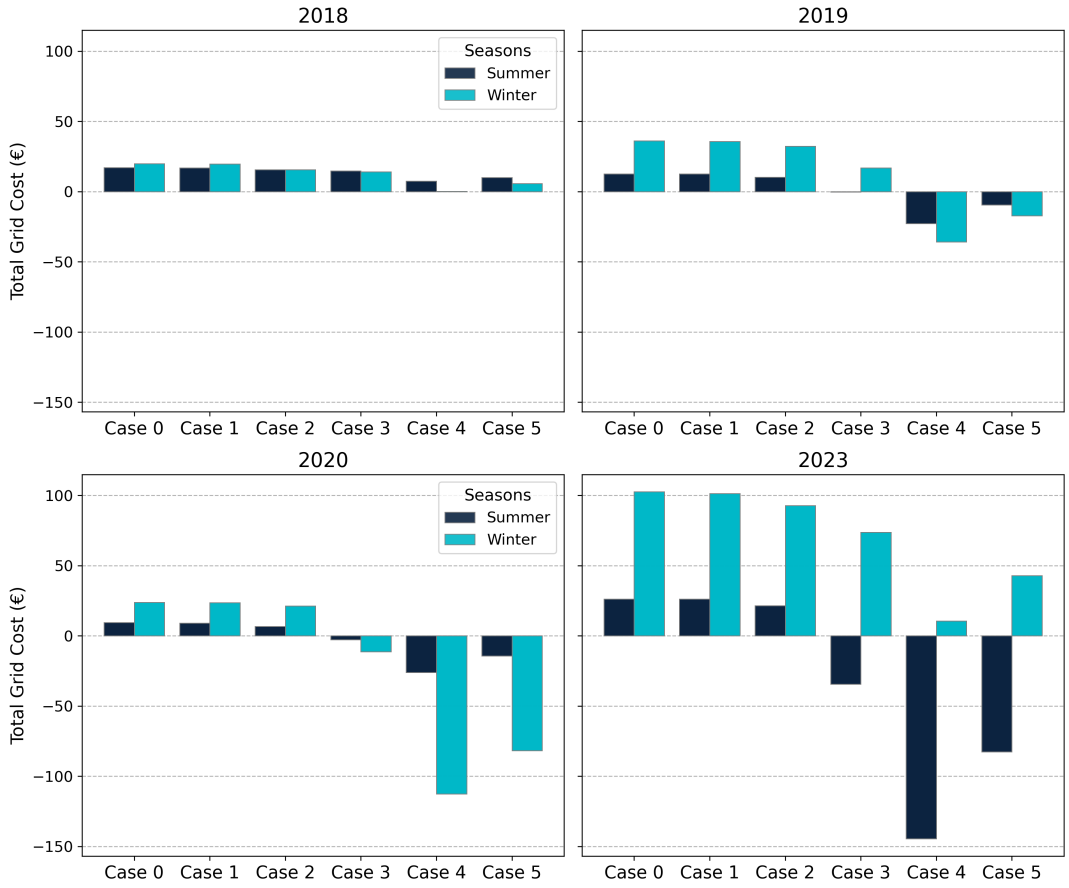

Figure 6.2.2: Total grid sum for each case, year and season. Grid cost consists of both cost of imported energy, as revenue from aFRR participation and exported energy.

6.3. aFRR Participation

Now it has become evident that aFRR plays a large role in node activity, we will take a closer look at how each aFRR asset performs within the node. In this simulation there are two types of technology that are able to participates in aFRR; BESS and EV. The difference between the two, apart from the size, is that the BESS remains stationary, but EVs arrive and leave according to a certain pattern and have to adhere to a minimal state of charge to ensure user comfort.

Figure 6.3.1 details the aggregated aFRR participation for Case 4 (B2N, V2N and joined aFRR) for each direction and asset. The upward delivered capacity is consistently higher, which can be attributed to the restriction of only scheduling downward power during a negative downward imbalance price, as stated in Paragraph 4.5, which is less common than a positive upward price. On certain days, such as Winter 2023 and Summer 2018, the downward imbalance price never falls below zero, leading to a complete absence of downward aFRR power delivery. This highlights how closely the provision of aFRR power is tied to the fluctuations in imbalance prices.

It becomes evident that the BESS outperforms EVs in terms of total delivered capacity in most cases and nodes. Only Node 3, the mixed node, shows a consistently similar delivered capacity from EVs compared to the stationary BESS. This can be attributed to the fact that the EV connection profile for Node 3 is characterised by longer connection periods and more simultaneously connected cars, resulting in more moments where EV batteries are available for aFRR participation. Figure 6.3.2 shows the number of cars that are connected to a charger for each node at a certain time instance. The presence of a car directly influences the total availability of battery storage, thus the potential to deliver aFRR power.

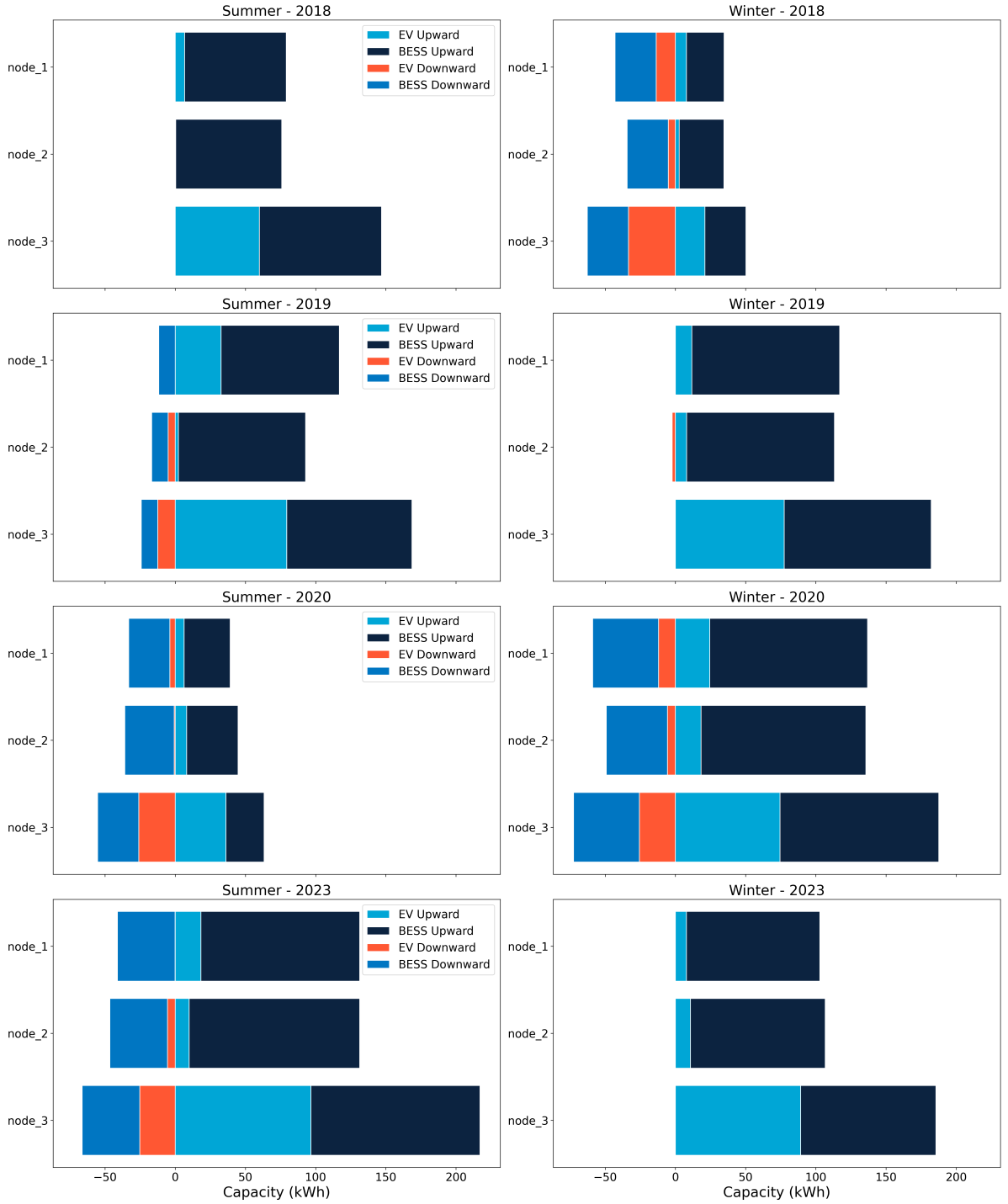

Figure 6.3.1: Total sum of both upward and downward delivered aFRR power per asset, node, year and season for Case 4. Downward power is indicated in the negative direction.

Furthermore, 6.3.1 shows some significant seasonal differences in certain years. Especially in 2020 upward BESS activity increased by 320 % from summer to winter in Node 3, which can likely be attributed to the higher average upward imbalance prices as displayed in Figure 6.1.10 and more clearly from Figure 6.3.3, where an increase in both amount and duration is visible. However, 2018 sees a 190 % increase from winter to summer in upward BESS activity but shows little difference in upward imbalance price distribution in Figure 6.1.10, apart from some outliers. Figure 6.3.3 however clearly indicates a more constant non-zero upward price in the summer which explains the increase in aFRR activity. Although there are differences between seasons, the short duration of the one-day simulations

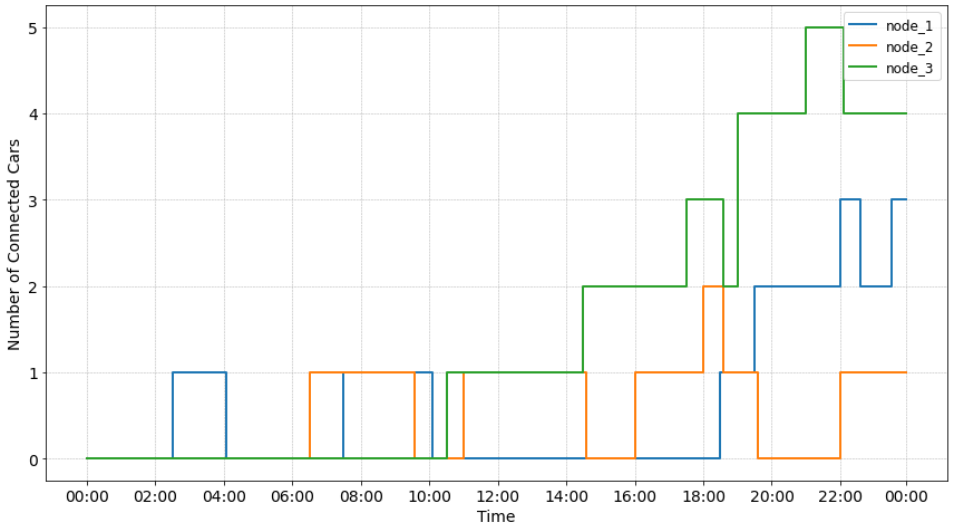

Figure 6.3.2: Sum of connected cars per node. Node 1: Residential node. Node 2: Commercial node. Node 3: Mixed node

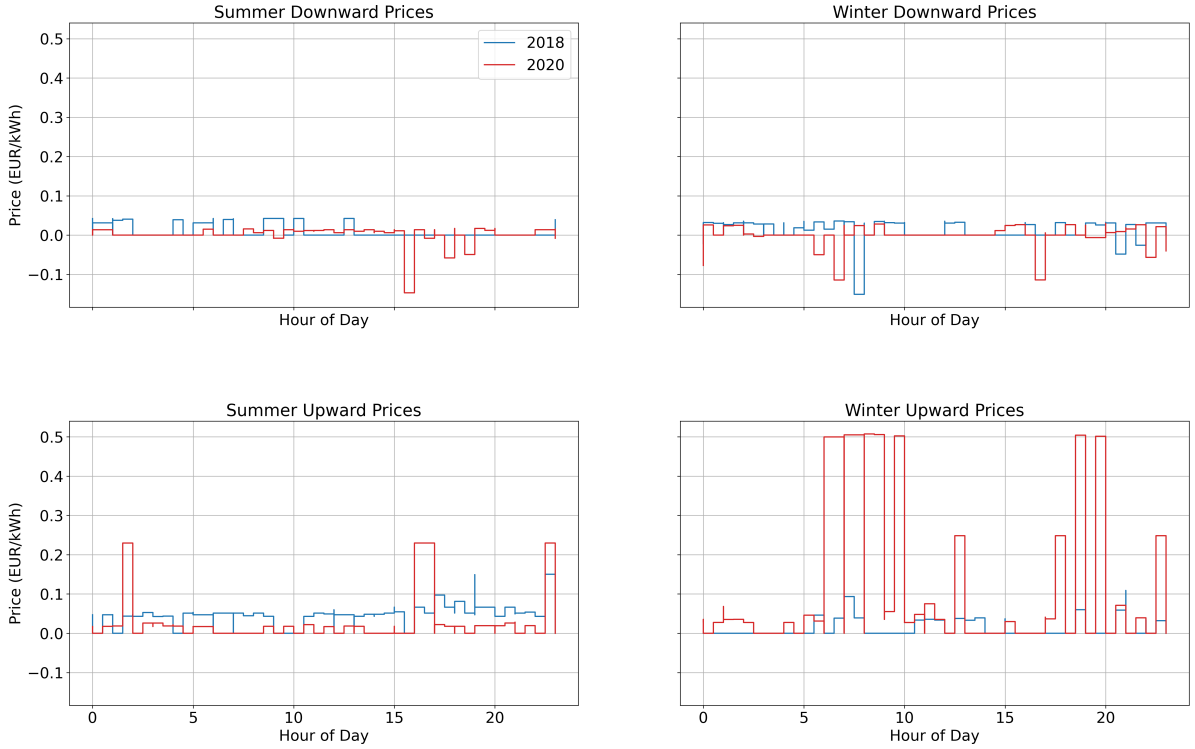

Figure 6.3.3: Step function of upward and downward imbalance price for both summer and winter season. For other years, see A.3.

makes it challenging to draw firm conclusions. Therefore, a more comprehensive assessment of long-term price trends is essential to gain deeper insights into these variations.

Figure 6.3.4 offers a visual representation of the variations in aFRR participation across nodes, aggregating both upward and downward aFRR provision from EVs and BESS. This comparison is focused on Case 4 in 2023 for both seasons. While all years were analysed, the outcomes were consistent, with the greatest difference in participation share for Node 3 across all years and seasons being 6.4%, see Appendix A.4.

The comparatively high amount of EV aFRR provision for Node 3 is visible in Figure 6.3.5, which details the total delivered aFRR capacity per node over all cases and seasons for 2020. Each year

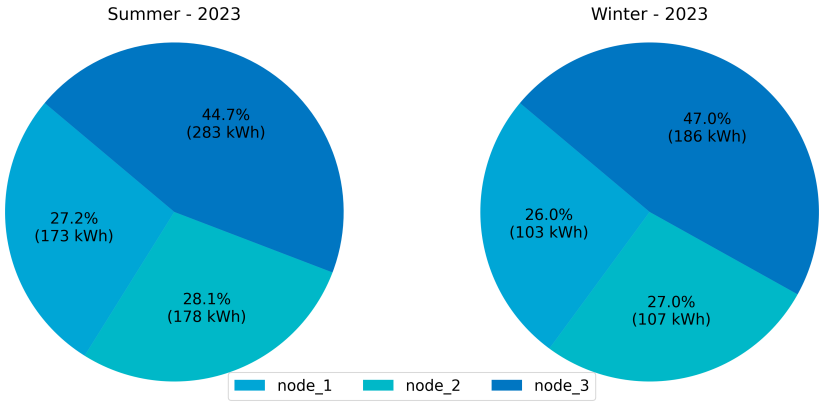

Figure 6.3.4: Aggregated sum of both EV and BESS upward and downward delivered aFRR power per node, year and season for Case 4.

showed similar line trends, where Node 3 in nearly all years surpassed the other nodes in terms of EV aFRR provision in both directions, in line with the findings that are displayed in Figure 6.3.1. Cases 3 and 4 see little to no difference in EV aFRR provision, which can be attributed to sufficient grid space in each node. Since favourable aFRR prices often trigger simultaneous participation from both EVs and BESS, tight constraints on grid capacity might lead to a reduction in the total aFRR capacity delivered.

Figure 6.3.6 displays similar data but for BESS aFRR activity only. The stationary nature of the BESS removes any large deviations between nodes when focusing on either upward or downward power. Again, all years showed similar line trends between the cases. Consistent in nearly every year, Winter outperformed Summer in terms of aggregated downward and upward power with as much as 144% in 2020. Only 2023, a year characterised by the highest day-ahead and imbalance prices, showed more aFRR activity in the summer than winter.

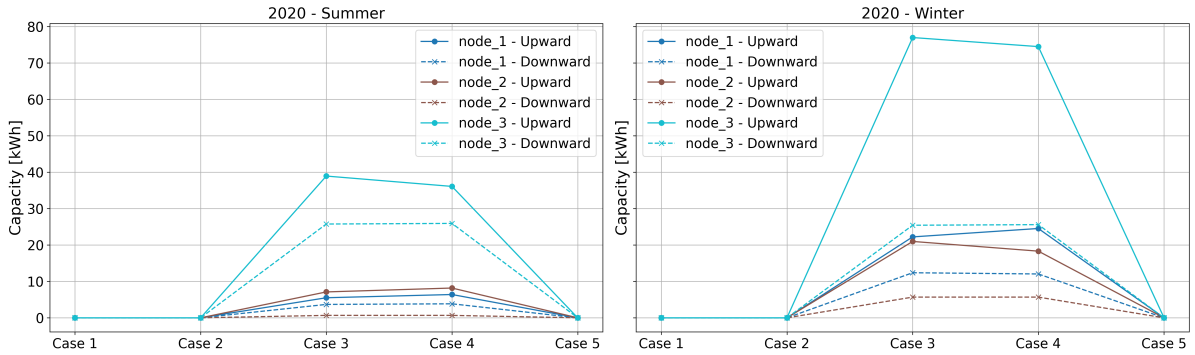

Figure 6.3.5: Sum of upward and downward aFRR EV power per node, season and case.

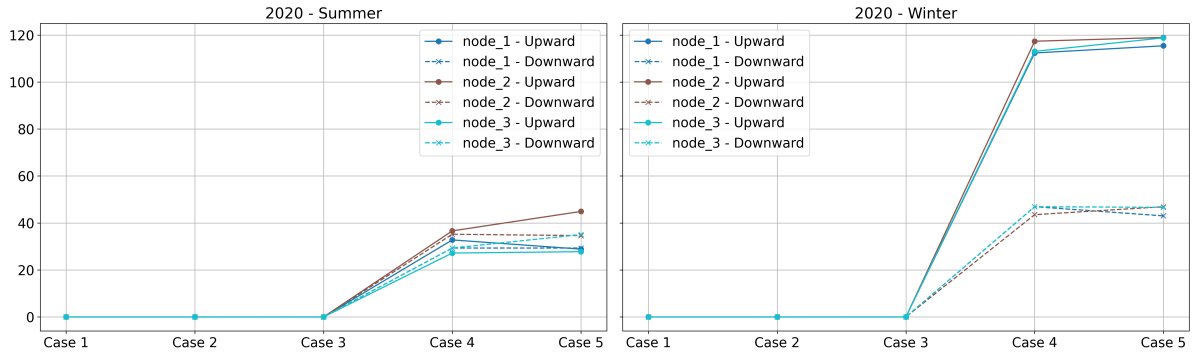

Figure 6.3.6: Sum of upward (solid) and downward (striped) aFRR BESS power per node, season and case.

6.4. Vehicle to Node Activity

This paragraph focuses on the V2N activity, which is regarded as energy taken from the EV battery and directly fed into the node to be consumed by any load that requires it.

Discharging an EV has two efficiency losses; charger efficiency (97%) and car battery efficiency (97%) (Damianakis, 2024). Since all cars arrive with <98% SoC, which is the minimal departure SoC, all discharged V2N energy must be charged again to ensure user satisfaction and thus avoid penalties in the simulation. We therefore have to take into account the round trip efficiency of charging and discharging the car, which translates to $(0.97 \times 0.97)^2 = 88.57\%$. For V2N to make sense, the difference in day-ahead price during discharging (V2N) and regular charging must exceed this efficiency loss, just like the BESS which operates with identical efficiencies. However, as these price fluctuations need to occur within individual charging sessions rather than throughout the entire day, V2N activity is typically less than B2N. Consequently, it is reasonable to anticipate that increased DAM price variability would lead to higher V2N capacity delivery.

Figure 6.4.1 and 6.4.2 show the aggregated V2N capacity over all nodes, for each case, year and season. In addition, a pie chart details the difference in V2N activity per node, summed over all cases and years. Figure 6.4.3 shows the corresponding DAM price profiles, with the maximum measured difference between the maximum and minimum of that day.

Figure 6.4.1 shows results for a summer day, where Case 1 outperforms other cases in terms of delivered V2N capacity. Node 3 clearly delivers the largest share of V2N activity, which can again

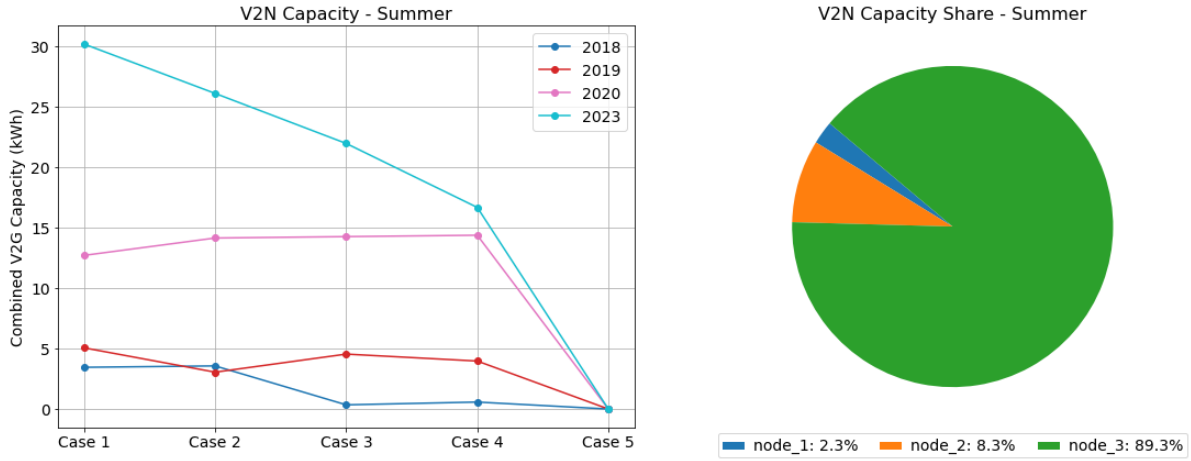

Figure 6.4.1: Aggregated sum over all nodes per case and year of delivered V2N capacity (left) and its corresponding share per node (right) for summer, plotted for one day. V2N capacity share is aggregated over all years and cases.

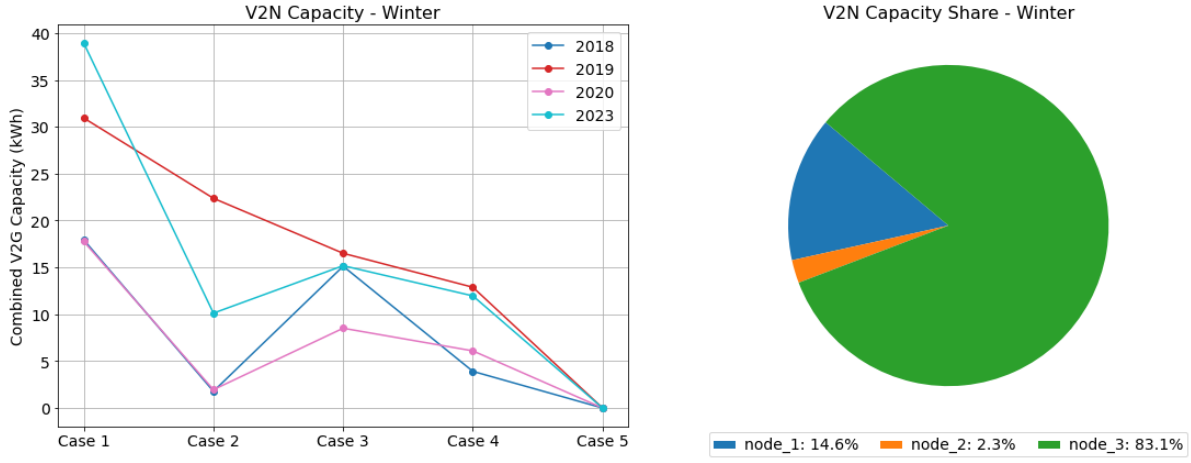

Figure 6.4.2: Aggregated sum over all nodes per case and year of delivered V2N capacity (left) and its corresponding share per node (right) for winter, plotted for one day.

be attributed to the longer charging periods which are clustered towards the second half of the day. Incorporating BESS in Case 2 appears to reduce the reliance on V2N activity relative to Case 1. This reduction is likely because BESS can capitalise more effectively on daily DAM price fluctuations, potentially achieving a higher percentage of profit. By comparing Figure 6.4.1 with the DAM price profile in Figure 6.4.3, a correlation between the years with the highest (2023) and lowest (2018) V2N capacity performance and the corresponding daily DAM price variations can be noticed. The year 2023, which shows the most amount of V2N activity, aligns with the year of the most significant DAM price fluctuations. In contrast, 2018, with the lowest V2N activity, corresponds to the year with the minimal DAM price changes, indicating the influence of DAM price variations on V2N capacity effectiveness across different years.

However, in contrast to the summer, the winter does not show as strong a correlation between the maximum DAM price delta and V2N activity. Although the year experiencing the greatest price delta (2023) does show higher V2N delivery compared to the year with the smallest delta (2020), the V2N capacities for other years are more closely aligned. This could be attributed to the varying timings of price spikes or dips between summer and winter, an aspect that calls for further investigation in future studies. However, as in the summer season, Case 1 performs best in winter and Node 1 delivers the largest amount of V2N capacity.

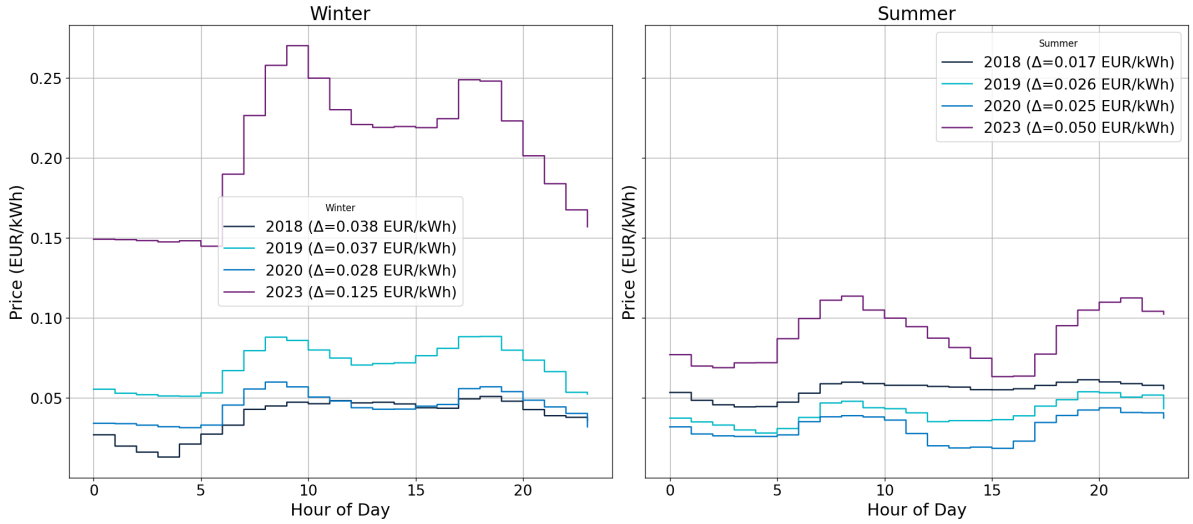

Figure 6.4.3: Price plot showcasing the day-ahead price profile for one (simulated) day, for both summer and winter. Line labels indicate the delta between the maximum and minimum for that day.

6.5. Passive Balancing

The graph presented in Figure 6.5.1 is a heatmap showing the percentage of grid cost savings due to passive balancing for each case compared to a baseline scenario (Case 0), across different years and seasons. Passive balancing refers to the revenue achieved from adjusting a BRP portfolio position based on the original E-program during favourable imbalance prices. Since this is not the original objective of the simulation, the initially allocated downward and upward aFRR power for both EV and BESS is treated as standard imported and exported energy respectively. By doing so, we remove any aFRR revenue from the equation. As a result, as discussed in Paragraph 5.3, this case only regards one grid player; the BRP.

The analysis explores two approaches for handling excess power meant for upward aFRR. The first approach, shown in Figure 6.5.1, sells this excess power at a reduced day-ahead market price (feed-in tariff), similar to how surplus solar power is sold. The second approach, in contrast, assumes this power has no market value and 'sells' it at 0 EUR/MWh. This second case simulates a scenario that avoids dependence on day-ahead prices since they might become uncertain in the future.

In both seasons, Case 4 consistently shows the highest passive balancing savings across all years, which indicates the synergistic benefits when combining BESS, aFRR and V2N technologies. In addition, an increase in imbalance and DAM prices results in higher savings, as demonstrated in 2023

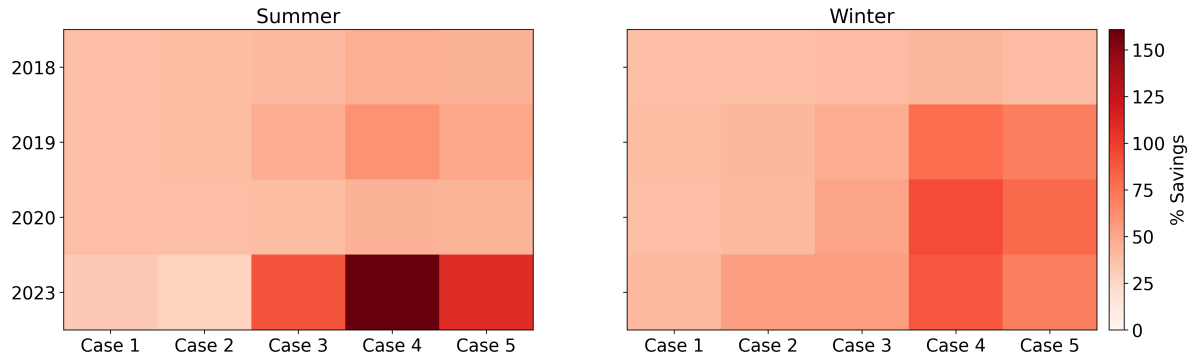

Figure 6.5.1: Percentage of grid cost savings due to passive balancing for each case, compared to Case 0. Upward power is fed into the grid against a feed-in tariff (95% DAM). Downward power is bought against day-ahead prices and is part of regular imported power costs.

which shows up to 150% savings in grid costs in summer. Furthermore, Cases 3, 4 and 5 outperform Cases 1 and 2, which is expected since these cases participate in aFRR provision, thus directly integrating the imbalance price in the optimisation. Any savings achieved in Cases 1 and 2 can be attributed to the selling of upward power against feed-in tariffs as can be seen when comparing Figure 6.5.1 with Figure 6.5.2, showing that savings are significantly reduced when upward power does not create revenue.

Excluding revenue from exported energy against feed-in tariffs shows a clear distinction between cases that do include aFRR provision and those that do not. Cases 1 and 2 show barely any savings, apart from some due to load shifting, which is the only difference in optimisation strategy between the base Case 0. Clearly, 2023 outperforms other years due to higher imbalance prices, as can be seen in both Figure 6.1.10 and 6.1.8 and Figure 6.5.3, which details the hourly up- and downward imbalance price for each simulated day per year and season. Significant savings of up to 120% can still be achieved through passive balancing, even when exported BESS and EV energy hold no value and are only used to offset the E-program, provided there is an exact prediction of imbalance and DAM prices.

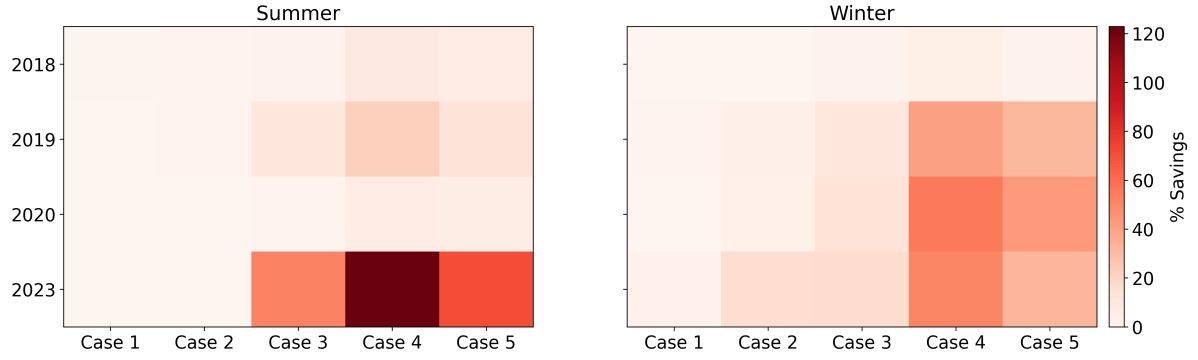

Figure 6.5.2: Percentage of grid cost savings due to passive balancing for each case, compared to Case 0. Upward power is fed into the grid against 0% of DAM prices and thus does not contribute to the earnings from exported power. Downward power is bought against day-ahead prices and is thus part of regular imported power costs.

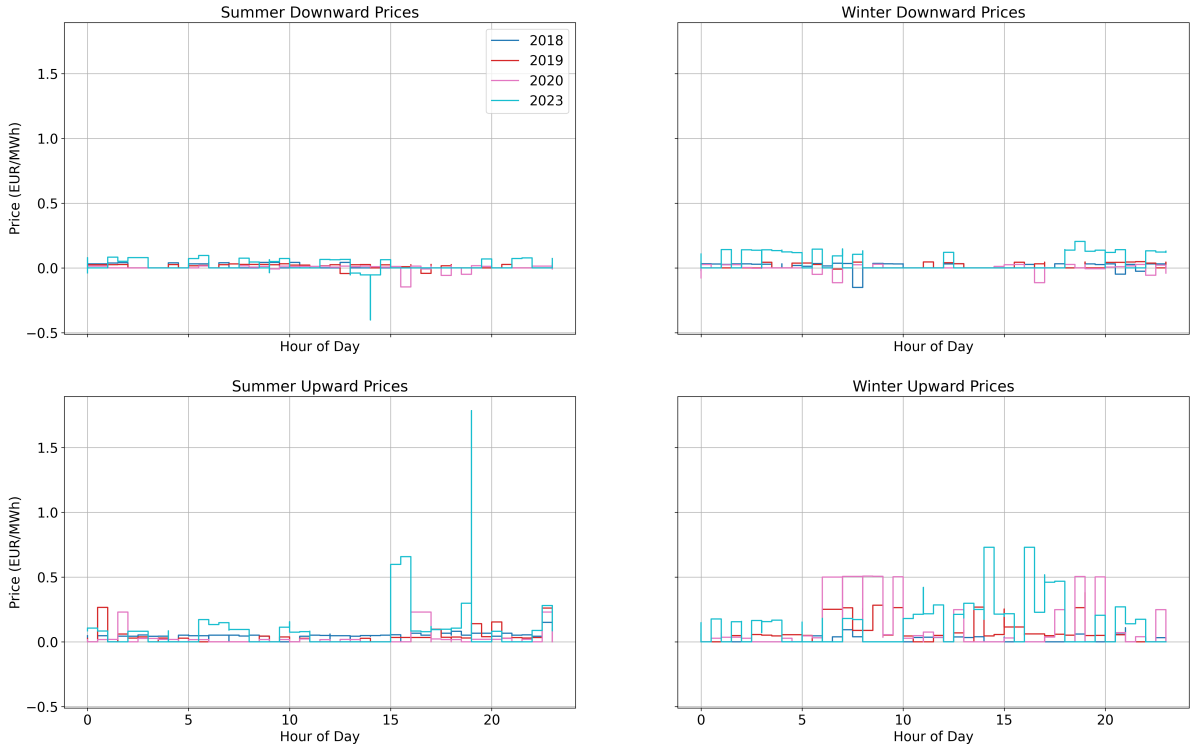

Figure 6.5.3: Upward and downward imbalance price profile for one simulated day, for each season, year and direction.

6.6. BESS Specifics

While the BESS sizing optimisation is out of the scope of this research, Figure 6.6.1 gives an insight into BESS C-rate performance per year and case. We compare Case 2 (B2N) with Case 5 (B2N + aFRR) to compare B2N activity with the introduction of aFRR provision. Here, the y-axis indicates the aggregated amount of occurrences (5-minute time step) of the BESS charged or discharged with a certain C-rate, summed over all nodes. Within the optimisation, the battery is limited to deliver a maximum of 0.5C. It becomes evident that Case 5 is operating near the maximum C-rate more often than Case 2. This likely occurs because, besides EV charging, the node load in Case 0 is typically below 25 kW, which is the restricting factor for B2N power in Case 2. In contrast, aFRR power in Case 5 is not subject to such constraints, only bounded by the overall grid capacity limits, which results in an increased occurrence of high C-rates.

Figure 6.6.2 represents the distribution of P_{imp} per case and season, aggregated across all years. The width of each violin plot reflects the frequency of P_{imp} occurrences, where a broader section indicates a higher density of values at that level, suggesting a more frequent occurrence of certain import capacities. Conversely, narrower sections point to less frequent values. The overall length of each violin illustrates the range of P_{imp} values observed.

A wider violin base in Case 0 indicates that a large share of P_{imp} values are at a lower level than other cases (87% below 15 kW, Summer Case 0). The maximum B2N power is limited to the maximum power usage of of the node. Comparing Case 2 (B2N and V2N) with Case 5 (B2N and aFRR) it is expected that the width of the base of the violin will decrease and be more distributed across the high power reason since aFRR power is often delivered against the maximum BESS C-rate. From Figure 6.6.2 this is indeed visible, especially during the summer day. It is important to note that this B2N power limitation applies only to discharging; charging is unaffected. Comparing Figure 6.6.1 with the findings of the violin plot, it is indeed seen that Case 5 exhibits a higher occurrence of high C-rates, and Case 2 higher occurrence at low C-rates. Given that charging power is not constrained by the maximum nodal power consumption, the high charge rates in Case 2, as depicted in Figure 6.6.1, are not reduced to zero.

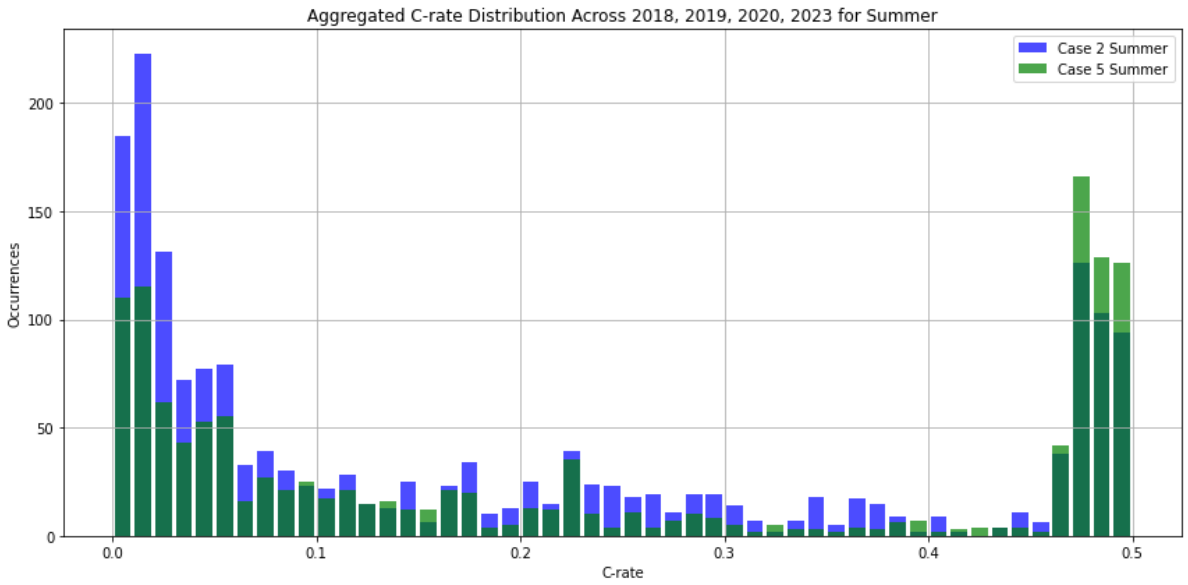

Figure 6.6.1: Charge and discharge C-rate occurrences for BESS per case, aggregated over all years for summer. For each year, see Appendix

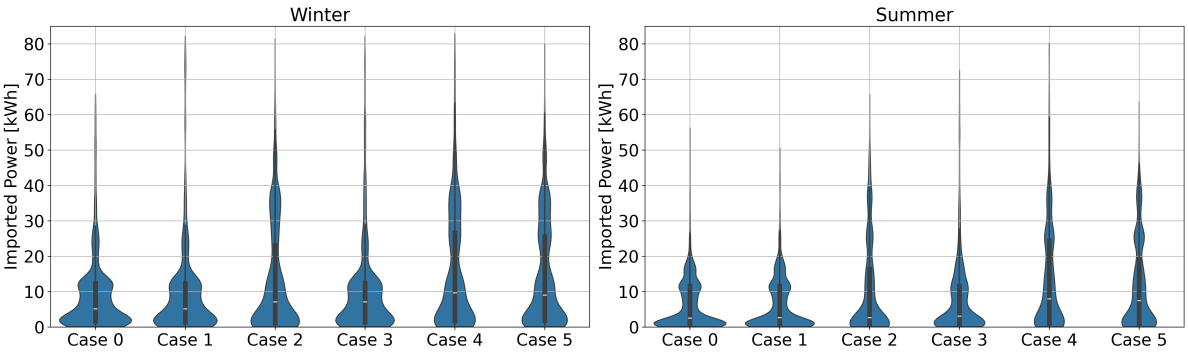

Figure 6.6.2: Violin plot that illustrates the distribution of imported power in kW across different cases for both seasons, aggregated over all years. The width represents frequency, and the length indicates the value range.

Table 6.6.1 includes the parameters that are part of the violin plot in Figure 6.6.2. The following conclusions can be made:

- **Mean:**
  In summer, Case 4 has the highest mean imported power consumption (13.04 kWh), while in winter, Case 4 also has the highest mean consumption (15.55 kWh). This suggests that Case 4 consistently exhibits higher average energy consumption compared to other cases, regardless of the season.
- **Maximum:**
  The maximum imported power varies across cases and seasons. For instance, in summer, Case 4 has the highest maximum imported power (80.29 kWh), while in winter, Case 4 again records the highest maximum (82.95 kWh). This indicates that Case 4 experiences the highest peak demand for imported power in both summer and winter.
- **Seasonal Differences:**
  Generally, we observe higher mean and maximum imported power values in winter compared to summer across all cases. This could be attributed to increased heating requirements and longer periods of darkness in winter, leading to higher overall energy consumption. However, Case 4 stands out with consistently high mean and maximum values in both summer and winter, indicating a significant demand for imported power regardless of the season.

- **Case Differences:**
  Comparing the mean and maximum values between cases within the same season reveals variations in energy consumption patterns. For instance, Case 4 consistently exhibits higher mean and maximum values compared to other cases, likely attributed to the presence of aFRR and nodal power of both EV and BESS.

In conclusion, Case 4 consistently exhibits higher mean and maximum imported power values across both summer and winter seasons, indicating a consistent increased demand for energy. Seasonal differences highlight increased energy consumption in winter, while Case 4 again has the highest average power demand.

Table 6.6.1: Statistical values of imported power values used in violin plot for cases and seasons. Each value apart from the Case column is expressed in [kWh]. Zero values are excluded from all data except 'min'.

Case	Summer				Winter			
	Mean	Median	Min	Max	Mean	Median	Min	Max
0	6.21	2.56	0	56.30	8.76	5.12	0	65.81
1	6.34	2.62	0	50.60	9.20	5.12	0	82.17
2	10.15	2.62	0	65.72	13.08	7.10	0	81.46
3	7.75	3.09	0	72.66	9.95	7.09	0	82.17
4	13.04	7.95	0	80.29	15.55	9.66	0	82.95
5	11.59	7.47	0	63.68	14.42	9.05	0	80.04

6.7. Discussion

This research addressed the growing issue of grid congestion due to the rapid electrification and the increasing demands placed on the power infrastructure by residential heating, transportation, and intermittent renewable energy sources. As these elements increase grid pressure, creating imbalances between energy generation and consumption, the need for efficient power management becomes increasingly important. This study focused on the deployment of flexible assets and loads as a strategic solution to these challenges. By simulating the flow of electricity from and to various sources, and integrating smart loads like heat pumps, electric vehicles and stationary battery storage, the EMS test the the potential for localised smart grids to adhere to load profiles while participating in the aFRR market. The primary objective of this research was to investigate the influence of integrating diverse smart loads and energy storage systems on total energy costs and participation in ancillary services within a localised smart grid. This study aimed to show how using flexible assets in smart grid management could enhance reliability in energy supply, reduce energy costs, and contribute to ancillary services.

6.8. Interpretation and Implications

The results indicate the capability for localised smart grids with flexible assets to ensure grid stability, reduce grid costs due to load shifting and participate in aFRR services, potentially turning grid costs into grid profits. Both EVs and stationary BESS showed individual capabilities to participate in aFRR services, while still adhering to minimum SOC requirements for EVs. A study done by Nelson and Johnson (2020) showed the capability to participate in both spinning (FCR/aFRR) and non-spinning (aFRR) reserves with BESS, and significantly reduce grid operating costs. However, the study assumed that the capacity bids were never called upon to be dispatched, thus simulating reserve capacity only, similar to Gomez-Gonzalez et al. (2021) that simulated FCR participation with HESS. Additionally, the research by Mohamed et al. (2023) assessed the revenues generated by BESS from FCR and aFRR both separately and combined, through simulations of actual energy delivery, showing that aFRR provided higher returns compared to FCR. However, the study did not simulate a BESS within a localised grid, focusing solely on optimisation for wholesale and imbalance market participation. Our study expands on this by including actual energy delivery and local grid power management, providing a practical view of how BESS operates within a local grid while contributing to the aFRR and providing battery-to-Node power.

Our findings reveal that the combined use of EVs and BESS shows the greatest savings in grid costs and generates the most revenue from aFRR participation. This aligns with the findings of Vermeer et

al. (2022), which showed similar outcomes for FCR participation only. However, FCR revenues are earned by the availability of reserve power rather than for actual energy delivery, as is the case with voluntary aFRR. This distinction means the actual impact of FCR on the grid is less visible within the nodal electricity flows, as well as within the asset battery dynamics itself. Particularly with regard to EVs, our study emphasises the impact of the duration and moments of charging sessions. By focusing on actual energy provision rather than reserve capacity, this approach showcases how EVs can play an active role in correcting grid imbalances, thereby creating a more practical example of a localised smart grid that participates in ancillary services.

7

Limitations and Recommendations

This chapter discusses each limitation present in the model, subdivided into three groups; pricing model, merit order and battery degradation. Each limitation is accompanied by relevant recommendations for future research.

7.1. Efficiencies, Performance and Climate

The coefficient of performance (CoP) of a heat pump varies depending on external conditions like the temperature of the heat source and the desired temperature output (Carnot cycle). In this model, the coefficient of performance is set to have a constant value of 3, and thus does not depend on ambient temperature. All efficiencies are assumed to be constant. Given that component degradation falls outside the scope of this thesis, the assumption is maintained that all efficiencies, including those of the EV and BESS battery round trip, as well as any converter/inverter efficiencies, remain stable. While Vermeer et al. (2022) has shown significant battery degradation in batteries engaged in frequency regulation over their entire 15-year lifespan, it is important to note that the model presented in this thesis simulates performance for only a single day. As a result, any potential degradation is expected to be minimal and is presumed to have negligible effects on component performance. Ramping rates are assumed to be instant. While lithium-ion batteries typically have a ramping rate of only milliseconds, the ramping rate in real-life situations should not be neglected. However, since the step-time of this simulation (5 minutes) exceeds the order of milliseconds by a hundredfold, the ramping rates are assumed to be instant. Furthermore, weather profiles are assumed to be without uncertainties; irradiation and ambient temperature profiles are perfectly known. To address these limitations, future recommendations could involve incorporating temperature-dependent coefficients of performance for heat pumps and dynamic efficiency models for batteries to account for degradation over time, while also introducing realistic ramping rates for batteries and uncertainty analysis into weather profiles to improve the realism of energy system simulations.

7.2. Pricing Model

The pricing model in this study is based on two specific prices: day-ahead prices for identifying the best times to import and export power, and imbalance prices for finding the most profitable moments to schedule and deliver aFRR power. Yet, the actual market price formulation is complex, as outlined in Paragraph 5.1.6. While day-ahead energy prices are often used in power optimisation research to model day-ahead scheduling, as shown in studies like those by Maeyaert et al. (2020), Mohamed et al. (2023) and Yan et al. (2019), there are studies, such as those by Zhou et al. (2023) and Imani et al. (2018), that incorporate real-time (intraday) electricity prices.

In our work, we chose to use day-ahead prices for initial simulations, acknowledging that this method does not fully capture the quick shifts in market prices that can occur within a day. This limitation is crucial as it points to a gap between assumptions within the simulation and the volatile real-world energy markets. The ideal method would have been to start with day-ahead prices in the one-shot optimisation and then shift to intraday prices in the RHO optimization, adding a layer of price prediction to increase

the accuracy and respect the causal relations shown in Figure (5.3.1). Such an approach is suggested for future research.

Secondly, imbalance prices are assumed to be perfectly forecasted, presenting the ideal scenario in terms of price prediction. A real-world scenario would use real-time balancing energy prices -published every minute by the TSO- to predict eventual imbalance prices per ISP. Such price forecasting models are a widely researched topic and examples of forecasting models are presented in works from Cardo-Miota et al. (2023) and Terpstra (2020). The findings of this research thus give an optimal scenario, demonstrating the potential of integrating flexible assets within localised smart grids. Future studies could consider implementing a more realistic price prediction model to provide more accurate aFRR revenue projections.

7.3. Merit Order

Furthermore, this research calculates revenues from aFRR with the assumption that all aFRR bids scheduled are part of the merit order and accepted in full. As discussed in Paragraph 4.5.1 and Chapter 2, bids are submitted through a merit-order system where various market participants offer balancing power at specific bid prices. In our simulation, each aFRR bid is simulated as not being the closing bid, therefore not receiving a partial activation request. In addition, each upward bid is considered to be offered at 0 EUR/kWh. Therefore, when the model schedules aFRR power, it is assumed to always be part of the closed merit order. Although it may appear unrealistic, submitting bids at 0 EUR/kWh in small quantities will lead to acceptance since the demand for balancing energy is always > 1 MW when it is not zero.

Shifting the focus to the bid limitations, we note the minimum aFRR bid capacity of 1 MW, which, while not incorporated in our model, is an aspect worth considering for its practical implications. Current aFRR market conditions require a minimum bid size of 1 MW, with the potential for pooling. An upscaled adaptation of the simulated model comprising 40 nodes could result in 1 MW BESS power at 0.5C. To ensure simultaneous capacity availability, the simulated model calls for a more complex BESS EMS. An upscaled version smaller than 40 nodes would be sufficient depending on the simultaneous EV charging sessions. Luckily, state-of-the-art BESS and EV modules show full wireless connection potential. Including such extensive EMSs could be implemented in future research to simulate localised smart grids with actual practical potential.

Lastly regarding the aFRR structure, is the previously discussed aFRR bid acceptance rates. Even when a bid is accepted, it is not called for the full duration of one ISP. For upward and downward ancillary power this is about 71% and 41% percent of each ISP respectively. In future research, these acceptance rates can be implemented as pseudo-random integers that are multiplied with scheduled aFRR bids, with an X per cent chance (determined by the BAR) of staying 1 for each timestep aFRR power was scheduled. This way, the model needs to adapt to last-minute changes, therefore increasing its robustness against unexpected market behaviour.

7.4. Battery Sizing and Degradation

Both EV and BESS are simulated without battery degradation which would impact charging and discharging behaviour and in turn affect potential grid cost reduction and revenue generation. From research done by Mohamed et al. (2023), BESS degradation significantly impacts the system operation and must be taken into account when evaluating market applications. Since in this research the maximum simulation duration was one day, little degradation would be visible. However, future research could include cycle degradation and ageing in terms of EUR/cycle, or simulate actual battery degradation and calculate the lifetime net present costs of each system similar to research done by Vermeer et al. (2022).

BESS dynamics within a grid are influenced by its size and C-rate. Since optimising size is out of scope of this project, more attention could be given to optimally sizing each BESS, possibly differentiating between nodes. Not only would this give more practical results in terms of component sizing, but it would also give more realistic insights into the capital costs of the introduced localised smart grid, in addition to more specific component lifetime predictions.

7.5. Passive Balancing

Considering that the assessment of passive balancing occurred after optimisation and was not the primary aim of the initial objective, it is advisable to conduct further research with a narrower focus on passive balancing and its complexities. Part of this narrower focus is in combination with the previously mentioned real-time price prediction dynamics. As explained in Paragraph 2.4, passive balancing E-program adjustments must be done within the period of one ISP, reacting to live imbalance prices. Utilising perfect price prediction in simulations offers an understanding of how localised smart grids can adapt an E-program, rather than giving a precise revenue figure.

8

Conclusion

Our investigation explored the integration of smart loads and energy storage systems, particularly BESS and EVs, into a localised smart grid, assessing their influence on grid costs and aFRR service participation. Through simulations across multiple years and seasons, we gained valuable insights into the financial dynamics of the grid and the effectiveness of these flexible assets. The introduction of BESS in Case 2 demonstrated a capacity to mitigate peak demand significantly resulting in the lowest cost of imported energy of all cases, although it resulted in higher nodal peak demand -up to 350%- due to the clustering of loads around moments of low energy prices. In addition, BESS showed excellent capabilities to even out the cost of imported energy between different nodes.

The combination of increased energy consumption of HPs and EVs and decreased PV production in the winter led to an increased amount of imported energy consistently over all years. In combination with higher day-ahead energy prices, the cost of imported energy is consistently higher in winter over all years. Furthermore, BESS showed increased amounts of both upward and downward power in winter in nearly all years. While it is clear that seasonal variations exist, the one-day simulation horizon limits conclusive observations, necessitating an examination of long-term price profiles.

The largest difference between grid types (Residential, Commercial or Mixed) is indicated by the amount of EV aFRR participation. Consistently, the mixed node is capable of delivering the largest amount of aFRR power due to the longer connection times and a higher amount of simultaneously connected EV cars.

When BESS was combined with aFRR services (Cases 4 and 5), it not only managed peak loads but also contributed to additional revenue streams, highlighting its dual role in grid stability and ancillary service revenues. The integration of aFRR services was essential in transforming grid costs into profits, notably in 2020 and 2023, during which aFRR participation reached its highest levels. For instance, in Case 4 2023, the grid costs were turned into profits, with reductions reaching up to 650% compared to the base scenario Case 0. In addition, observations on BESS C-rate performance provided operational insights, showing a higher frequency of high C-rates in scenarios where aFRR was included.

EVs showcased great potential in aFRR participation, especially in more recent years when market conditions were favourable. The dynamic charging and discharging capabilities of EVs allowed them to participate in aFRR services, turning grid costs into grid profits while still adhering to minimum departure SOC. This demonstrates their potential as flexible assets and a possible solution for grid congestion management by participating in the aFRR market. Furthermore, the analysis highlighted the large influence of day-ahead and imbalance prices on the profitability of aFRR engagement, which was significantly affected by the changing market prices, emphasising the necessity for accurate price prediction algorithms.

In our analysis of the impact of passive balancing on grid cost savings Case 4 stands out, showing the benefits of a synergy from BESS, aFRR, and V2N technologies. This case consistently shows

the highest savings across different years and seasons, highlighting the benefits of this integrated approach in enhancing grid efficiency and cost-effectiveness. By adjusting a BRP portfolio in response to favourable imbalance prices, 2023 resulted in the highest savings on grid costs of up to 150% in summer. The exploration of two methods for handling excess upward aFRR power, one valuing it at feed-in tariff rates and the other at zero market value, highlights the influence of market price variations on passive balancing strategies. The reduced grid costs of Cases 3, 4, and 5 over Cases 1 and 2 emphasise the significance of aFRR participation, incorporating the imbalance price directly into the optimisation. These findings show the potential of passive balancing as a strategy to improve grid cost efficiency, particularly when market imbalance price dynamics are included, offering a promising path for future grid optimisation strategies within the evolving energy landscape.

In conclusion, our study highlights the considerable advantages of integrating BESS and EVs with aFRR services (or imbalance prices) within a localised smart grid, for each season and grid type. The financial profitability and effective asset use emphasised in our findings demonstrate the potential of these technologies to advance smart grid functionalities and achieve economic efficiencies in grid operations.

A

Appendix

A.1. Power Flows

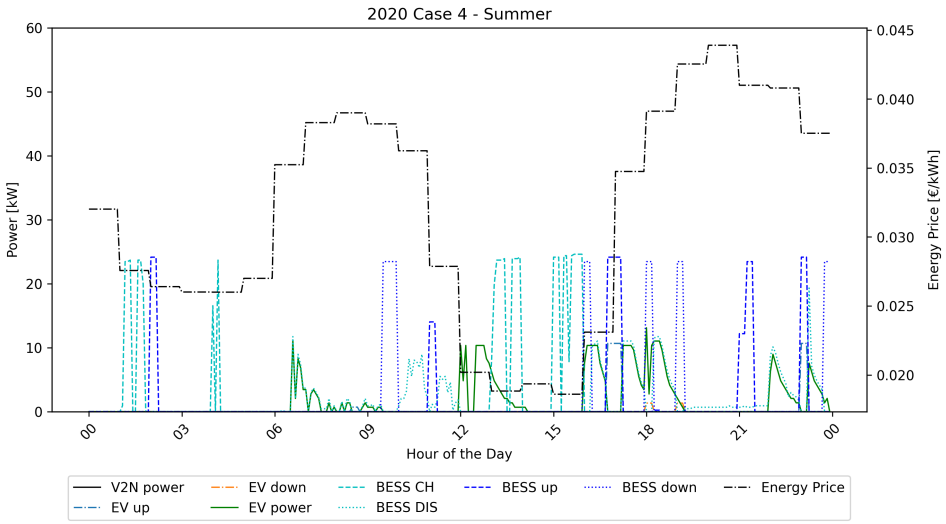

Figure A.1.1: Nodal power flow and day-ahead energy price for Case 4 Summer 2020 Node 2: Commercial Node.

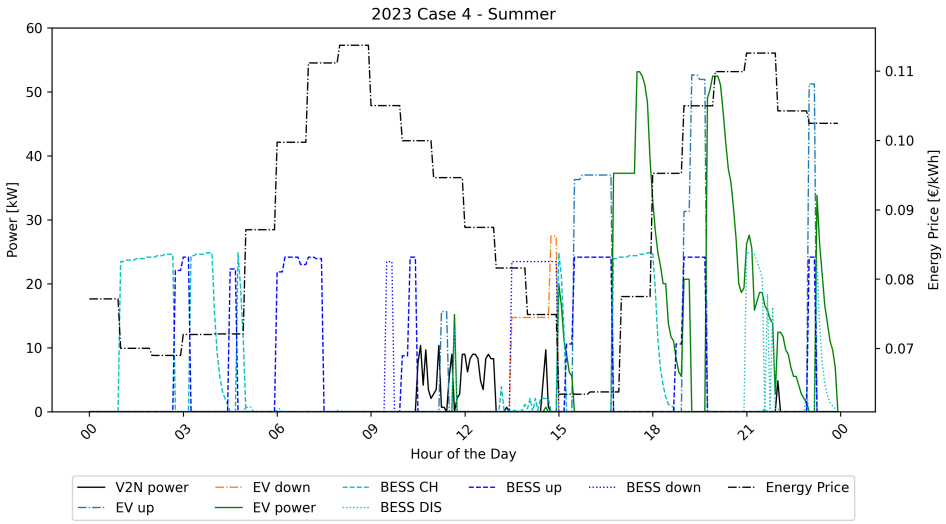

Figure A.1.2: Nodal power flow and day-ahead energy price for Case 4 Summer 2023 Node 2: Commercial Node.

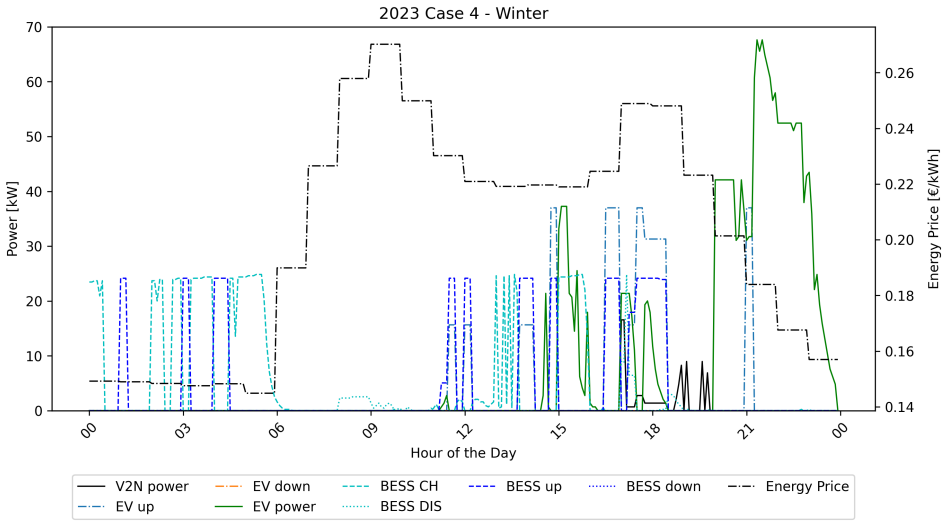

Figure A.1.3: Nodal power flow and day-ahead energy price for Case 4 winter 2023 Node 2: Commercial Node.

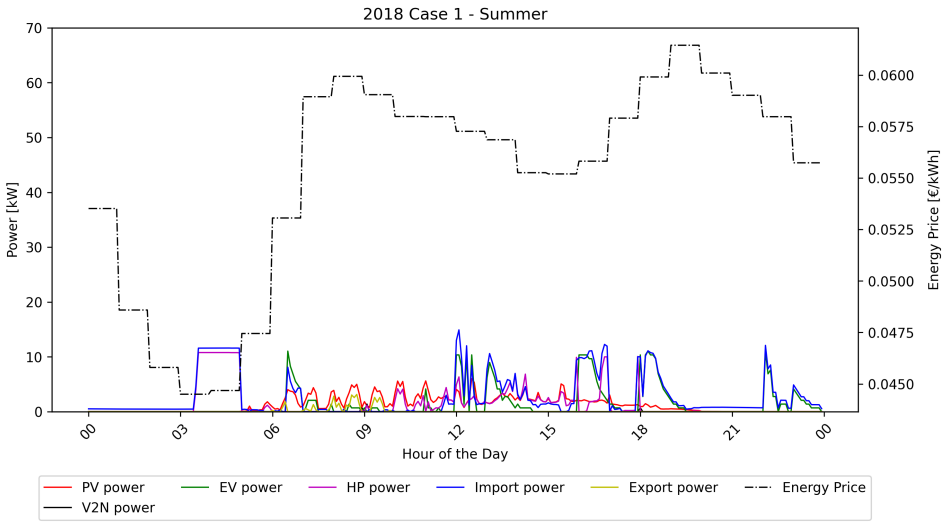

Figure A.1.4: Nodal power flow and day-ahead energy price for Case 1 Summer 2018 Node 2: Commercial Node.

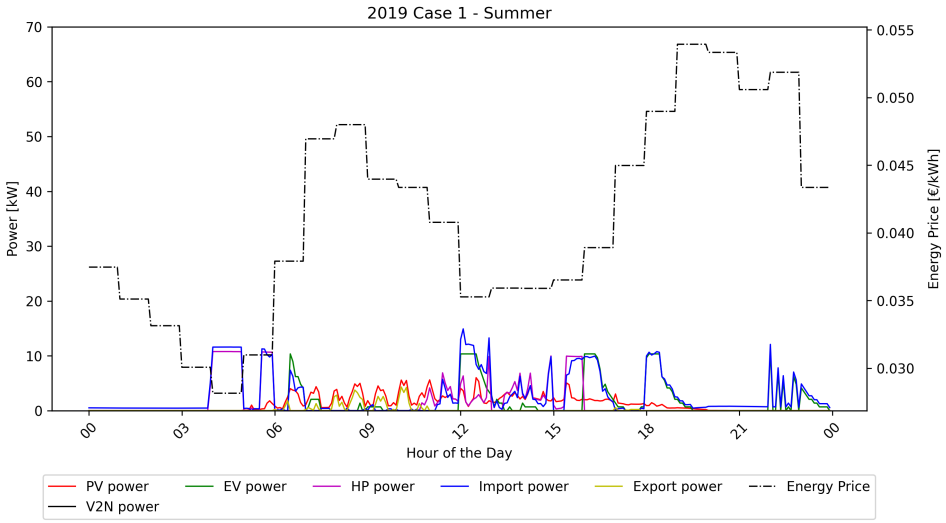

Figure A.1.5: Nodal power flow and day-ahead energy price for Case 1 Summer 2019 Node 2: Commercial Node.

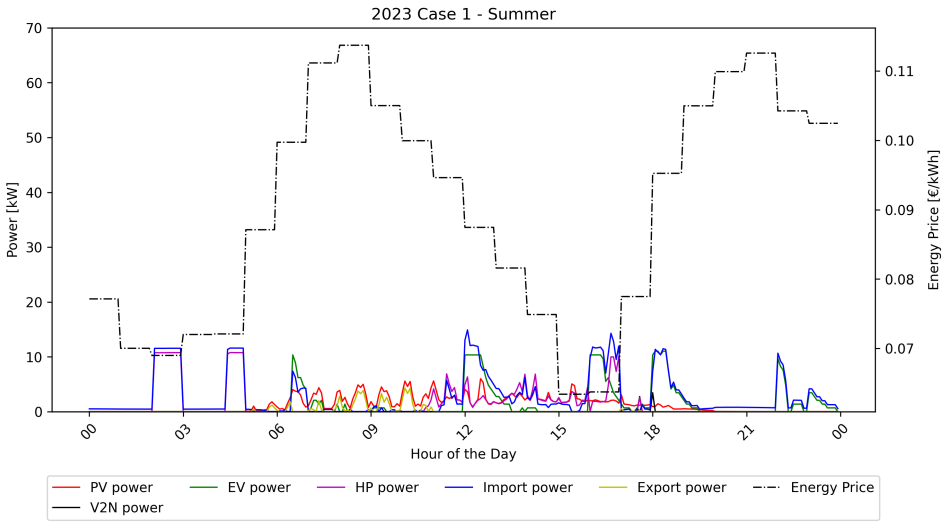

Figure A.1.6: Nodal power flow and day-ahead energy price for Case 1 Summer 2023 Node 2: Commercial Node.

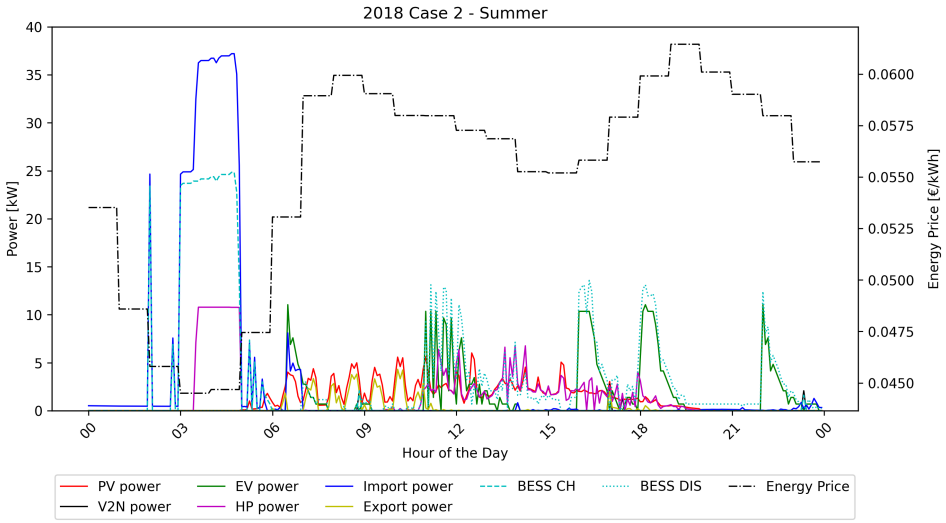

Figure A.1.7: Nodal power flow and day-ahead energy price for Case 2 Summer 2018 Node 2: Commercial Node.

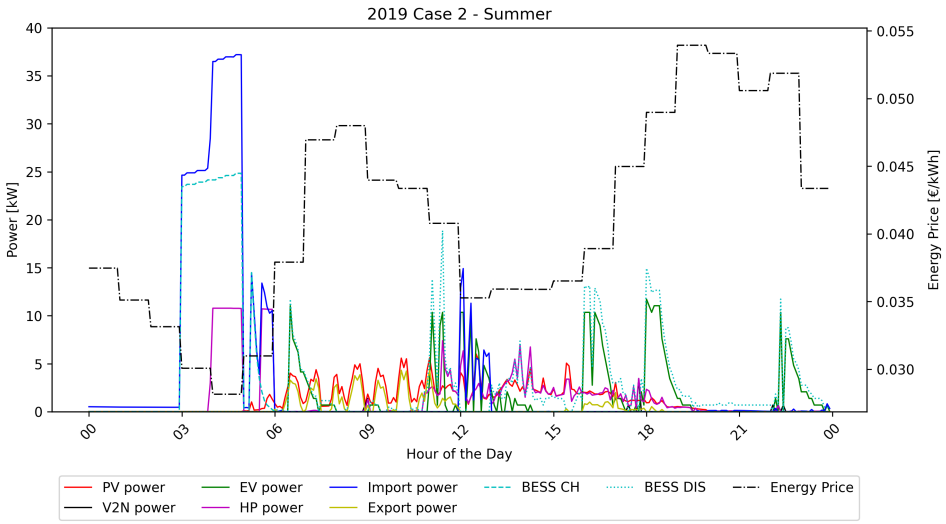

Figure A.1.8: Nodal power flow and day-ahead energy price for Case 2 Summer 2019 Node 2: Commercial Node.

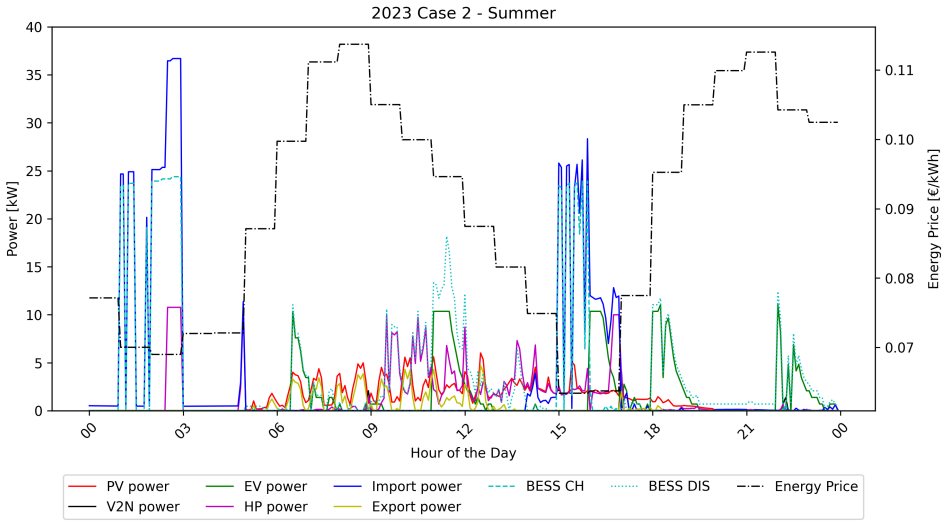

Figure A.1.9: Nodal power flow and day-ahead energy price for Case 2 Summer 2023 Node 2: Commercial Node.

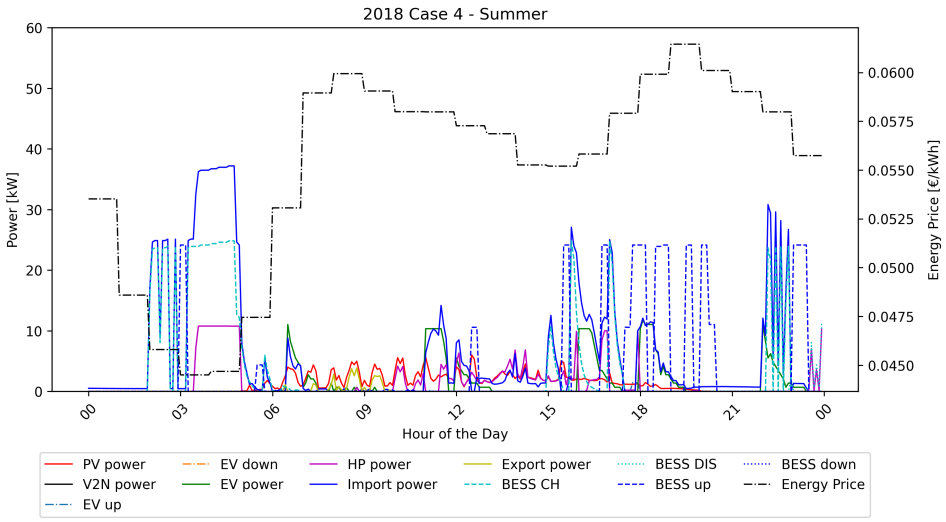

Figure A.1.10: Nodal power flow and day-ahead energy price for Case 4 Summer 2018 Node 2: Commercial Node.

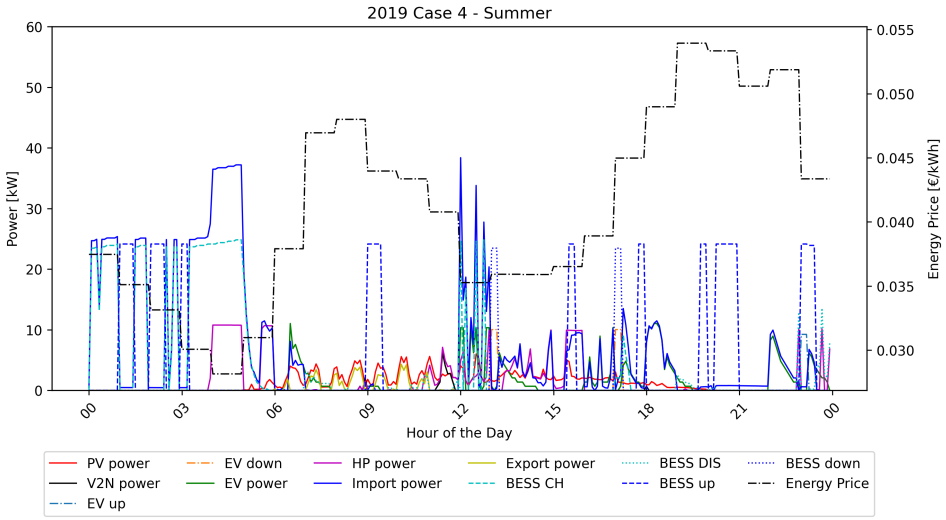

Figure A.1.11: Nodal power flow and day-ahead energy price for Case 4 Summer 2019 Node 2: Commercial Node.

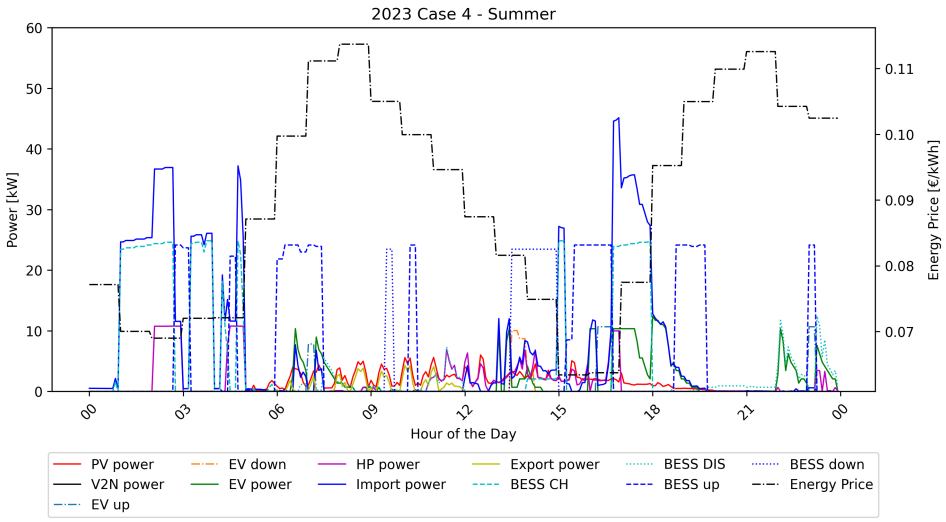

Figure A.1.12: Nodal power flow and day-ahead energy price for Case 4 Summer 2019 Node 2: Commercial Node.

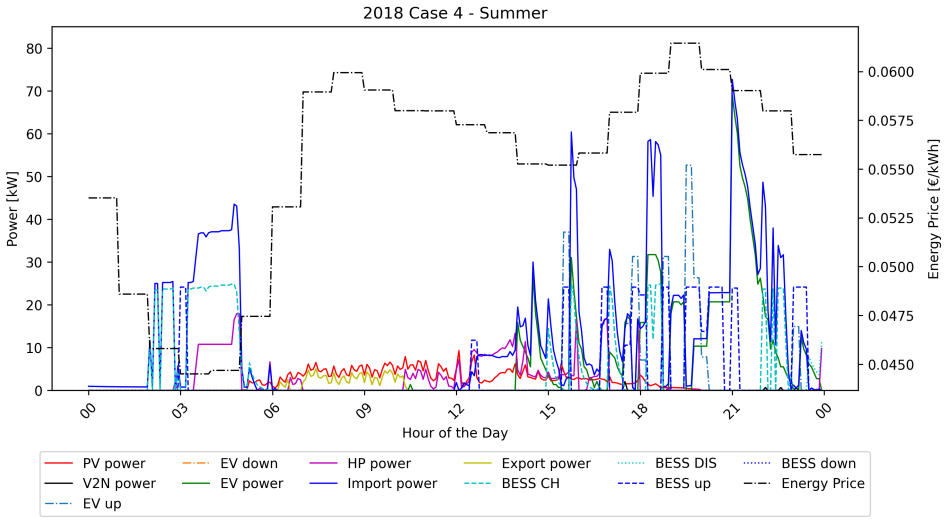

Figure A.1.13: Nodal power flow and day-ahead energy price for Case 4 Summer 2018 Node 3: Mixed Node.

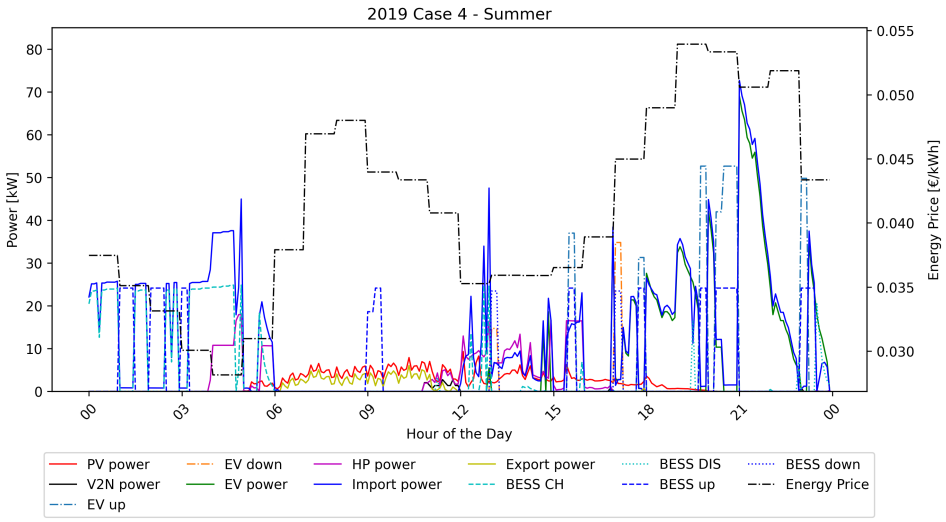

Figure A.1.14: Nodal power flow and day-ahead energy price for Case 4 Summer 2019 Node 3: Mixed Node.

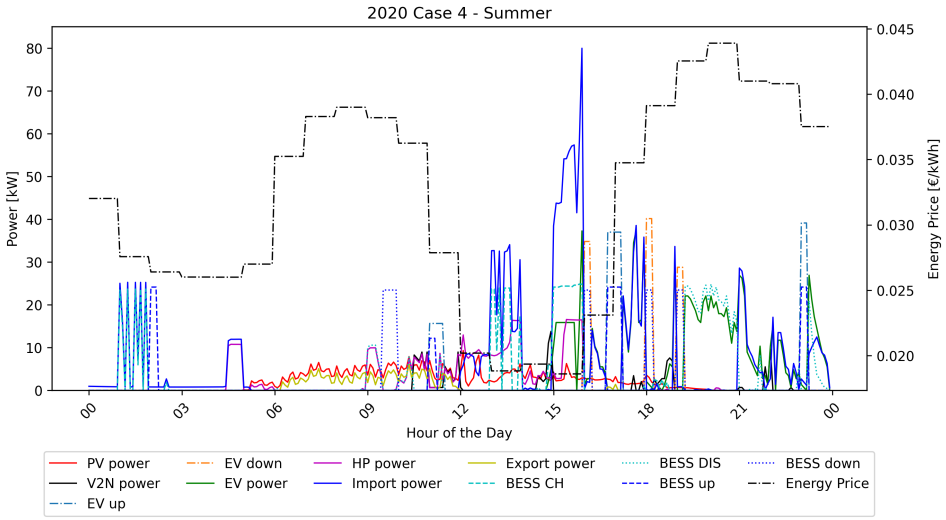

Figure A.1.15: Nodal power flow and day-ahead energy price for Case 4 Summer 2020 Node 3: Mixed Node.

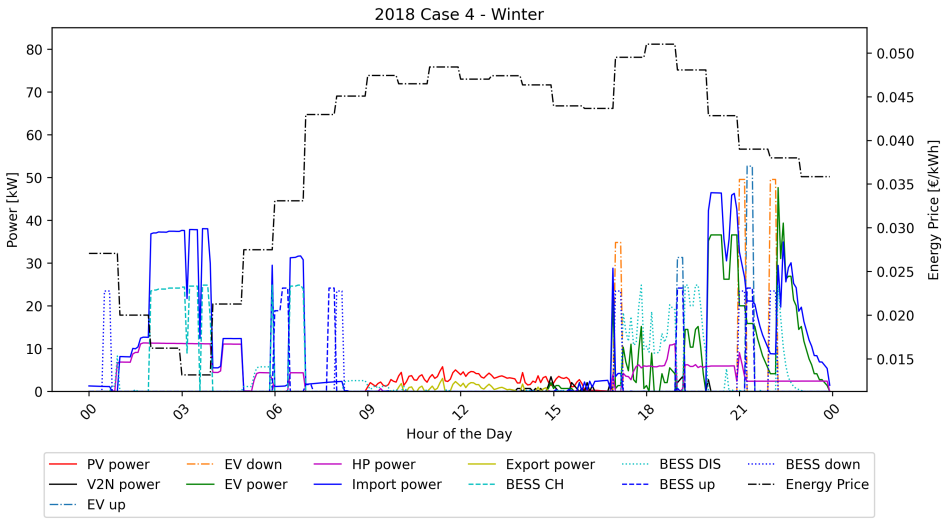

Figure A.1.16: Nodal power flow and day-ahead energy price for Case 4 Winter 2018 Node 3: Mixed Node.

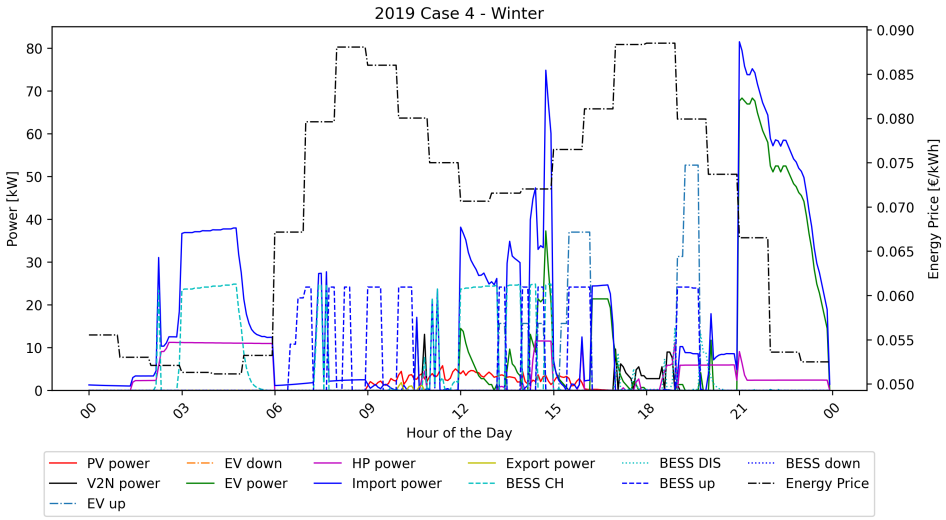

Figure A.1.17: Nodal power flow and day-ahead energy price for Case 4 Winter 2019 Node 3: Mixed Node.

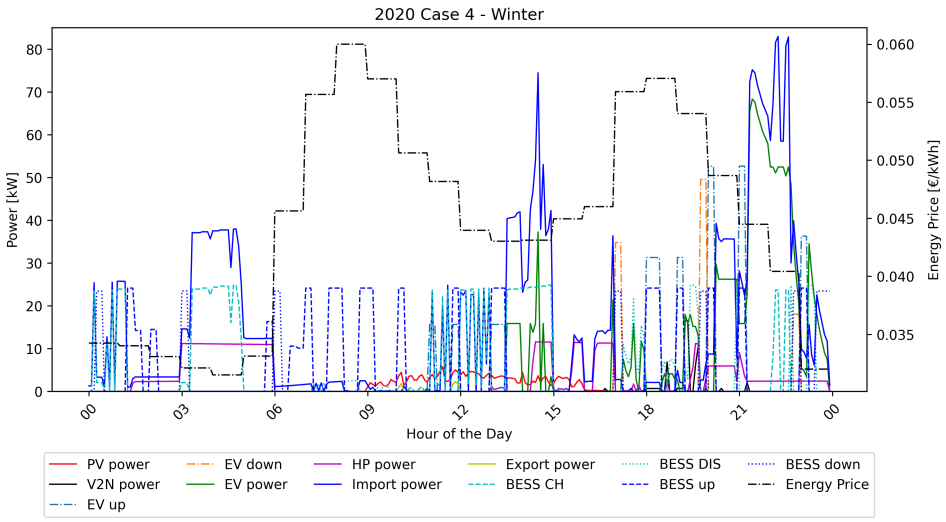

Figure A.1.18: Nodal power flow and day-ahead energy price for Case 4 Winter 2020 Node 3: Mixed Node.

A.2. Cost of Imported Energy

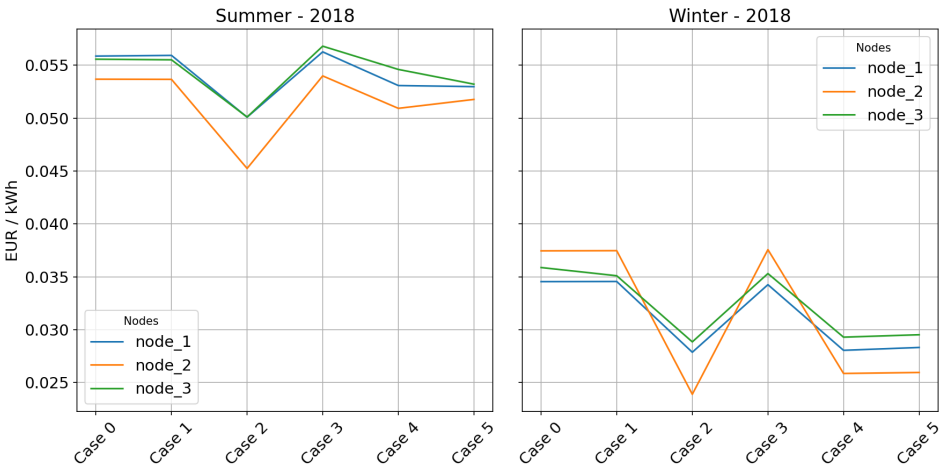

Figure A.2.1: Cost of imported energy for each case, and season in 2018. aFRR imported power is not considered as energy that is paid for against the DAM price, thus not part of the cost of imported energy

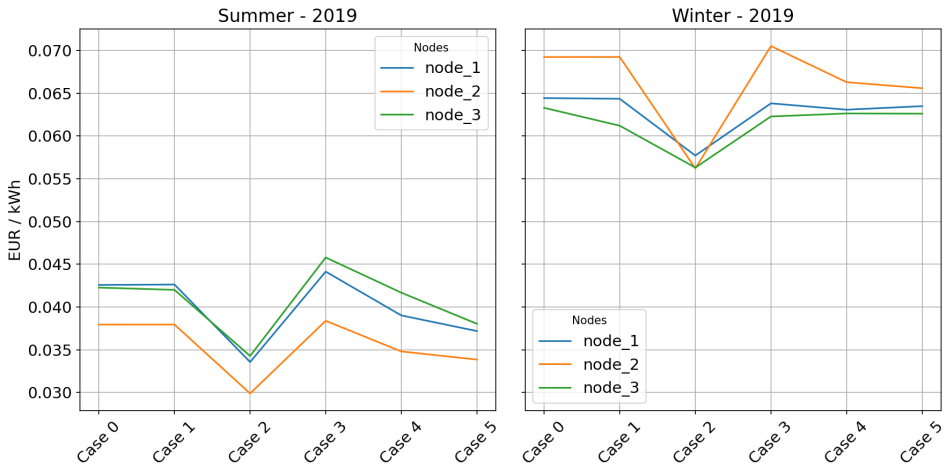

Figure A.2.2: Cost of imported energy for each case, and season in 2019. aFRR imported power is not considered as energy that is paid for against the DAM price, thus not part of the cost of imported energy

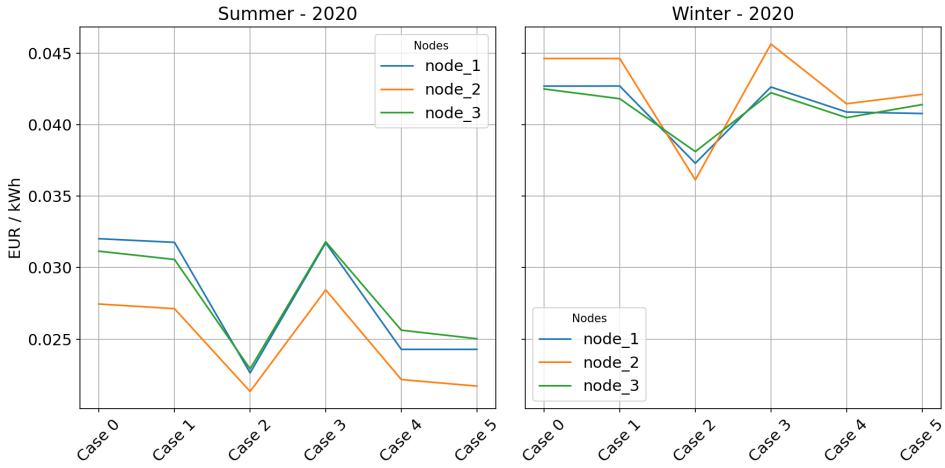

Figure A.2.3: Cost of imported energy for each case, and season in 2020. aFRR imported power is not considered as energy that is paid for against the DAM price, thus not part of the cost of imported energy

A.3. Prices

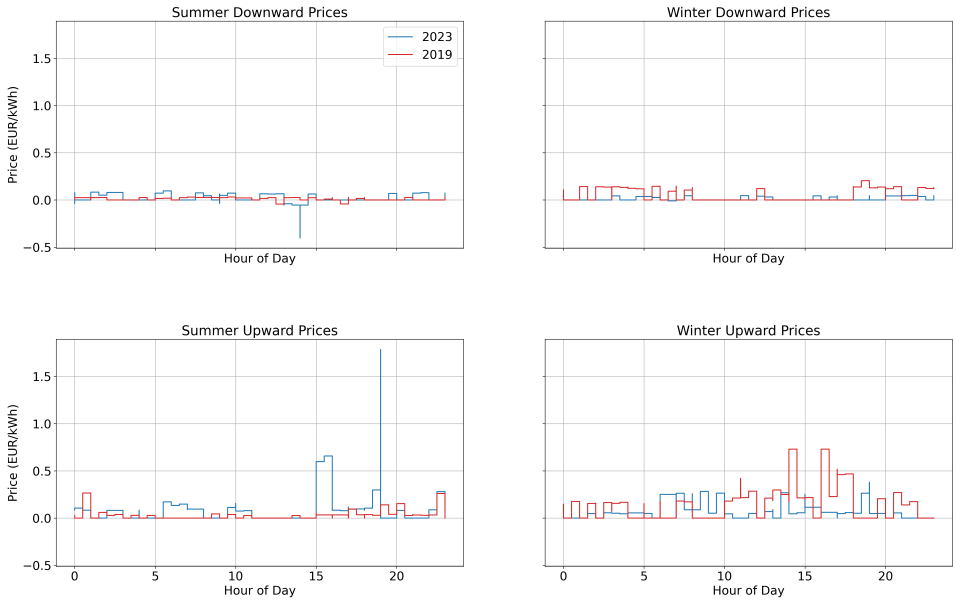

Figure A.3.1: Step function of upward and downward imbalance price for both summer and winter season.

A.4. aFRR Provision

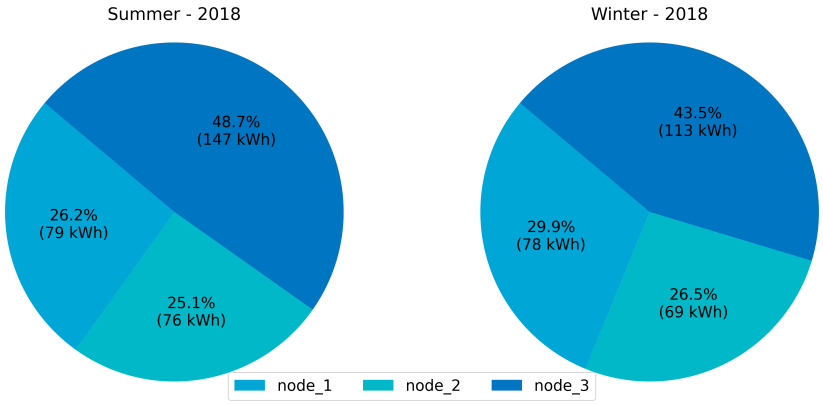

Figure A.4.1: Aggregated sum of both EV and BESS upward and downward delivered aFRR power per node and season for Case 4.

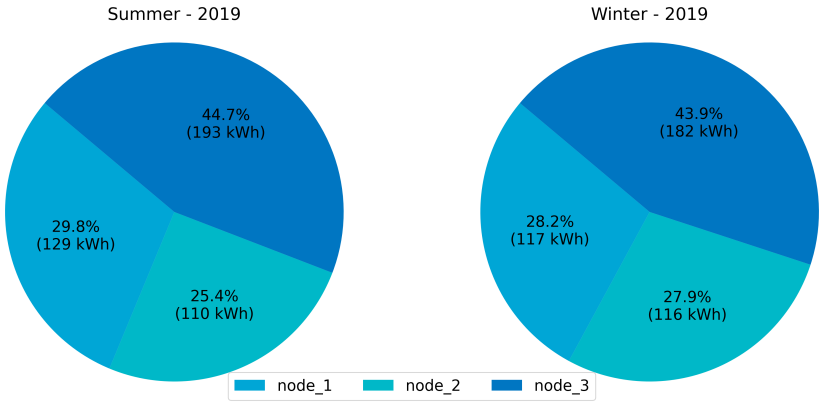

Figure A.4.2: Aggregated sum of both EV and BESS upward and downward delivered aFRR power per node and season for Case 4.

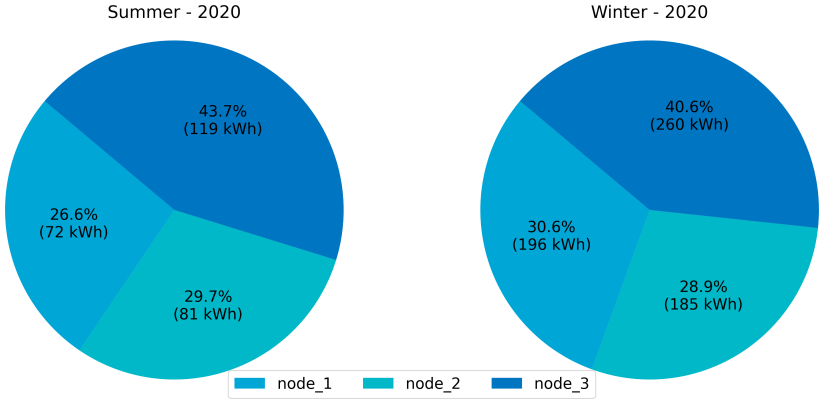

Figure A.4.3: Aggregated sum of both EV and BESS upward and downward delivered aFRR power per node and season for Case 4.

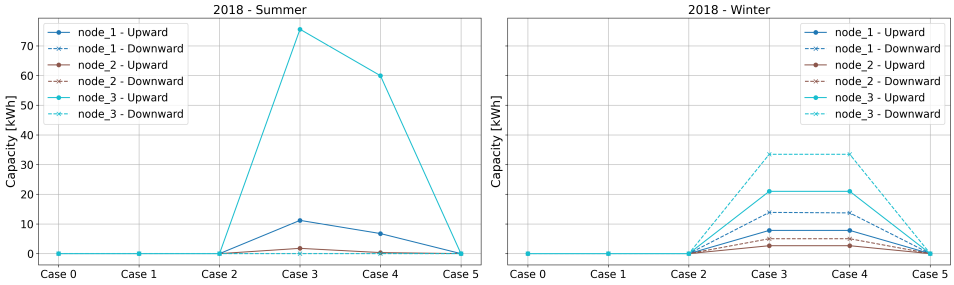

Figure A.4.4: Sum of upward and downward aFRR EV power per node, season and case.

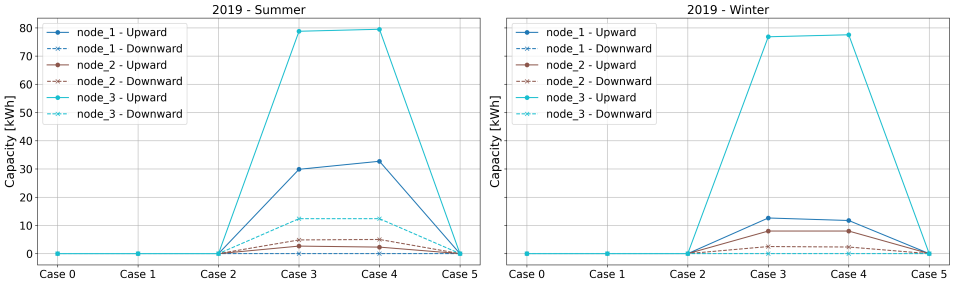

Figure A.4.5: Sum of upward and downward aFRR EV power per node, season and case.

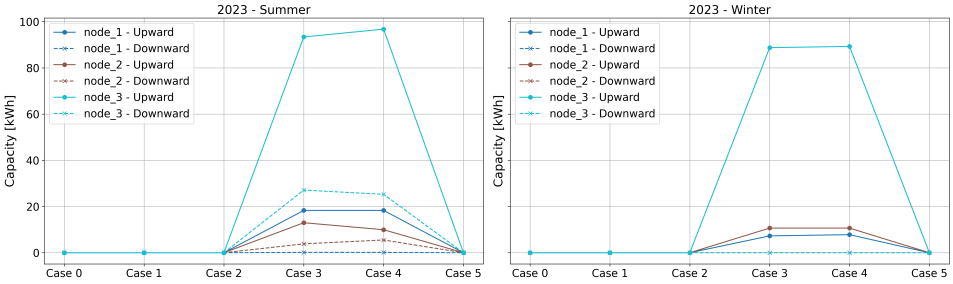

Figure A.4.6: Sum of upward and downward aFRR EV power per node, season and case.

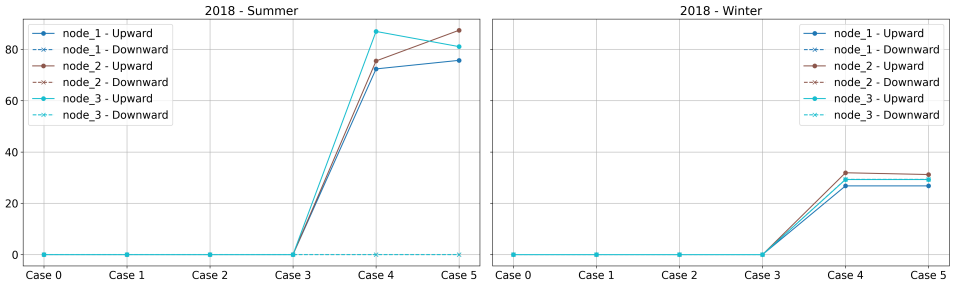

Figure A.4.7: Sum of upward (solid) and downward (striped) aFRR BESS power per node, season and case

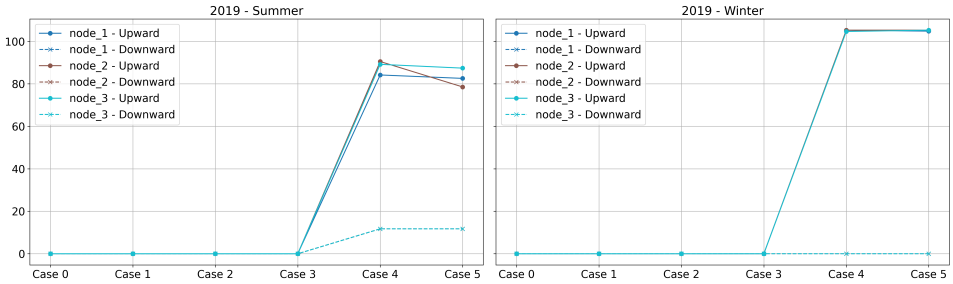

Figure A.4.8: Sum of upward (solid) and downward (striped) aFRR BESS power per node, season and case

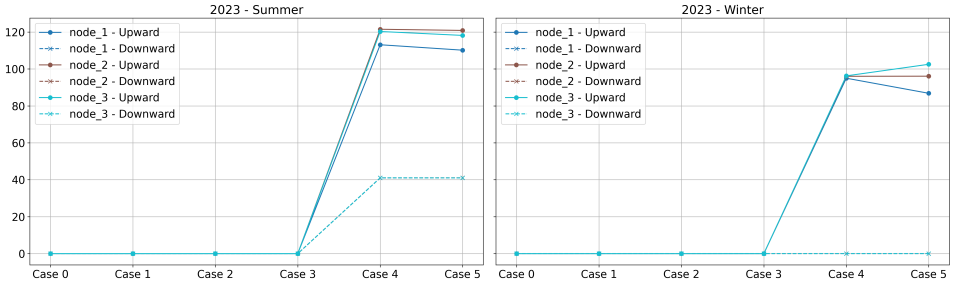

Figure A.4.9: Sum of upward (solid) and downward (striped) aFRR BESS power per node, season and case

A.5. C-rate

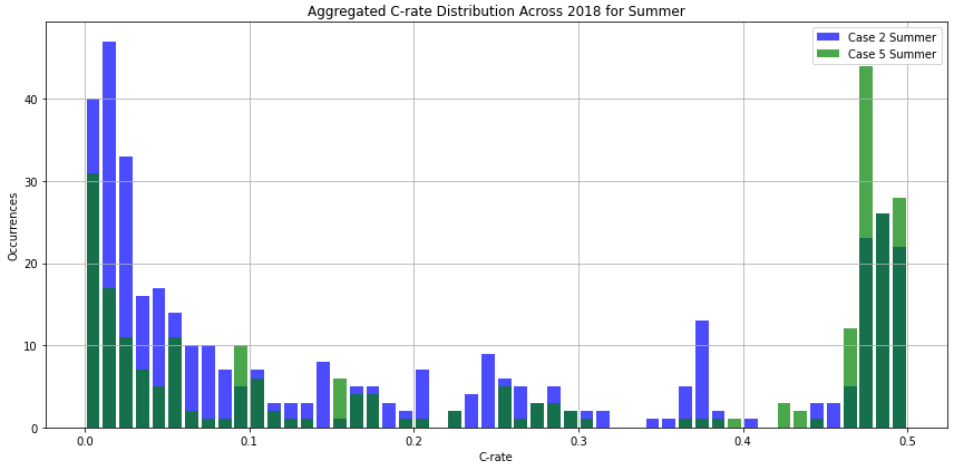

Figure A.5.1: Sum of upward (solid) and downward (striped) aFRR BESS power per node, season and case

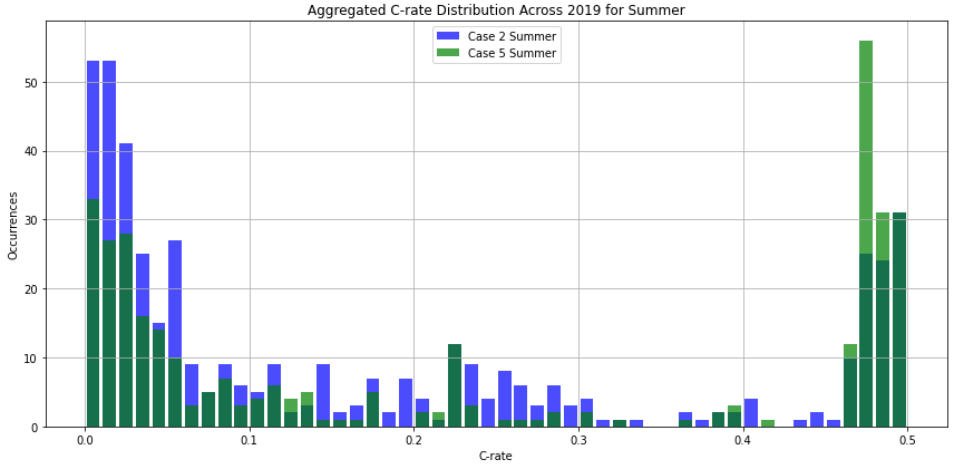

Figure A.5.2: Sum of upward (solid) and downward (striped) aFRR BESS power per node, season and case

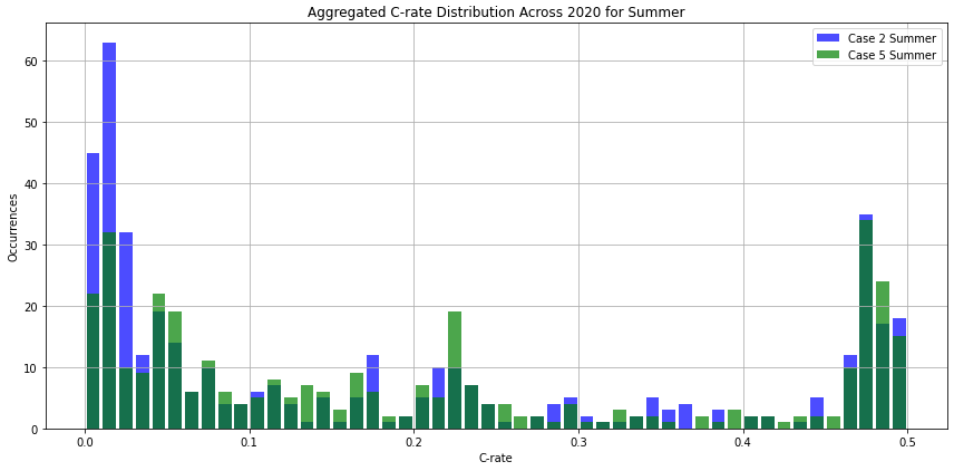

Figure A.5.3: Sum of upward (solid) and downward (striped) aFRR BESS power per node, season and case

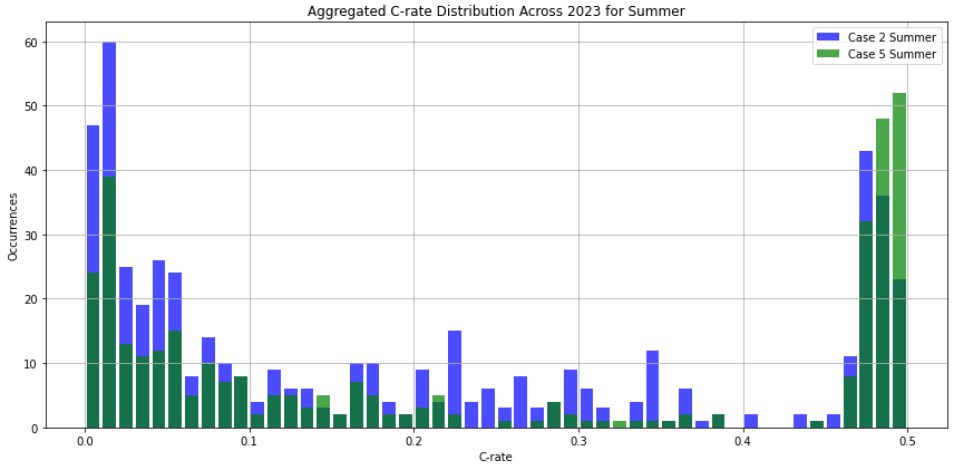

Figure A.5.4: Sum of upward (solid) and downward (striped) aFRR BESS power per node, season and case

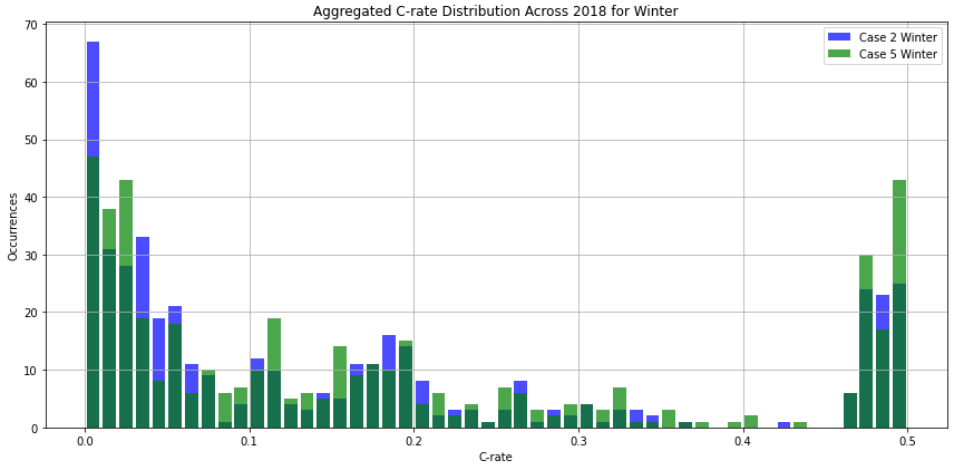

Figure A.5.5: Sum of upward (solid) and downward (striped) aFRR BESS power per node, season and case

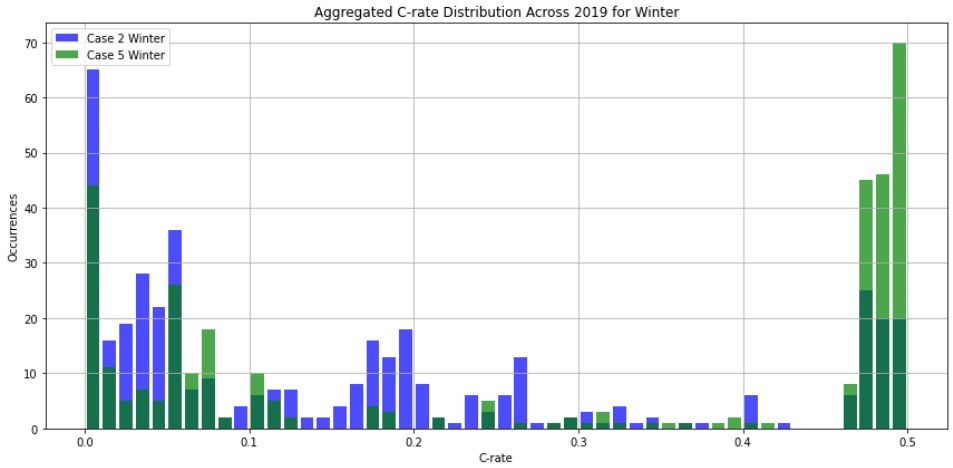

Figure A.5.6: Sum of upward (solid) and downward (striped) aFRR BESS power per node, season and case

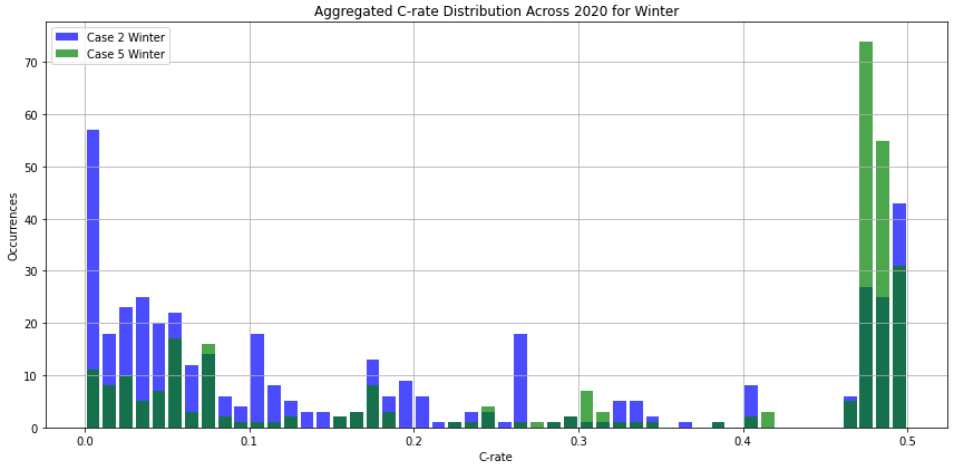

Figure A.5.7: Sum of upward (solid) and downward (striped) aFRR BESS power per node, season and case

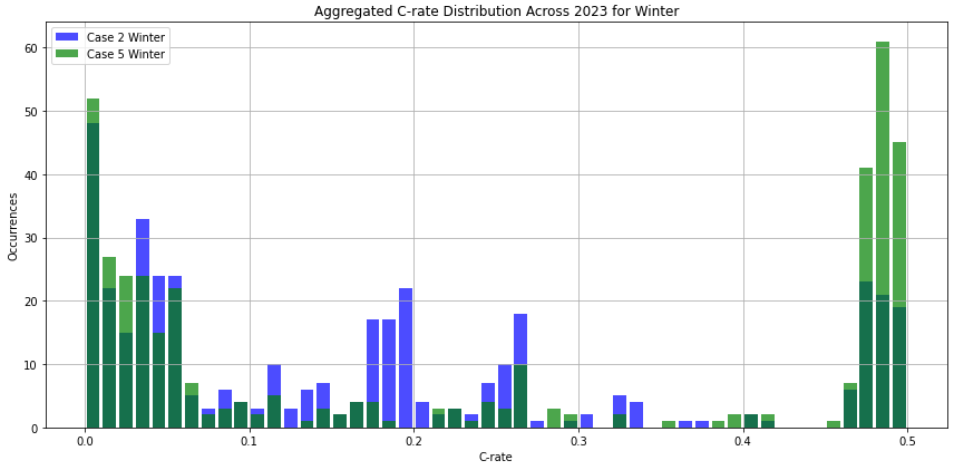

Figure A.5.8: Sum of upward (solid) and downward (striped) aFRR BESS power per node, season and case

Bibliography

ABB Brochure [Accessed 2024]. (Publication date unavailable). https://library.industrialsolutions.abb.com/publibrary/checkout/DEA-642?TNR=Brochures%7CDEA-642%7CPDF&filename=DEA-642.pdf

Akram, U., Shah, R., & Mithulananthan, N. (2019). Hybrid energy storage system for frequency regulation in microgrids with source and load uncertainties. *IET Generation, Transmission Distribution*, *13*, 5048–5057. https://doi.org/10.1049/iet-gtd.2018.7064

Alsharif, A., Tan, C. W., Ayop, R., Dobi, A., & Lau, K. Y. (2021). A comprehensive review of energy management strategy in vehicle-to-grid technology integrated with renewable energy sources. *Sustainable Energy Technologies and Assessments*, *47*, 101439. https://doi.org/10.1016/j.seta.2021.101439

Aneke, M., & Wang, M. (2016). Energy storage technologies and real-life applications – a state of the art review. *Applied Energy*, *179*, 350–377. https://doi.org/10.1016/j.apenergy.2016.06.097

Author(s). (2007). Supercapacitor energy storage for wind energy applications. *IEEE Transactions on Industry Applications*, *43*(5), 1309–1316. https://doi.org/10.1109/TIA.2007.895768

Baek, M.-K., Roh, J.-H., Park, J.-B., & Jeong, W.-C. (2021). Optimal sizing of battery/supercapacitor hybrid energy storage systems for frequency regulation. *Journal of Electrical Engineering & Technology*, *17*, 111–120. https://doi.org/10.1007/s42835-021-00867-6

Bandyopadhyay, S., Mouli, G. R. C., Qin, Z., Elizondo, L. R., & Bauer, P. (2020). Techno-economical model based optimal sizing of pv-battery systems for microgrids. *IEEE Transactions on Sustainable Energy*, *11*, 1657–1668. https://doi.org/10.1109/tste.2019.2936129

Behabtu, H. A., Messagie, M., Coosemans, T., Berecibar, M., Fante, K. A., Kebede, A. A., & Mierlo, J. V. (2020). A review of energy storage technologies' application potentials in renewable energy sources grid integration. *Sustainability*, *12*(24), 10511. https://doi.org/10.3390/su122410511

Berckmans, G., Messagie, M., Smekens, J., Omar, N., Vanhaverbeke, L., & Van Mierlo, J. (2017). Cost projection of state of the art lithium-ion batteries for electric vehicles up to 2030. *Energies*, *10*, 1314. https://doi.org/10.3390/en10091314

Blonsky, M., Munankarmi, P., & Balamurugan, S. P. (2021). Incorporating residential smart electric vehicle charging in home energy management systems. *2021 IEEE Green Technologies Conference (GreenTech)*. https://doi.org/10.1109/greentech48523.2021.00039

Bocklisch, T. (2015). Hybrid energy storage systems for renewable energy applications. *Energy Procedia*, *73*, 103–111. https://doi.org/10.1016/j.egypro.2015.07.469

Cardo-Miota, J., Pérez, E., & Beltran, H. (2023). Deep learning-based forecasting of the automatic frequency reserve restoration band price in the iberian electricity market. *Sustainable Energy, Grids and Networks*, *35*, 101110. https://doi.org/10.1016/j.segan.2023.101110

CBS News. (2024a). *An innovative way to estimate solar energy yields*. Retrieved April 2024, from https://www.cbs.nl/en-gb/about-us/innovation/project/an-innovative-way-to-estimate-solar-energy-yields

CBS News. (2024b). *Nearly half the electricity produced in the netherlands is now renewable*. Retrieved April 2024, from https://www.cbs.nl/en-gb/news/2024/10/nearly-half-the-electricity-produced-in-the-netherlands-is-now-renewable

Chen, H., Cong, T., Yang, W., Tan, C., Li, Y., & Ding, Y. (2009). Progress in electrical energy storage systems: A critical review. *Progress in Natural Science*, *19*, 291–312. https://doi.org/10.1016/j.pnsc.2008.07.014

Cole, W. J., Marcy, C., Krishnan, V. K., & Margolis, R. (2016). Utility-scale lithium-ion storage cost projections for use in capacity expansion models. *2016 North American Power Symposium (NAPS)*. https://doi.org/10.1109/naps.2016.7747866

Coppitters, D., De Paepe, W., & Contino, F. (2021). Robust design optimization of a photovoltaic-battery-heat pump system with thermal storage under aleatory and epistemic uncertainty. *Energy*, *229*, 120692. https://doi.org/10.1016/j.energy.2021.120692

Damianakis, N. (2024, xx). Energy management system for smart charging of evs.

Damianakis, N., Mouli, G. R. C., Bauer, P., & Yu, Y. (2023). Assessing the grid impact of electric vehicles, heat pumps & pv generation in dutch lv distribution grids. *Applied Energy*, *352*, 121878. https://doi.org/10.1016/j.apenergy.2023.121878

Das, C. K., Bass, O., Kothapalli, G., Mahmoud, T. S., & Habibi, D. (2018). Overview of energy storage systems in distribution networks: Placement, sizing, operation, and power quality. *Renewable and Sustainable Energy Reviews*, *91*, 1205–1230. https://doi.org/10.1016/j.rser.2018.03.068

Eicke, A., Ruhnau, O., & Hirth, L. (2021). Electricity balancing as a market equilibrium: An instrument-based estimation of supply and demand for imbalance energy. *Energy Economics*, *102*, 105455. https://doi.org/10.1016/j.eneco.2021.105455

Enexis Netbeheer. (n.d.). Welke aansluiting heb ik nodig? [Accessed: 2023-06-01].

ENTSOE. (2023, February). Capacity: Volumes of contracted balancing reserves [17.1.b] [Accessed: 2023-02-01].

ENTSO-E. (2024, January). Explanatory note to the methodology for pricing balancing energy and cross-zonal capacity used for the exchange of balancing energy or operating the imbalance netting process. https://eepublicdownloads.entsoe.eu/clean-documents/nc-tasks/240131_Art%2030(1)_EB%20Regulation_Pricing%20Methodology_AllTSOamendment%20-%20Explanatory%20document_final.pdf

Entura. (2016). *Is pumped storage hydro the key to increasing renewables in australia?* https://www.entura.com.au/is-pumped-storage-hydro-the-key-to-increasing-renewables-in-australia/

European Commission. (2023a). REPowerEU: Affordable, Secure and Sustainable Energy for Europe [Accessed: 2023-04-22]. https://commission.europa.eu/strategy-and-policy/priorities-2019-2024/european-green-deal/repowereu-affordable-secure-and-sustainable-energy-europe_en

European Commission. (2023b). The European Green Deal [Accessed: 2023-04-22]. https://commission.europa.eu/strategy-and-policy/priorities-2019-2024/european-green-deal_en

European Commission, Joint Research Centre. (2018). *Li-ion batteries for mobility and stationary storage applications: Scenarios for costs and market growth*. Publications Office. https://doi.org/10.2760/87175

European Network of Transmission System Operators for Electricity (ENTSO-E). (2023). Objectives of entso-e [Accessed: 2023-08-22]. https://www.entsoe.eu/about/inside-entsoe/objectives/

Fanti, M. P., Mangini, A. M., Roccotelli, M., & Ukovich, W. (2017). Optimal energy management integrating renewable energy, energy storage systems and electric vehicles. *2017 IEEE 14th International Conference on Networking, Sensing and Control (ICNSC)*. https://doi.org/10.1109/icnsc.2017.8000146

Formsma, A. (2023, July). Factsheet 'glastuinbouw en het elektriciteitssysteem'.

Franz, J., & Röben, F. (2020). Market response for real-time energy balancing: Simulation using field test data. *2020 17th International Conference on the European Energy Market (EEM)*, 1–5. https://doi.org/10.1109/EEM49802.2020.9221882

Gomez-Gonzalez, M., Hernández, J. C., Vidal, P. G., & Jurado, F. (2021). Novel optimization algorithm for the power and energy management and component sizing applied to hybrid storage-based photovoltaic household-prosumers for the provision of complementarity services. *Journal of Power Sources*, *482*, 228918. https://doi.org/10.1016/j.jpowsour.2020.228918

Guena, T., & Leblanc, P. (2006). How depth of discharge affects the cycle life of lithium-metal-polymer batteries. *INTELEC 06 - Twenty-Eighth International Telecommunications Energy Conference*. https://doi.org/10.1109/intlec.2006.251641

Hadjipaschalis, I., Poullikkas, A., & Efthimiou, V. (2009). Overview of current and future energy storage technologies for electric power applications. *Renewable and Sustainable Energy Reviews*, *13*(6–7), 1513–1522. https://doi.org/10.1016/j.rser.2008.09.028

Hajiaghasi, S., Hosseini Ahmadi, M. M., Goleij, P., Salemnia, A., & Hamzeh, M. (2021). Hybrid energy storage sizing based on discrete fourier transform and particle swarm optimization for microgrid applications. *International Transactions on Electrical Energy Systems*, *31*. https://doi.org/10.1002/2050-7038.13156

Hajiaghasi, S., Salemnia, A., & Hamzeh, M. (2019). Hybrid energy storage system for microgrids applications: A review. *Journal of Energy Storage*, *21*, 543–570. https://doi.org/10.1016/j.est.2018.12.017

Huang, P., Lovati, M., Zhang, X., Bales, C., Hallbeck, S., Becker, A., Bergqvist, H., Hedberg, J., & Maturi, L. (2019). Transforming a residential building cluster into electricity prosumers in sweden: Optimal design of a coupled pv-heat pump-thermal storage-electric vehicle system. *Applied Energy*, *255*, 113864. https://doi.org/10.1016/j.apenergy.2019.113864

IEA. (2023). *Tracking clean energy progress 2023* [Licence: CC BY 4.0]. IEA. https://www.iea.org/reports/tracking-clean-energy-progress-2023

Imani, M. H., Ghadi, M. J., Ghavidel, S., & Li, L. (2018). Demand response modeling in microgrid operation: A review and application for incentive-based and time-based programs. *Renewable and Sustainable Energy Reviews*, *94*, 486–499.

International Renewable Energy Agency. (2012, April). *Electricity storage: Technology brief* (Technology Policy Brief). Energy Technology Systems Analysis Programme. https://www.irena.org/-/media/Files/IRENA/Agency/Publication/2012/IRENA-ETSAP-Tech-Brief-E18-Electricity-Storage.pdf

Kaldellis, J. (2015). Photovoltaic-energy storage systems for remote small islands. In B. Sørensen (Ed.), *Solar energy storage* (pp. 291–326). Academic Press. https://doi.org/10.1016/B978-0-12-409540-3.00013-X

Killer, M., Farrokhseresht, M., & Paterakis, N. G. (2020). Implementation of large-scale li-ion battery energy storage systems within the emea region. *Applied Energy*, *260*, 114166. https://doi.org/10.1016/j.apenergy.2019.114166

Krishnan, K., Kalam, A., & Zayegh, A. (2013). H2 optimisation and fuel cell as a back-up power for telecommunication sites. *2013 International Conference on Circuits, Power and Computing Technologies (ICCPCT)*, 1274–1277. https://api.semanticscholar.org/CorpusID:16007413

Kumar, K., & Pahariya, D. Y. (2017). A review-on analysis of battery lifetime extension in small-scale wind-energy system using supercapacitors. *IARJSET*, *4*, 77–82. https://doi.org/10.17148/iarjset.2017.4515

Lei, S., He, Y., Zhang, J., & Deng, K. (2023). Optimal configuration of hybrid energy storage capacity in a microgrid based on variational mode decomposition. *Energies*, *16*, 4307.

Liao, J.-T., Chuang, Y.-S., Yang, H.-T., & Tsai, M.-S. (2018). Bess-sizing optimization for solar pv system integration in distribution grid. *IFAC-PapersOnLine*, *51*, 85–90. https://doi.org/10.1016/j.ifacol.2018.11.682

Luo, X., Wang, J., Dooner, M., & Clarke, J. (2015). Overview of current development in electrical energy storage technologies and the application potential in power system operation. *Applied Energy*, *137*, 511–536. https://doi.org/10.1016/j.apenergy.2014.09.081

Maeyaert, L., Vandevelde, L., & Döring, T. (2020). Battery storage for ancillary services in smart distribution grids. *Journal of Energy Storage*, *30*, 101524. https://doi.org/10.1016/j.est.2020.101524

Mohamed, A., Rigo-Mariani, R., Debusschere, V., & Pin, L. (2023). Stacked revenues for energy storage participating in energy and reserve markets with an optimal frequency regulation modeling. *Applied Energy*, *350*, 121721. https://doi.org/10.1016/j.apenergy.2023.121721

Mouli, G. R. C., Schijffelen, J. H., Bauer, P., & Zeman, M. (2017). Design and comparison of a 10-kw interleaved boost converter for pv application using si and sic devices. *IEEE Journal of Emerging and Selected Topics in Power Electronics*, *5*(2), 610–623. https://doi.org/10.1109/JESTPE.2016.2601165

Nelson, J. R., & Johnson, N. G. (2020). Model predictive control of microgrids for real-time ancillary service market participation. *Applied Energy*, *269*, 114963.

Netbeheer Nederland. (2023a). Capacity map [Accessed: 2023-04-22]. https://capaciteitskaart.netbeheernederland.nl/

Netbeheer Nederland. (2023b, May). Wachtlijsten voor stroomaansluitingen nemen toe [Accessed: 2024-04-22]. https://www.netbeheernederland.nl/artikelen/nieuws/wachtlijsten-voor-stroomaansluitingen-nemen-toe

Netbeheer Nederland. (2024, February). Wachtlijsten nemen toe [Accessed: 2024-04-22]. https://www.netbeheernederland.nl/artikelen/nieuws/wachtlijsten-nemen-toe

Next Kraftwerke. (2023). Balancing responsible party (brp) [Accessed: 2023-04-22]. https://www.next-kraftwerke.be/knowledge-hub/balancing-responsible-party-brp

Ni, F., Zheng, Z., Xie, Q., Xiao, X., Zong, Y., & Huang, C. (2021). Enhancing resilience of dc microgrids with model predictive control based hybrid energy storage system. *International Journal of Electrical Power Energy Systems*, *128*, 106738.

Okhuegbe, S., Mwaniki, C., & Akorede, M. (2019). Optimal sizing of hybrid energy systems in a microgrid: A review.

Panasonic. (2021). *Evac-105 / evdc-105 energy storage*. panasonic.com. https://ftp.panasonic.com/batterystorage/datasheet/evervolt_datasheet.pdf

Papakonstantinou, A. G., Psarros, G. N., & Papathanassiou, S. A. (2024). Frequency regulation in island grids with battery storage participating in automatic generation control. *School of Electrical and Computer Engineering, National Technical University of Athens (NTUA), Greece*.

Rancilio, G., Rossi, A., Falabretti, D., Galliani, A., & Merlo, M. (2022). Ancillary services markets in europe: Evolution and regulatory trade-offs. *Renewable and Sustainable Energy Reviews*, *154*, 111850. https://doi.org/10.1016/j.rser.2021.111850

Rassaei, F., Soh, W.-S., & Chua, K.-C. (2015). Demand response for residential electric vehicles with random usage patterns in smart grids. *IEEE Transactions on Sustainable Energy*, *6*, 1367–1376. https://doi.org/10.1109/tste.2015.2438037

Rassaei, F., Soh, W.-S., & Chua, K.-C. (2018). Distributed scalable autonomous market-based demand response via residential plug-in electric vehicles in smart grids. *IEEE Transactions on Smart Grid*, *9*, 3281–3290. https://doi.org/10.1109/tsg.2016.2629515

Rezaei Mozafar, M., Monaghan, R. F. D., Barrett, E., & Duffy, M. (2022). A review of behind-the-meter energy storage systems in smart grids. *Renewable and Sustainable Energy Reviews*, *164*, 112573. https://doi.org/10.1016/j.rser.2022.112573

Rijksdienst voor Ondernemend Nederland (RVO). (2023). *Cijfers over elektrisch rijden in nederland*. Retrieved April 22, 2023, from https://www.rvo.nl/onderwerpen/duurzaam-ondernemen/energie-en-milieu-innovaties/elektrisch-rijden/stand-van-zaken/cijfers

Schmidt, O., Hawkes, A., Gambhir, A., & Staffell, I. (2017). The future cost of electrical energy storage based on experience rates. *Nature Energy*, *2*. https://doi.org/10.1038/nenergy.2017.110

Schmidt, O., Melchior, S., Hawkes, A., & Staffell, I. (2019). Projecting the future levelized cost of electricity storage technologies. *Joule*, *3*, 81–100. https://doi.org/10.1016/j.joule.2018.12.008

Seo, H., Kim, A., Park, M., & Yu, I. (2011). Power quality enhancement of renewable energy source power network using smes system. *Physica C: Superconductivity and its Applications*, *471*(21–22), 1409–1412. https://doi.org/10.1016/j.physc.2011.05.205

Shen, W., Vo, T. T., & Kapoor, A. (2012). Charging algorithms of lithium-ion batteries: An overview. *2012 7th IEEE conference on industrial electronics and applications (ICIEA)*, 1567–1572.

Shigematsu, T., Kumamoto, T., Deguchi, H., & Hara, T. (2002, November). *Applications of a vanadium redox-flow battery to maintain power quality* (Vol. 2). https://doi.org/10.1109/TDC.2002.1177625

Singh, P., & Lather, J. S. (2020). Dynamic current sharing, voltage and soc regulation for hess based dc microgrid using cpismc technique. *Journal of Energy Storage*, *30*, 101509.

SolarPower Europe. (2023). *EU Market Outlook for Solar Power 2023-2027* (M. Schmela, Ed.) [Please cite as: SolarPower Europe (2023): EU Market Outlook for Solar Power 2023-2027.].

Stamatellos, G., Zogou, O., & Stamatelos, A. (2022). Interaction of a house's rooftop pv system with an electric vehicle's battery storage and air source heat pump. *Solar*, *2*(2), 186–214. https://doi.org/10.3390/solar2020011

Suzuki, Y., Koyanagi, A., Kobayashi, M., & Shimada, R. (2005). Novel applications of the flywheel energy storage system. *Energy*, *30*(11–12), 2128–2143. https://doi.org/10.1016/j.energy.2004.08.018

Tabar, V. S., Ghassemzadeh, S., & Tohidi, S. (2019). Energy management in hybrid microgrid with considering multiple power market and real-time demand response. *Energy*, *174*, 10–23.

Tennet. (n.d.).

TenneT. (2022a, March). Fcr manual for bsp's [Accessed: 2023-07-01].

TenneT. (2022b, March). Onbalansprijssystematiek (version 6) [Accessed: 2023-08-29].

TenneT. (2022c, October). Manual afrr for bsps [Accessed: 2023-07-05].

TenneT. (2023a). Dutch ancillary services - tennet [Accessed: 2023-12-01].

TenneT. (2023b). Soorten elektriciteitsmarkten [Accessed on: February 25, 2024]. https://tennet.eu/nl/soorten-elektriciteitsmarkten

TenneT. (2023c, February). Manual / product information incident reserves for bsps [Accessed: 2023-07-05].

Tennet. (2023a). Balance responsible party (brp) [Accessed: 2023-04-22]. https://www.tennet.eu/balance-responsible-party-brp

Tennet. (2023b). Balancing markets [Accessed: 2023-04-22]. https://www.tennet.eu/markets/market-news/balancing-markets

Tennet. (2023c). Balancing service providers (bsp) [Accessed: 2023-08-22]. https://www.tennet.eu/balancing-service-providers-bsp

Tennet. (2023d). Market roles [Accessed: 2023-08-22]. https://www.tennet.eu/market-roles

Tennet. (2023e). Tennet balanceringsmarkten [Retrieved December 1, 2023].

Tennet TSO. (2023). System Balance and Price Information [Accessed: December 2023].

TenneT TSO B.V. (2022, March). Imbalance pricing system: How are the (directions of) payment determined? [Version 6.0].

Terpstra, N. R. (2020, June). *Day-ahead and imbalance price forecasting on the dutch electricity market: A comparison between time series and artificial neural networks models* [Retrieved from https://research.tue.nl/en/studentTheses/day-ahead-and-imbalance-price-forecasting-on-the-dutch-electricit].

Tesla. (2023). *Tesla powerwall 2 datasheet - north america* [Accessed July 31, 2023]. https://www.tesla.com/sites/default/files/pdfs/powerwall/Powerwall%202_AC_Datasheet_en_northamerica.pdf

Tesla, Inc. (Accessed 2024). *Megapack*. https://www.tesla.com/megapack

Toprakci, O., Toprakci, H. A. K., Ji, L., & Zhang, X. (2010). Fabrication and electrochemical characteristics of LiFePO4 powders for lithium-ion batteries [Released on J-STAGE March 29, 2014]. *KONA Powder and Particle Journal*, *28*, 50–73. https://doi.org/10.14356/kona.2010008

Torkashvand, M., Khodadadi, A., Sanjareh, M. B., & Nazary, M. H. (2020). A life cycle-cost analysis of li-ion and lead-acid besss and their actively hybridized esss with supercapacitors for islanded microgrid applications. *IEEE Access*, *8*, 153215–153225.

Traore, A., Taylor, A., Zohdy, M. A., & Peng, F. Z. (2017). Modeling and simulation of a hybrid energy storage system for residential grid-tied solar microgrid systems. *Journal of Power and Energy Engineering*, *05*, 28–39. https://doi.org/10.4236/jpee.2017.55003

Tushar, M. H. K., Zeineddine, A. W., & Assi, C. (2018). Demand-side management by regulating charging and discharging of the ev, ess, and utilizing renewable energy. *IEEE Transactions on Industrial Informatics*, *14*, 2671–2679.

Vermeer, W., Mouli, G. R. C., & Bauer, P. (2022). Optimal sizing and control of a pv-ev-bes charging system including primary frequency control and component degradation. *IEEE Open Journal of the Industrial Electronics Society*, *3*, 236–251. https://doi.org/10.1109/OJIES.2022.3161091

Wakui, T., Sawada, K., Yokoyama, R., & Aki, H. (2019). Predictive management for energy supply networks using photovoltaics, heat pumps, and battery by two-stage stochastic programming and rule-based control. *Energy*, *179*, 1302–1319. https://doi.org/10.1016/j.energy.2019.04.148

Worighi, I., Geury, T., El Baghdadi, M., Van Mierlo, J., Hegazy, O., & Maach, A. (2019). Optimal design of hybrid pv-battery system in residential buildings: End-user economics, and pv penetration. *Applied Sciences*, *9*, 1022. https://doi.org/10.3390/app9051022

Worku, M. Y. (2022). Recent advances in energy storage systems for renewable source grid integration: A comprehensive review. *Sustainability*, *14*, 5985. https://doi.org/10.3390/su14105985

Yan, Q., Zhang, B., & Kezunovic, M. (2019). Optimized operational cost reduction for an ev charging station integrated with battery energy storage and pv generation. *IEEE Transactions on Smart Grid*, *10*, 2096–2106. https://doi.org/10.1109/tsg.2017.2788440

Yıldız, S., Gunduz, H., Yildirim, B., & Özdemir, M. T. (2022). An islanded microgrid energy system with an innovative frequency controller integrating hydrogen-fuel cell. *Fuel*, *326*, 125005. https://doi.org/10.1016/j.fuel.2022.125005

Yousefi, M., Hajizadeh, A., Soltani, M. N., & Hredzak, B. (2021). Predictive home energy management system with photovoltaic array, heat pump, and plug-in electric vehicle. *IEEE Transactions on Industrial Informatics*, *17*(1), 430–440. https://doi.org/10.1109/TII.2020.2971530

Zhou, C., Wang, P., Bao, T., Yao, S., Tang, Y., & Yang, P. (2023). Flexible load optimal regulation strategy of commercial buildings under the environment of electricity market. *Energy Reports*, *9*, 1705–1716. https://doi.org/10.1016/j.egyr.2023.04.173

Zhuo, W., & Savkin, A. V. (2019). Profit maximizing control of a microgrid with renewable generation and bess based on a battery cycle life model and energy price forecasting. *Energies*, *12*, 2904. https://doi.org/10.3390/en12152904

Ziegler, M. S., & Trancik, J. E. (2021). Re-examining rates of lithium-ion battery technology improvement and cost decline. *Energy & Environmental Science*, *14*, 1635–1651. https://doi.org/10.1039/d0ee02681f